FINITE ELEMENT MODELING OF PRECAST R.C.C. JOINTS AND FRAME UNDER CYCLIC LOADING

A thesis submitted in the partial fulfillment of
requirement for the award of the degree of

MASTER OF ENGINEERING

IN

CIVIL ENGINEERING

Submitted By

Saurav Khanna

Roll No. 801022017

Under the supervision of

Dr. Naveen Kwatra

Associate Professor

Department of Civil Engineering

Thapar University, Patiala.

DEPARTMENT OF CIVIL ENGINEERING

THAPAR UNIVERSITY

PATIALA – 147004, (INDIA)

July -2012

CERTIFICATE

This is to certify that the work presented in this thesis titled **'Finite Element Modeling of Precast RCC Joints and Frames Under Cyclic Loading'** being submitted by **Saurav Khanna** in the partial fulfillment of requirement for the award of the **MASTER'S DEGREE**, in **CIVIL ENGINEERING (Structures)**, submitted in the **CIVIL ENGINEERING DEPARTMENT, THAPAR UNIVERSITY, PATIALA** is an authentic record of student's own work carried out under my supervision & guidance. The matter presented in this thesis has reached the standards fulfilling the requirements of the regulation of award of said degree.

Dr. Naveen Kwatra
Associate Professor
Civil Engineering Department
Thapar University, Patiala.

Dr. Maneek Kumar
Professor & Head
Civil Engineering Department
Thapar University, Patiala.

Dean Academic Affairs
Thapar University, Patiala.

ACKNOWLEDGEMENTS

"SUCCESS BEGINS WITH A SINGLE STEP"

This thesis could not be completed without the help of many people who contribute directly or indirectly through there constructive criticism in the evolution and preparation of this work. A special debit of gratitude is owned to my thesis supervisor, Associate Professor, **Dr. Naveen Kwatra** for his gracious efforts and keen pursuit, which has remained as a valuable asset for the successful fulfillment of my thesis. His dynamism and diligent enthusiasm has been highly instrumental in keeping my spirit high. His flawless & forthright suggestions blended with an innate intelligent application have crowned my task with success.

I would also like to thanks my parents for their constant encouragement during the entire course of my work.

I would also like to thank my friends and class mates or their kind support during the completion of my thesis.

I am also like to offer my sincere thanks to all faculty, teaching and non-teaching, of Civil Engg. Deptt. (CED), and staff of central library, TU, Patiala for there assistance.

SAURAV KHANNA

Reg. No. 801022017

ABSTRACT

Precast concrete has been widely accepted as a viable means of constructing safe, durable, reliable, high quality, and cost-effective structural systems. Its full implementation in high seismic areas, however, has been some what limited, mainly due to scarce design guidelines as compared to those available for cast-in-place concrete structures. In particular, there is a lack of design provisions for seismic-resistant beam-to-column connections appropriate for precast concrete frame construction.

Connection is one of the crucial elements to limit building damage. In this investigation behavior of different types of precast beam column connection details used in precast construction under monotonic as well as cyclic loading is analyzed by using Finite Element based software ATENA. The various parameters investigated by F.E. modeling of these connections are their load carrying capacity, energy dissipation characteristics, ductility & cracks development pattern under monotonic as well as under cyclic displacements. The results obtained by F.E. modeling of precast connection are compared with the results of F.E. modeling of monolithic connection so as to compare the behavior of precast connection in comparison to monolithic connection. The comparison of results of these joints shows that precast joints if properly detailed can be as effective as monolithic construction. Another parameter investigated in this work is the behavior of precast frame during its erection stage under cyclic loading. During the erection stage a precast frame is most venerable to lateral forces because precast frame attains its full lateral strength by interlocking of all components and any accidental lateral load on precast frame at this stage may cause complete failure of structure. By F.E. modeling of precast frame it is found that precast frame requires proper supporting mechanism in its initial stage of erection because cast in place concrete grout placed in connection is not strong enough to keep the frame intact during lateral forces.

TABLE OF CONTENTS

LIST OF FIGURES

LIST OF TABLES

CHAPTER-1
INTRODUCTION

Precast concrete systems for buildings are cost-efficient, structural systems that provide speed and ease of erection. They allow for improved quality control in the precast plants, and freedom in the architectural form of the members. The increased usage of such members is attributed to an increased interest on the part of contractors and engineers in order to find competitive alternatives to cast-in-place concrete elements.

Despite many advantages of precast concrete, it is not widely used, especially in regions of high seismic risk. The reason behind this is a lack of confidence and knowledge base about their performance in seismic regions as well as the absence of rational seismic design provisions in major model building codes. Several precast parking structures performed poorly in the 1994 Northridge earthquake(1), due to incorrect detailing. Connection in precast concrete structures is one of the crucial elements to limit building damage.

Linear finite element analysis (LFEA) is one of the tools which may be used to improve the prediction of strength of precast frame. This research focuses on analyzing the behavior of various beam column joints as well as of a frame under inelastic cyclic loading of the precast structure constructed by the detailing developed by various researchers using finite element based software ATENA & comparing the result of connection details used in precast construction with a monolithic constructed frame so as to find the suitability of the proposed detailing in precast construction under seismic forces.

1.1 Precast Structures

A precast concrete structure is an assemblage of precast elements which, when suitably connected together, form a 3D framework capable of resisting gravitation and wind (or even earthquake) loads. The framework is ideally suited to buildings such as offices, retail units, car parks, schools, stadium and other such buildings requirement minimal internal obstruction and multi-functional leasable space. Recently, several high-rise low and medium buildings of reinforced concrete frame structures has been constructed using precast element for efficiency. The construction members consist of beams, columns, slabs and walls The

selection of construction methods for different frame members is decided by many factors such as detailing and design, condition of mechanical design, production site scale, time schedule and costing. These factors are the key points for employing a precast structure. The decision is frequently decided by considering productivity, transportation and the ability of crane system. Joint section should be located at the less stressed position. However, it must take into account erection capacity and joint gaps.

The very existence of a precast concrete industry and the numerous successful building projects achieved using precast concrete, for the whole or just a part of the structure, is proof that the technique is practical and economical. In global terms, the market share of precast 'grey' frames (structural concrete with no architectural qualities) is probably around 5 percent of the multi-storey business **(1)**

Many people believe that in certain countries, especially where the ratio of labour to-materials or plant is low, say one man-hour pay is less than 1/500 daily hire of a large mobile crane, precast cannot compete with cast in situ concrete. Where local labour policies demand high levels of unskilled site labour, heavy concrete prefabricates create the potential for new safety hazards due to transportation, handling and temporary stability. Similarly in countries with a strong steel industry and widespread education in steel work design, the popular opinion is that precast cannot compete with structural steelwork frames. In many circumstances however precast concrete is the only economical and practical solution and if the designer is unwilling to consider precast concrete as a total solution the result of this is the so-called 'mixed' solution **(1)**

1.2 CHALLENGES IN PRECAST CONSTRUCTION

Precast concrete has been widely accepted as a viable means of constructing safe, durable, reliable, high quality, and cost-effective structural systems. Its full implementation in high seismic areas, however, has been somewhat limited, mainly due to scarce design guidelines as compared to those available for cast-in-place concrete structures. In particular, the lack of design provisions for seismic-resistant beam-to-column connections appropriate for precast concrete frame construction.

Another obstacle to the use of precast concrete construction in seismic areas has been the imposition of prescriptive provisions developed to promote ductility in cast-in-place concrete construction **(2)**. This set of design and detailing requirements makes a standard methodology for establishing equivalence of energy dissipation and ductility between

precast concrete and cast-in-place systems desirable. In the past, some precast concrete framed structures have performed poorly in earthquakes because of inadequate connection details**.(3)** To gain confidence in the use of precast concrete in moment-resisting frames, satisfactory methods for connecting the precast elements together were required. Therefore, recommendations developed for the seismic design of cast-in-place systems were straightforwardly adapted – that is, the objective of the design method was to emulate monolithic construction.

The challenge in precast frame construction lies in finding economical and practical methods of connecting the precast concrete elements together to ensure adequate stiffness, strength, ductility and stability.

1.3 DESIGN PROVISIONS FOR PRECAST CONSTRUCTION

The Indian codes of practice give guidelines for design and construction of precast reinforced or prestressed concrete ribbed, cored and waffle units**(4,5)**. Although seismic analysis and design requirements are given for precast structures involving large panel prefabricates, design and details of connections are not specified for precast structures in seismically-active areas **(6,7).** On the other hand, among the international codes, NEHRP code permits both elastic and inelastic designs of connections9. For the design of precast members, the UBC and ACI code provisions recommend that all loading and restraint conditions be considered from initial fabrication to completion of structure, and provide strength requirements for various connections **(8,9).**

The New Zealand code of practice recommends that precast elements be designed based on all critical stages of loading**(10).** Load-paths need to be provided in the structure for effective transfer of seismic forces through the lateral load resisting system to maintain the structural integrity. The NZS code recommends two-fold general specification onfixings, namely

(i) resistance to all applied forces and accommodation of imposed deformations

(ii) accommodation of structural damage within a permitted level of strength degradation.

Connections are designed between the precast elements themselves and between the precast and cast in-situ elements for

- **controlling the cracking**
- **developing a flexural failure mode through yielding of steel**

- **providing sufficient horizontal capacity in connectors to transfer the effects of horizontal seismic forces.**

For column bases and horizontal joints, vertical steel is specified. Also, for vertical precast wall panels, component strength requirements and number of ties are specified. The code also recommends the general requirements of ductility capacity, energy dissipating mechanisms and capacity design principles to be applied in the design method

1.4 Finite Element Analysis

To model the complex behavior of reinforced concrete analytically in its non-linear zone is difficult. This has led engineers in the past to rely heavily on empirical formulas which were derived from numerous experiments for the design of reinforced concrete structures. The Finite Element method makes it possible to take into account non-linear response. The FE method is an analytical tool which is able to model RCC or retrofitted structure and is able to calculate the non-linear behavior of the structural members. For structural design and assessment of reinforced concrete members, the non-linear finite element (FE) analysis has become an important tool. The method can be used to study the behavior of reinforced and pre-stressed concrete structures including both force and stress redistribution. With the advent of digital computers and powerful methods of analysis, such as the finite element method many efforts to develop analytical solutions which would obviate the need for experiments have been undertaken by investigators. The finite element method has thus become a powerful computational tool, which allows complex analyses of the nonlinear response of RC structures to be carried out in a routine fashion. FEM is useful for obtaining the load deflection behavior and its crack patterns in various loading conditions. Experiments can be ideal to study the behavior and failure of structures. However, they can be costly and time consuming. They require adequate facilities, space, setup, and manpower. If done properly, computational models could be used as an attractive alternative to the expensive experimental investigation.

1.5 IMPORTANCE OF THIS WORK

The precast concrete has many advantages like reliability, durability, faster construction, higher quality and all weather construction. But this type of construction is more preferred for construction of flyovers around the world. In the International arena precast concrete sector has experienced reasonable growth in the recent years. But there is hesitancy in extensively using precast concrete in highly seismic areas. There was a clear evidence of failure of precast parking structures during the 1994 Northridge earthquake **[11,12]**. Failure in these earthquakes was mainly due to poor connections between the precast elements themselves and between the precast elements and lateral load-resisting system. Hence, a lot of research is required in this area.

- For the past four decades though a lot of research has been done in precast structures, a complete understanding of the behavior of precast beam-column connections to various possible structural loadings has not been completely understood.
- Connections are one of the most essential parts in prefabricated structures as they constitute the weakest link in the structure. The behavior of a precast structure, to a large extent, depends on the behavior of the connections. A key aspect is the behavior of joints that should have larger capacity than elements, or having a dissipative behavior, should possess the necessary ductility resources. Therefore, the proper selection of the type of connection to be used and their design play a prominent role in the performance of precast structures.
- Hence, there is a necessity to carry out more research in this area which will help to improve the knowledge base and thus aid in arriving at improved codal provisions for construction of more durable precast structures.

1.6 AIM & OBJECTIVES

The objectives of this study are :-

1) To present finite element analysis of different types of beam column connection details used in precast construction under monotonic as well as inelastic cyclic displacements using finite element based software ATENA

2) To compare the results of F.E.M. analysis of beam column connection with F.E.M. analysis results of the monolithic connection so as to find difference in behavior of precast connections in comparison to that of monolithic connections.

3) To model & analyze the response, load carrying capacity & cracks development pattern of a single storey frame constructed with precast elements & connections during its erection stage under inelastic cyclic loading using finite element based software ATENA & comparing the result of same with a monolithic constructed frame.

1.7 SCOPE OF THE STUDY

1) This study focuses on modeling & analyzing the behavior of different types of beam column connection details used in precast structure under static and inelastic cyclic displacements. In this study only an exterior connection of a four store building frame is investigated under seismic loads.

2) Firstly various types of connection details for beam to column in precast structures proposed and investigated experimentally by different researchers are modeled using F.E.M. based software ATENA & then their response, load carrying capacity & cracks development pattern under monotonic as well as inelastic cyclic loading is investigated

3) After analyzing the different connection details for beam column joint in precast structure, a complete single storied, 2 bays frame constructed with precast elements & connection details analyzed before is modeled & its response, load carrying capacity & cracks development pattern during erection stage under inelastic cyclic loading is analyzed using

finite element based software ATENA. In this work the frame has been investigated during its initial stage of erection without slab been placed.

4) The results from the F.E. analysis of precast frame is then compared with F.E. analysis result of a monolithic frame of same dimensions, restrains & loading so as to find difference in behavior of precast frame in comparison to that of monolithic frame.

5) This study is restricted only to a single storied two bays frame during its erection stage without slab been placed, further investigations can be done on a complete building frame constructed with precast elements.

1.8 ORGANIZATION OF THE THESIS

The thesis is organized as par detail given below:
Chapter 1: Introduces to the topic of thesis in brief.

Chapter 2: Discusses the literature review i.e. the work done by various researchers in the field of precast joints & frames in R.C.C . structures experimentally as well as analytically

Chapter 3: Deals with the details of the structure modeled in Atena in its first part. Second part comprises of FEM modeling, theory related to the ATENA, material modeling and analytical programming procedure steps involved in modeling of the control frame. It also deals with the description of the material behaviour of concrete, reinforced steel bars.

Chapter 4: The result from the F.E. analysis of the different joints & frames are presented in this chapter. The comparison between the results of precast & monolithic joints are presented and compared under monotonic as well as cyclic displacements. In second part results of a precast frame at the stage of its erection are presented.

Chapter 5: Finally, salient conclusions and recommendations of the present study are given in this chapter followed by the references.

CHAPTER-2
LITERATURE REVIEW

2.1 GENERAL

In India, precast concrete structures are getting wide acceptance in construction industry as some of the major constructional projects have been constructed using precast system of construction. These includes major components of Delhi metro, other large span bridges & industrial buildings.

The use of precast concrete construction systems still lags behinds in comparison to monolithic system of R.C.C. construction because traditional construction system is more labor intensive & requires less technically sound labor & industrial infrastructure. The Indian codes of practice give guidelines for design and construction of precast reinforced or prestressed concrete ribbed, cored and waffle units **(4,5)**. Although seismic analysis and design requirements are given for precast structures involving large panel prefabricates, design and details of connections are not specified for precast structures in seismically-active areas **(6,7).**

2.2 PREACAST CONCRETE

Precast concrete means concrete which has been prepared for casting and the concrete either is statically reinforced or prestressed. Meanwhile a precast concrete element is of a finite size and must therefore connect with other elements to form a complete structure. When two elements are connected, problems such as shrinkage, thermal or load will induced strains and cause volumetric changes. The volumetric changes cause movement between the two elements and internal friction between the two elements surface is provided by using various methods such as inserting dowel between beam to column connection. Apart from that, local crushing at the top of column occurs due to the flexural rotation of the beam. Therefore, a bearing pad is provided to overcome this problem. Another factor need to be considered is the narrow bearing of the suspended element on the vertical element. Consideration for the overall stability of the structure is important too.

Precast concrete structure refers to the combination of precast concrete elements and the structure is able to sustain vertical and horizontal loads or even dynamic loads. The design and construction of the joints and connections is important to ensure the stability and robustness of the overall structure. According to Dr. Kim S. Elliot, a joint is a mechanism to take care of the forces action at the interface of two or more structural elements. A connection is a combination of one or more interfaces to sustain forces action. **(Kim S. Elliot, 2002)** The design of connection should be able to sustain various kinds of loads (static and dynamic) in terms of strength and ductility. Besides, the connection should be simple for construction. Constructability of connection is important to reduce fabrication period. As there is a lack of knowledge and information on the connection behavior in seismic load, this research is conducted to understand the behavior of several precast connections used in precast constrction.

2.3 LITERATURE SURVEY

In order to undertake an investigation on the connection behavior of various elements in precast concrete structures a comprehensive literature overview of the findings from studies conducted to analyze and investigate the behavior of precast concrete systems assembled with typical connections or joints under simulated earthquake loading is investigated & presented below : -

2.3.1 BEHAVIOUR OF PRECAST BEAM-COLUMN MECHANICAL CONNECTIONS UNDER CYCLIC LOADING (13)

R. Vidjeapriya and K.P. Jaya (2011) conducted an experimental investigation with the following objectives :-

1) To identify a simple and suitable precast beam – column connection for an exterior beam-column joint of a moment resisting framed structure.
2) To conduct experimental investigations on two types of precast connections and a monolithic connection.
3) To identify the most suited connection for the precast elements.

The beam-column connection in a three storey reinforced concrete residential building in Chennai, India was considered for their study. The building was modeled and analyzed using STAAD Pro software. The force resultants such as shear force, bending moment and axial force around the exterior beam-column joint due to various load combinations were computed. Seismic analysis was performed using equivalent lateral force method given in IS:1893-2002 [14]. The design and detailing of beam, column and exterior joint was carried out based on the guidelines given by IS:456-2000 [15] and IS:13920-1993 [16]. One-third scaled models were developed for monolithic and precast specimens. The dimensions of the beam were 100 mm x 100 mm x 550 mm. The column was of size 100 mm x 100 mm x 1200 mm.

In their work they used two types of connection details for connecting beam to column. The first type of connection detail used consists of J-Bolt connection & was designated as PC1. In this connection the beam was supported on concrete corbel using J-bolt. This connection transmits vertical shear forces. J-bolt of diameter 16 mm was kept inside the corbel and cast by keeping its straight portion protruding outside. The beam was inserted on to the J-bolt and the nut tightened. Iso-resin grout was used to fill the gap between the J-bolt and the hole in the beam. The schematic representation of the isometric view of precast concrete column with corbel and the beam connected using a J-bolt is shown in Figure 2.1

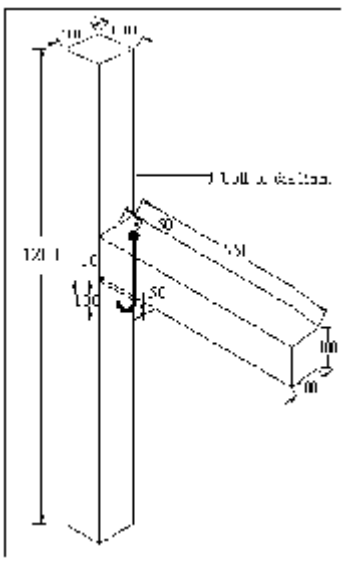

Fig. 2.1 Precast beam-column connection using J-bolt

The second type of connection detail used consists of using cleat angels for making connections & was designated as PC2. In this type of connection two 16mm diameter bolts

were used, in which one bolt connects the cleat angle with the column and the other connects the cleat angle with both the beam and the corbel. Figure 2.2 shows the schematic representation of the isometric view of the precast beam-column connection using cleat angle. The cleat angle used for the connection is ISA100x100x10. The bolts used were high tensile friction grip bolts. The gap between the bolts and the groove was filled using iso-resin grouts.

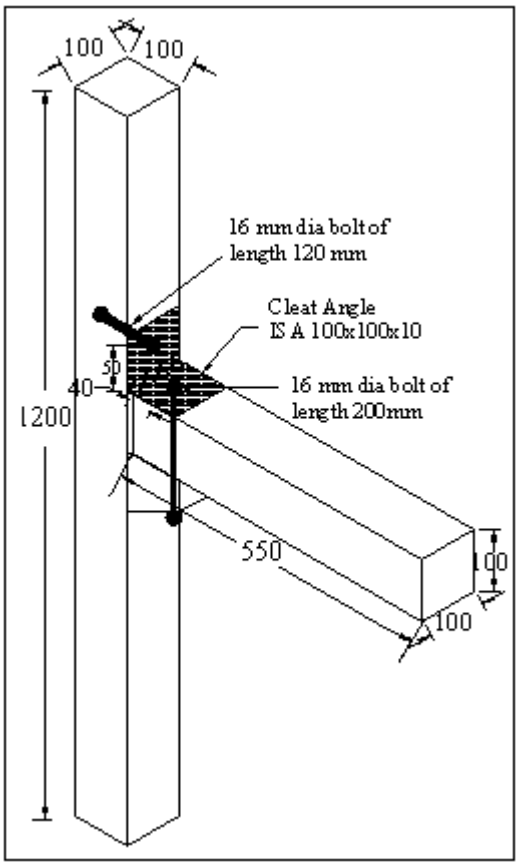

Fig. 2.2 Precast beam-column connection using cleat angle

The experiments were carried out on a loading frame of 2000kN capacity. A hydraulic jack was fixed to the loading frame for the application of the axial load along the axis of the column. Two hydraulic jacks were used to apply the reverse cyclic loading. Displacement controlled loading system was adopted. The specimens were tested in an upright position with column in vertical and beam in horizontal position. The column was hinged at floor and was laterally restrained at the top. The schematic representation of the experimental test setup is shown in Figure 2.3

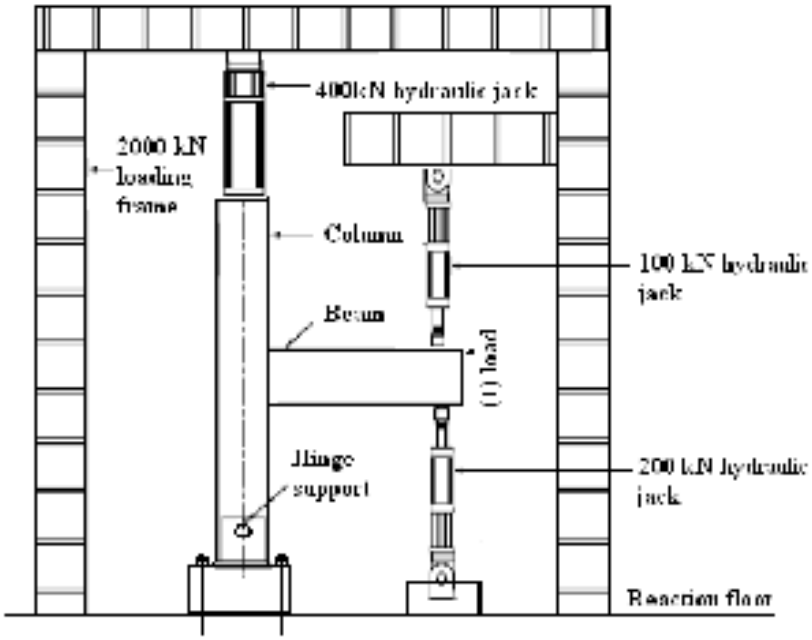

Fig. 2.3:- Schematic test setup(13)

Loading Sequences used in their investigation is as shown in table 2.1

Table 2.1: Displacement sequence for the displacement based loading of the specimens

Sl. No.	Displacement (mm)		Increment
	Start	End	
1	0.1	1.0	0.1
2	1.0	2.0	0.2
3	2.0	10.0	0.5
4	10.0	18.0	2.0
5	18.0	21.0	3.0
6	21.0	25.0	4.0
7	25.0	30.0	5.0

The following results & conclusions were obtained from their work :-

Strength :-The ultimate load carrying capacity of the specimen ML was found to be 11.29kN and11.75kN in positive and negative directions respectively. For the specimen PC1, the ultimate load carrying capacity was found to be 5.42kN and 4.57 kN in positive and negative directions respectively whereas for the specimen PC2, the ultimate load carrying capacity was found to be

4.33 kN and 3.58 kN in positive and negative directions respectively which is very much lesser than the monolithic specimen. From the results, it was observed that the load carrying capacity of the specimen PC1 was 51.99% and 61.11% lesser than the monolithic specimen in the positive and negative direction respectively. Similarly, the load carrying capacity of specimen PC2 was 61.65% and 69.53% lesser than the monolithic specimen in the positive and negative direction respectively. Out of the two precast specimens the specimen PC1 performed better than specimen PC2. While comparing with the precast specimens the monolithic specimen performed better in resisting the load.

Crack pattern :- All the specimens were subjected to reverse cyclic loading. For the specimen ML, the flexural crack initiated at the beam-column junction at 2 mm displacement cycle (5.13 kN) and propagated further. The flexural cracks in beams were initiated at 2.5 mm displacement cycle (6.15 kN) and were developed away from the beam-column junction. Shear cracks first occurred at the beam-column junction at 7 mm displacement cycle (9.92 kN) and cracks further propagated at 12 mm (10.61 kN), 15 mm (10.94 kN), 18 mm (10.95 kN), ±21 mm (11.29 kN), 25 mm (11.29 kN) displacement cycles. The failed monolithic specimen ML is shown in figure 2.4. For the specimen PC1, the first flexural crack initiated on the beam where the bolt had been fixed at 1.5 mm displacement cycle (2.7 kN). Further flexural cracks occurred at 3 mm (2.71 kN),-6 mm (3.09 kN), 8 mm (4.33 kN), and 18 mm (5.14 kN) displacement cycles. Cracks in the corbel occurred at 8 mm displacement cycle (4.33 kN) where the bolt had been fixed. Further cracks developed in the corbel at 18 mm displacement cycle (5.14 kN). All the cracks in the beam and corbel occurred at the position of J-bolt. No cracks were observed in the column except at the corbel region. The failed precast specimen PC1 is shown in figure 2.5**.** For the specimen PC2, the first flexural crack in the beam was initiated below the cleat angle at –2.5mm (3.64 kN) displacement cycle. Also flexural cracks occurs at –3mm (3.65 kN), –4 mm (4.18 kN), -7mm (4.56 kN),12 mm (2.01 kN) at the position where the recesses was provided for the bolt which connected the cleat angle with the column. Cracks occurred in the corbel at 1.4mm (2.7kN) displacement cycle and propagated at 2.5mm (217 kN) displacement cycle. Spalling of concrete was also observed at the position of bolts. The failed precast connection, PC2, is shown in figure 2.6**.**

Fig. 2.4 Failed monolithic specimen

Fig. 2.5. Failed J-bolt connection

Fig. 2.6. Failed cleat angle connection

Load displacement relationship :-The load-displacement relations for the monolithic and the precast specimens had been obtained from the test results and presented in figures 2.7, 2.8 and 2.9. The load displacement hysteresis curve of monolithic specimen ML shown in figure 2.7 exhibited similar load displacement pattern in both positive and negative directions. The strength and stiffness degradation has been observed only after 25mm displacement cycle. From figure 2.7 to 2.9 it is inferred that the energy dissipation in the positive direction is greater than that in the negative direction. This is because of the ductility offered by the J bolt. In the positive direction, strength degradation occurred beyond 18 mm displacement cycle whereas in the negative direction, the strength degradation occurred only beyond 25 mm displacement cycle. For monolithic and the two precast specimens the test was stopped after completion of 30 mm displacement cycles, as the strength dropped below 80 percent of ultimate strength in positive and negative displacement direction

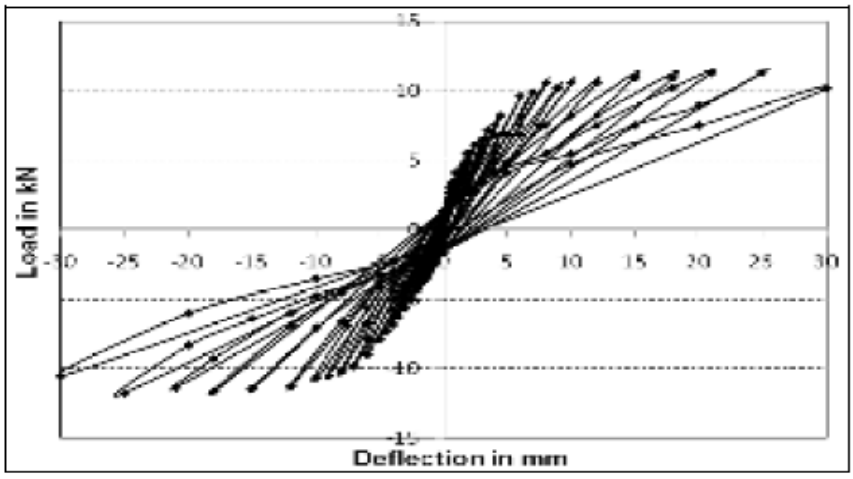

Fig. 2.7:-. Hysteresis curve for monolithic specimen ML

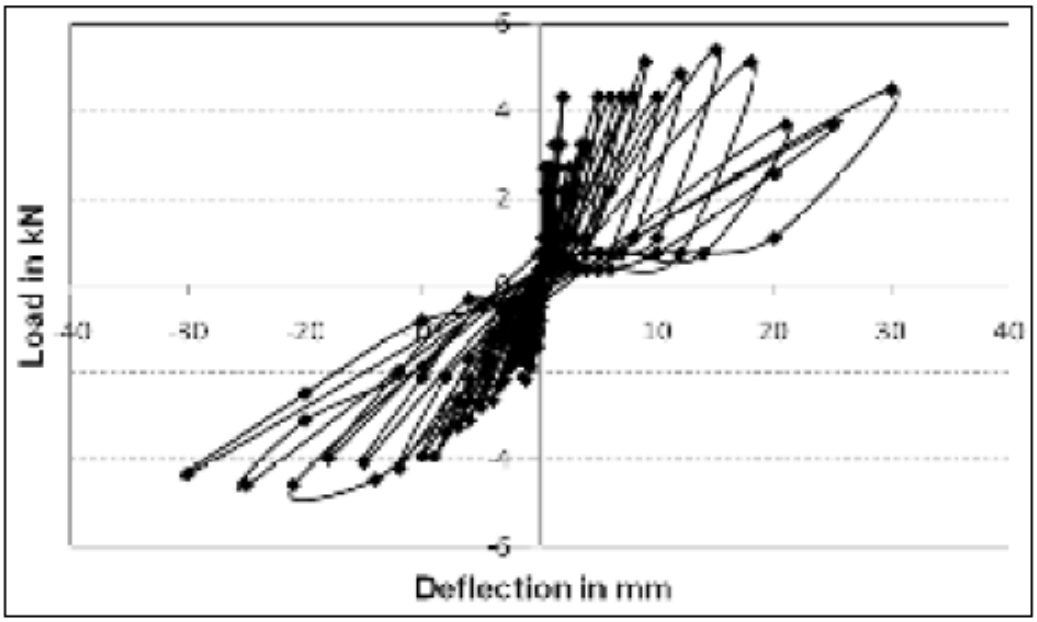

Fig. 2.8 :- Hysteresis curve for precast specimen PC1

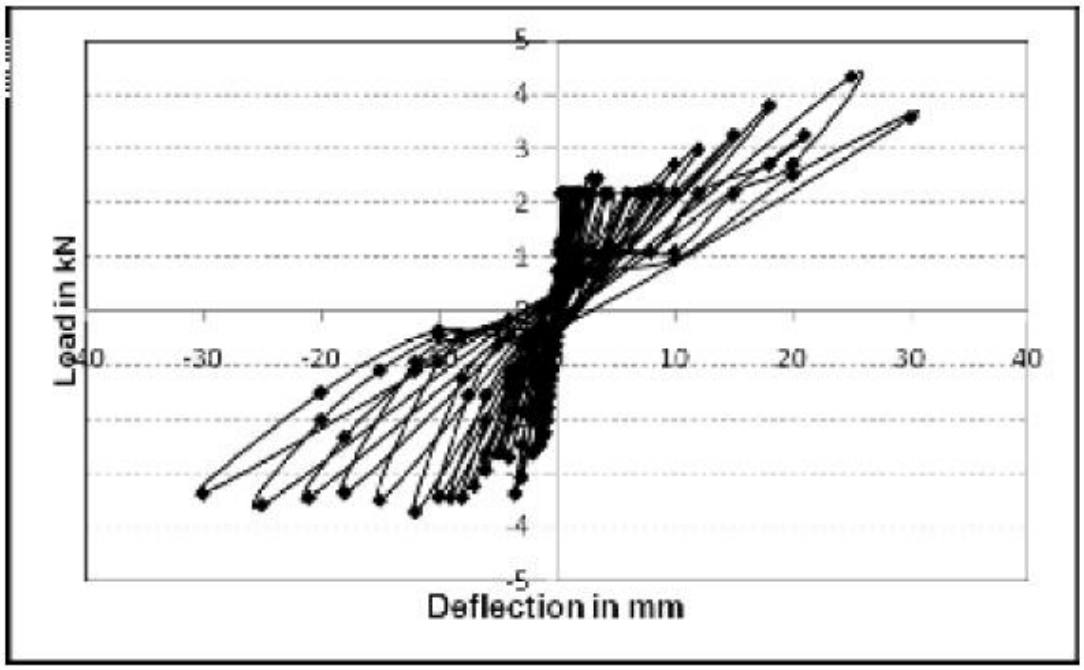

Fig. 2.9 :- Hysteresis curve for precast specimen PC2

Energy dissipation :- The area under the load displacement curve gives the energy dissipation of the specimen. Figure 2.10 shows the comparison of energy dissipation of the precast specimens with that of the monolithic specimen.

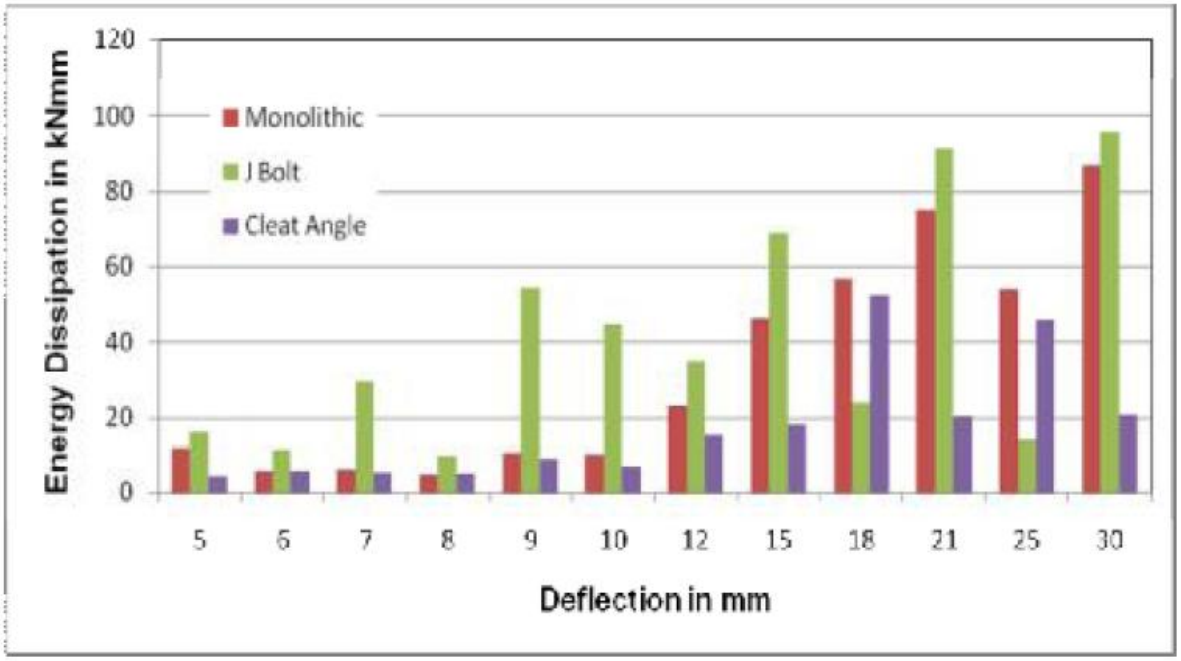

Fig. 2.10 :- Comparison of energy dissipation from 5mm to 30mm

It can be observed that the cumulative energy dissipation for the specimen PC1 was 22.87% greater than the ML connection whereas the energy dissipation for the specimen PC2 was 41.78% lesser than the monolithic connection. The specimen PC1 exhibits better performance because the J bolt is properly embedded within the concrete medium and provides sufficient ductility to the system.

Ductility :- The displacement ductility factor is determined as the ultimate displacement divided by the displacement at the occurrence of yielding of longitudinal steel bars. The ductility factor of the monolithic and precast specimens have been evaluated and given in Table 2.2

Table 2.2: Ductility factor of the three specimens

Specimen	Yield displacement	Ultimate displacement	Ductility factor
Monolithic	5	25	5
Precast (PC1)	1	18	18
Precast (PC2)	9	25	2.78

It can be observed from Table 2.2 that the displacement ductility of the specimen PC1 was found to be more than that of monolithic specimen. Hence the specimen PC1 is more ductile when compared to the specimen ML. As energy dissipation and ductility are the characteristics which make the structure perform better under seismic forces, the results

indicate that the precast specimen PC1 have favourable behaviour under seismic load whereas specimen PC2 does not have favorable behavior under seismic load.

From the results it was observed that the ultimate load carrying capacity of the monolithic specimen was more than the precast specimens PC1 and PC2. Precast specimen PC1 was more ductile and dissipates more energy compared to the monolithic specimen whereas precast specimen. PC2 was less ductile and dissipates less energy compared to the monolithic specimen. Precast specimens showed increased stiffness in the negative direction due to the presence of corbel. The bottom left reinforcement bar in the beam experiences the maximum strain due to the applied cyclic loading in the both the precast specimens. In precast connection, the column reinforcements were free from strains compared to that of monolithic connection.

2.3.2 Cyclic behaviour of precast RC connections (17)

Manoj K. Joshi, C.V.R. Murty and M. P. Jaisingh conducted a study aimed at identifying a suitable technique for connecting precast beam and column components at an exterior joint in moment resisting frames in high seismic areas. The study investigated two connection techniques; two precast and corresponding monolithic specimens were prepared and subjected to pseudo-static loading to investigate the effectiveness of the same. The properties of the specimens used in this work were as follows:-

Material characteristics :- OPC 43 grade cement from the same stock was used in all specimens. The grade of concrete used was M25 with a water cement ratio of 0.5 for the design mix. The 28-day average compressive strengths of the cubes of two monolithic specimens M1 and M2 were 28.1 MPa and 31.3 Mpa respectively, and those of the precast specimens P1 and P2 were 27.7 MPa and 32.4 MPa respectively. Reinforcement steel used in all the four specimens was of grade Fe 415; yield and ultimate strengths of 20 mm bars were 500 MPa and 630 MPa respectively, while those of 25 mm bars were 476 MPa and 641 MPa respectively.

Geometry and reinforcement detailing :- The specimens had a strong-column weak-beam configuration, and represented the exterior beam-column joint of the four-storey reinforced concrete building, Fig 2.11. The column portion was 2.6 m long with a 400 mm × 400 mm cross-section and the beam portion was 1.3 m long with a 300 mm × 400 mm cross-section. Two types of detailing were used in the specimens. In the first type of detailing a single U-bar is used as both top and bottom beam reinforcement, as in the specimens M1 and P1, Fig 2.12; here, letters M and P stand for monolithic and precast respectively. The other type of

detailing conforms to the Indian Standard code for ductile detailing of RC sections, as in the specimens M2, P2, Fig 2.13.

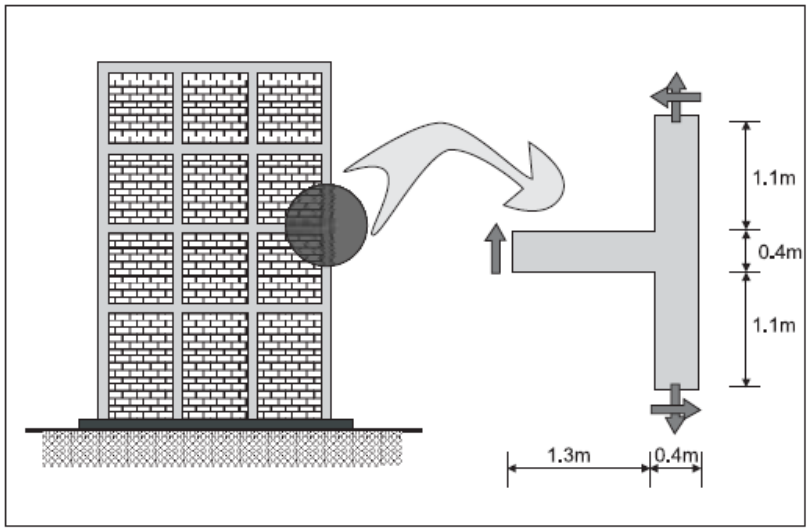

Fig.2.11 :- Exterior beam column sub. assemblage of an R.C. frame building, geometry and forces acting on it when it swings from right to left

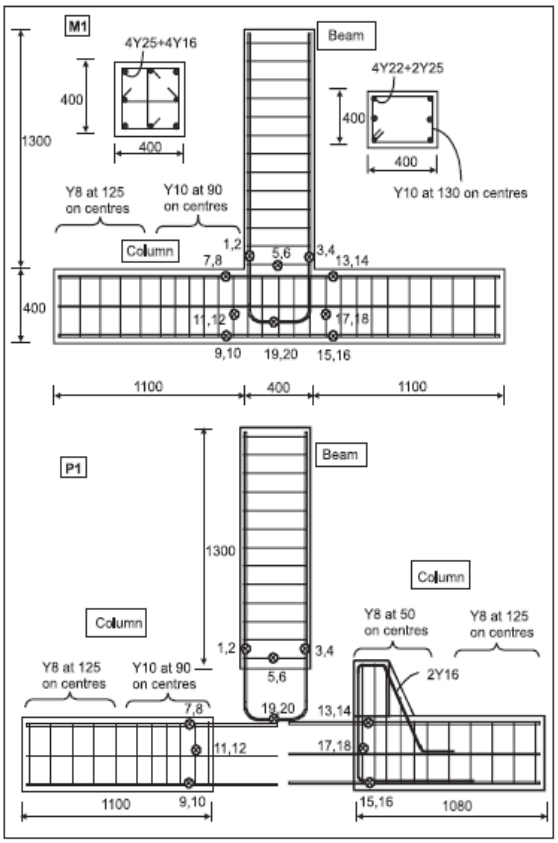

Fig. 2.12:- Details of geometry and reinforcements of the specimens M1 & P1.

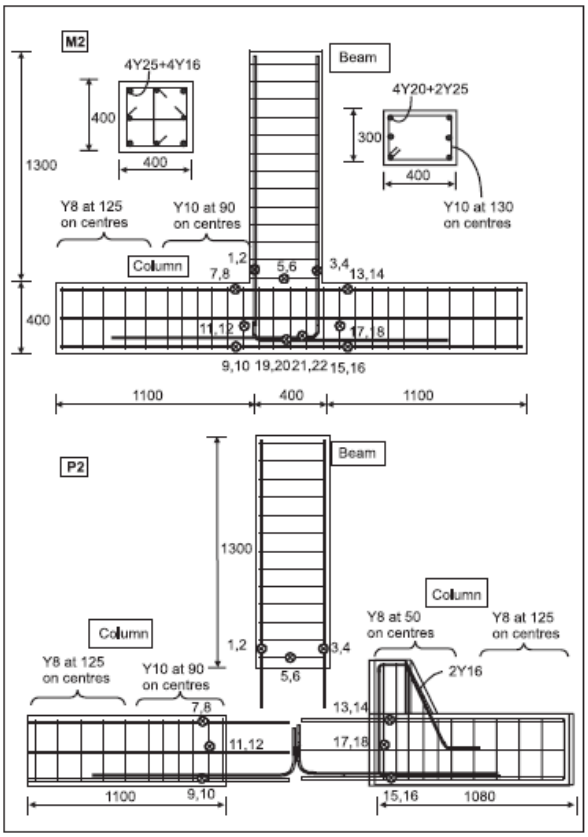

Fig. 2.13:- Details of geometry and reinforcements of the specimens M2 & P2.

The set up for the experimentation in this work is as shown in fig. 2.14 The specimens were loaded with the column stub horizontal and the beam stub vertical. The axial movement of the column was restrained at its ends by stiff supports fixed to the strong floor by steel studs. The ends of the column stub were supported by rollers equidistant from the beam centre. In specimen M1, plates were also provided along with the rollers to provide a larger bearing surface to the specimen. In the testing of precast specimen P1, the spacer piece of the collar arrangement was eliminated as it became unstable in the second cycle of 20 mm displacement. Also, the plates between the column stub and the strong floor at the location of rollers were eliminated that facilitated an increase in lever arm. This was necessary because during the testing of the precast specimen P1 the actuator load capacity of 250 kN was reached in the positive direction beyond 20 mm displacement cycle. An increased lever arm was expected to induce higher displacement under the same transverse load on the beam and with the same load capacity of the actuator.

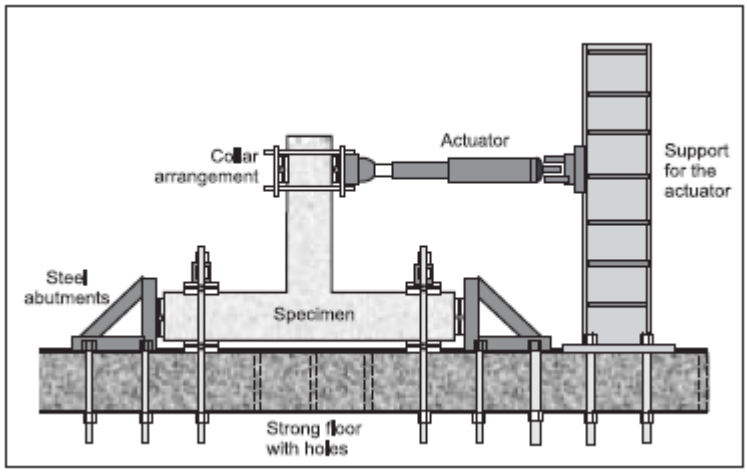

Fig. 2.14 :- Experimental setup used for cyclic loading of specimens.

The sub-assemblage specimens were subjected to cyclic displacement- controlled lateral loading applied at the end of the beam. A 250-kN capacity MTS hydraulic actuator with a displacement range of ± 150 mm was used. Two loading histories were adopted. The first one was used for the monolithic specimens. The loading history consisted of displacement cycles of ± 1, ±2, ±3, ±5, ±7.5, ±10, ±15, ±20,precast and corresponding monolithic specimens were prepared and subjected to pseudo-static loading to investigate the effectiveness of the same.

Displacements were measured in the specimen by LVDTs. LVDT 1 and LVDT 2 at the point of application of load in the positive and negative displacement directions. The

displacement at the actuator support was measured using LVDT7. LVDTs 3, 4 and 5 were used to measure the displacement at locations along the beam.

As the testing of the precast specimen P1 was conducted in two stages with the load applied at different levels in both the experiments, LVDT 8 and LVDT 9 were added to measure the response at the earlier load application level. LVDT1 and LVDT2 were used to measure the displacement at the new point of application of the load. Strain gauges were pasted on longitudinal and shear reinforcements for measuring strains in them at the probable plastic hinge sections.

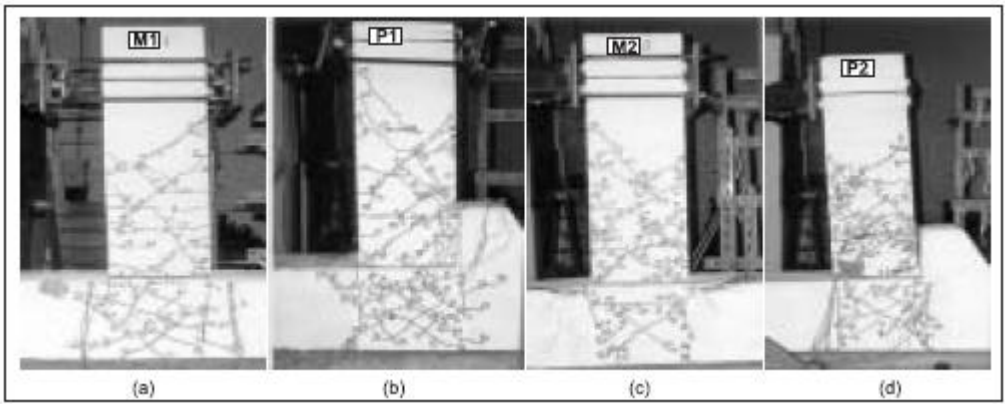

Fig. 2.15:- Crack patterns of the four specimens at the end of displacement loading

The various observations made during the cyclic loading of the specimens were as follows. The diagrams of crack patterns observed in the various specimens at the end of the experiment are shown in Fig 2.15. For both specimens M1 and P1, the first flexural cracks appeared in the 3 mm-displacement cycle at the junction of the beam and the column. The first crack runs across the full depth of the beam for the specimen M1. Flexural cracks in the beam away from the beam column junction were also observed in the 5 mm, 7.5 mm and 10 mm displacement cycles for both the specimens. For the specimen P1, flexural cracks also appeared in the 25 mm and 30 mm displacement cycles. The first shear crack appeared in the 10 mm displacement cycle for both the specimens in both the beam and the joint regions.

For both specimens M2 and P2, the first crack develops in the 2 mm displacement cycle with the crack forming at the junction of beam and column for M2 and at the junction of the beam and the corbel for P2 respectively. Flexural cracks also appear in the beam in displacement cycles of 5 mm, 15 mm and 25 mm for specimen M2. For specimen P2, additional flexural cracks appear in the beam in displacement cycles of 7.5 mm, 10 mm and

15 mm. The first shear crack in the beam appears in the 7.5 mm displacement cycle for the specimen M2, and in the 5 mm displacement cycle for the specimen P2.

The various results obtained from this work were :-

Hysteresis loops :-

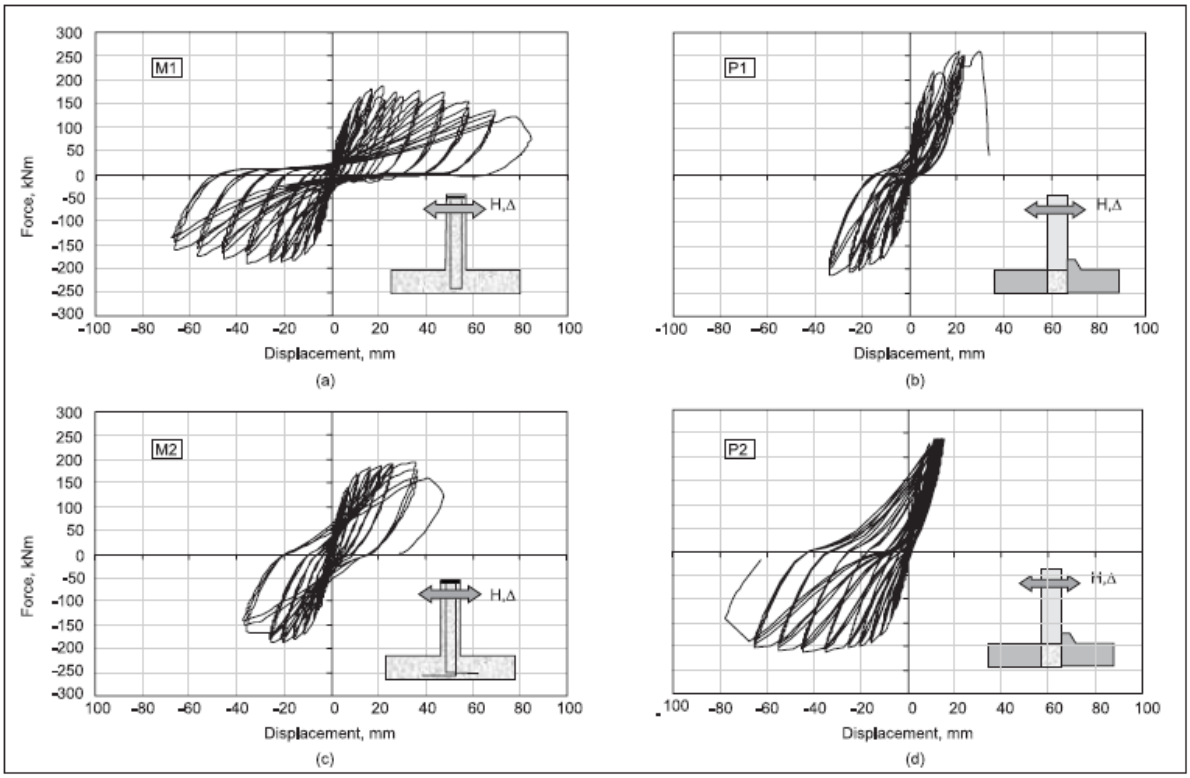

Fig. 2.16 :- Hysteresis loops of the four specimens studied.

The load-displacement hysteresis loops for the three cycles of loading at each displacement excursion level are shown in Fig 2.16. Maximum pinching was observed for the specimen M1, with predominant bond and shear failure in the joint region. Bond failure of U-shaped beam reinforcement and concrete in the joint occurred at the maximum displacement excursion level in the displacement cycles of 40 mm. This was accompanied by a steady degradation in strength.

Both the precast specimens, P1 and P2, showed increased stiffness in the direction of positive displacement due to the presence of corbels. Pinching was less compared to M1. Both the specimens show extensive flexural and shear cracking in beam with spalling of beam concrete at the column face for specimen P2. Only for the specimen P2, sliding of RC beam was observed along the through flexural crack at the face of the corbel. Longitudinal

bar in the beam snapped, causing failure in the first cycle of 50 mm displacement for P1 and in the first cycle of 90 mm displacement for P2.

Specimen M2 exhibited fat hysteresis loops with very less pinching, due to good bonding between reinforcement and joint concrete. Shear cracks were also very few in the joint region. The cause of failure was the snapping of longitudinal beam bar in the first cycle of 50 mm displacement.

The comparisons of the results of the all specimens in this work shows that in all the four specimens, the displacement controlled loading was not applied at the same location in the beam. Hence, to compare the overall behaviour of the specimens, the hysteresis loops were derived for moment in the beam at the face of the column as function of transverse displacement applied at the end of the beam. The calculated flexural strength of the beam is 157.03 kN-m, while calculated over strength is 15 percent. The specimens were compared for the different observed and calculated characteristics.

Comparison of specimen M1 and M2 :-

(i) The pinching in hysteresis loops of the specimen M1 reflects predominant shear and bond failure, also corroborated by shear cracking in the joint, the gap between beam and column at the face of column, and the sub-yield strains in the longitudinal beam reinforcement. The relatively fat and stable loops of specimen M2 reflect predominant flexural failure, which is evident from the fewer shear cracks in the joint and snapping of beam reinforcement bar at failure.

(ii) The strength achieved in specimen M2, exceeds that obtained for the specimen M1. The strength and stiffness degradations in the second and third cycles for most displacement excursion levels, are higher for M1 compared to M2

(iii) The cumulative energy dissipation for specimen M1 is more than that of specimen M2 after the 30 mm displacement cycles due to pinching in the hysteresis loops of M1.

Comparison of specimens M1 and P1

(i) Although the crack patterns extending into the columns in the joint region, are similar for both the specimens, the hysteresis loops of M1 show more pinching. The specimen P1 failed with the snapping of longitudinal reinforcement bar in the beam, while for specimen M1, failure is marked by the strength dropping below 80 percent in the post-ultimate response.

(ii) The ultimate strengths of both the specimens in the positive direction are nearly same, while in the negative direction, P1 has 11 percent more strength.

(iii) At low displacement levels, the specimen P1 hashigher average strength and stiffness deterioration than the specimen M1.

(iv) The cumulative energy dissipated by the M1 is higher than that of P1 except at low displacement excursions. The energy dissipated by P1 may have been higher if the displacement in the positive direction was not restricted by the limitation in the force capacity of the actuator.

(v) Specimen M1 has a displacement ductility much higher than that of P1. The yield displacement of specimen M1 is nearly equal in both the directions, while in the specimen P1 the yield displacement in the positive direction is smaller than that of negative direction, because of higher stiffness due to corbel

Comparison of specimen M2 and P2

(i) At higher displacement cycles, the specimen M2 has stable hysteresis loops than P2.

(ii) In the negative loading direction, P2 shows 12 percent higher strength than specimen M2. In the positive direction, P2 could not be loaded to its ultimate strength due to the restriction of applied displacement; thus it shows lower strength than M2 in that direction.

(iii) At low displacement level, M2 has less stiffness degradation than P2, while at higher displacement levels, the stiffness degradation increases for M2.

(iv) For both the specimens, maximum energy dissipated in the first cycle is the same. Till the 40 mm displacement cycle, which is the last displacement cycle sustained by M2, the cumulative energy dissipated by M2 is about 35 percent higher than specimen P2. However, at failure, the cumulative energy dissipated by specimen P2 is about 75 percent higher than specimen M2.

Comparison of specimen P1 and P2

(i) The hysteresis loops for specimen P2 show less pinching than those of specimen P1. Both specimensfail with the snapping of longitudinal beam bars. The damage in the specimen P2 is mostly concentrated in the beam with a few shear cracks in the joint, whereas in specimen P1, there is extensive shear cracking in the joint. In specimen P2, sliding of the beam takes place in higher displacement cycles, along the flexural crack at the face of the corbel, which does not occur in specimen P1.

(ii) The specimen P2 has marginally higher strength than the specimen P1 in both the directions. Strength and stiffness deterioration are greater in specimen P1 for both repeat cycles.

(iii) Till the maximum displacement cycle for P1, the cumulative energy dissipated by specimen P1 is about more than that of P2. But the maximum cumulative energy dissipated at failure by P2 is about 60 percent higher than that at its failure by P1. The displacement ductility factor achieved by the specimen P2 is about 32 percent higher than P1.

The following conclusions were drawn from this study :-

(i) The monolithic specimen with beam bars anchored into the column performed better than the monolithic specimen with continuous U-bars as beam reinforcement.

(ii) The precast specimen with continuous U-bars as beam reinforcement performed worse than the corresponding monolithic specimen. This is attributed to the sliding of the beam stub at the interface with the beam-column joint, which was absent in the monolithic specimen.

(iii) Of the two precast specimens, the one with beam bars anchored into the column with welding of the lap splices performed better than the one with continuous U-bars as beam reinforcement.

2.3.3 Connections Behavior in Precast Concrete Structures Due to Seismic Loading (18)

Ehsan Noroozinejad Farsangi, 2010 (18) conducted a finite element analysis on 4 types of precast connections which were pinned, rigid, semi rigid and a new proposed connection. The stiffness of the new connection in his work was obtained from the slope of the total load versus deflection graph in the elastic range. Then the seismic loading from El Centro earthquake modified with 0.15g and 0.5g was applied to the whole structure. From the analysis results, it was found that new connection has sufficient stiffness, strength and also higher ductility. The whole structure analysis results showed that the new connection behaves as semi rigid connection. LUSAS and SAP2000 were used for analysis.

In this study investigator used plane stress theory in FE analysis for simplification of the modeling. Although, it is probable that plane-stress formulation can not reflect the exact behavior, but can give results with a good accuracy. A plane stress is subjected with stress at two directions and it is suitable to thin element such as beam and column body. This means that there is no zero stress at z direction.

Proposed connection**:-** The geometry and dimension of typical connection from experiment and proposed new connection used in his work are shown in figures 2.17 and 2.18

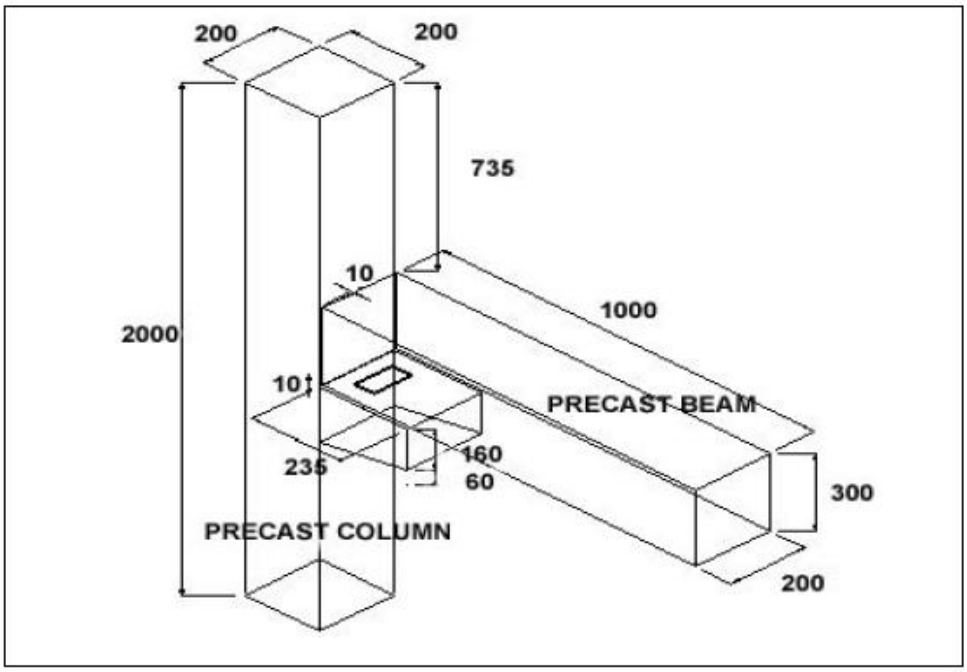

Figure 2.17:- Experimental Connection

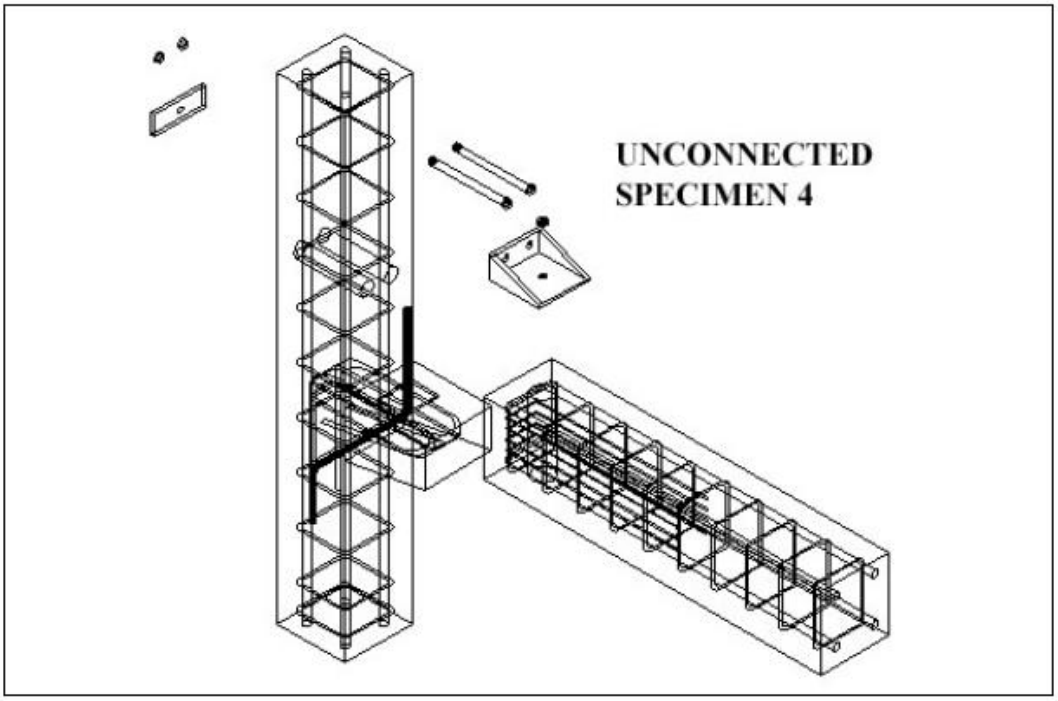

Figure 2.18 :- Proposed new connection

STRUCTURAL MODELING (SAP2000):- In this investigation 3 dimensional frame consisting of 2 x 3 bays was loaded with dead load 4kN/m_2 and live load 2.5kN/m_2. The length and width of the frame were 6m and 3m respectively. Besides, the column height was 3m. The frame was analyzed without any bracing. This frame was then compared with pin jointed frames and fixed frames.

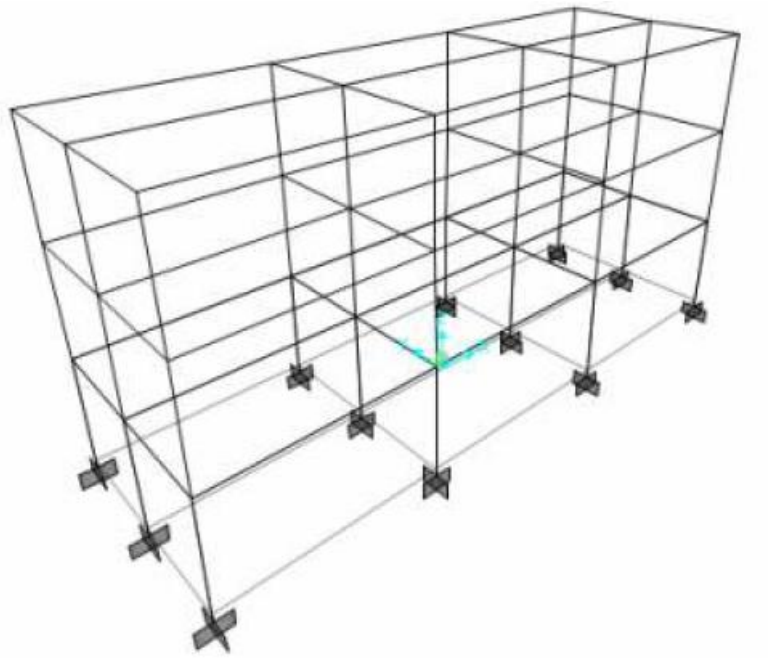

Figure 2.19 :- 3 Storey 3 Dimensional Frame (SAP2000)

Figure 2.19 shows the three storey frame used for F.E. analysis in his work. The dead load and live load were distributed along the 6m length main span as the slab spans in one direction. The end column was fully fixed. Besides that, seismic load for linear time history analysis was introduced on the frames. The time history loading was El Centro and amplifies with 0.15g and 0.50g.

Finite element modeling (LUSAS):- Finite element models used in this work are shown in Figures 2.20 to 2.23. The geometry for column, beam and corbel was same for all the models either it is new or it is old. In this paper, column, beam, dowel, plate, stiffener and bolt were assigned with plane stress because they were subjected by two forces in two directions which were x-direction and y direction. Since the reinforcement bar was subjected by x direction only, the reinforcement was modeled as bar element.

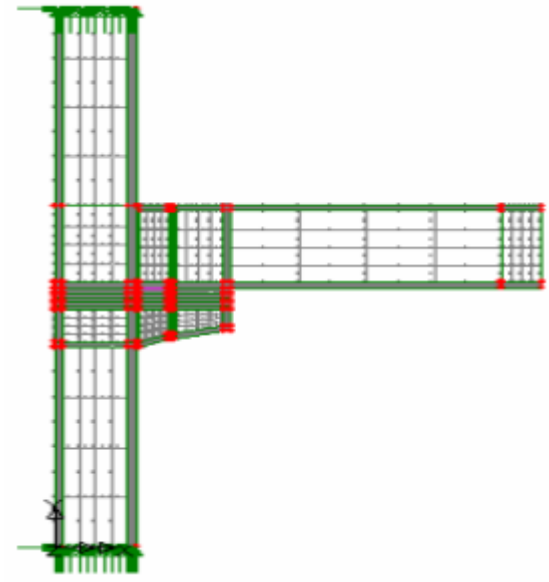

Figure 2.20:- Corbel Only Model

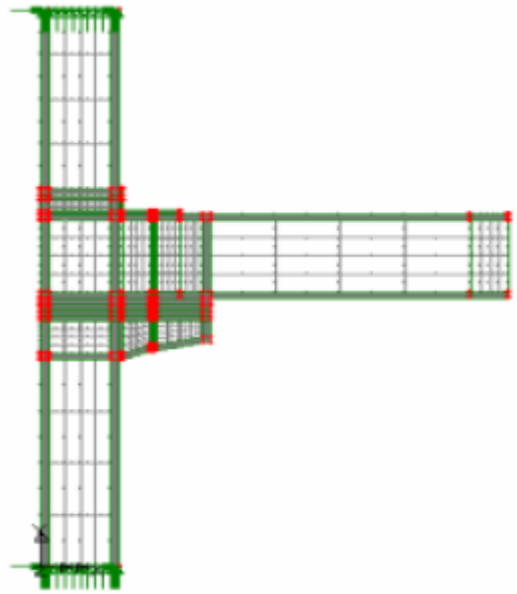

Figure 2.21 :- Corbel + Plate and Bolt on beam Top Model

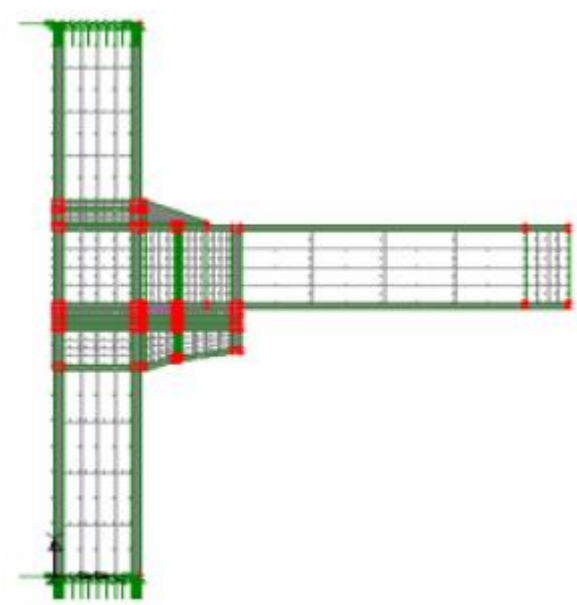

Figure 2.22 :- Corbel+ Plate and Bolt on Beam Top + Stiffener

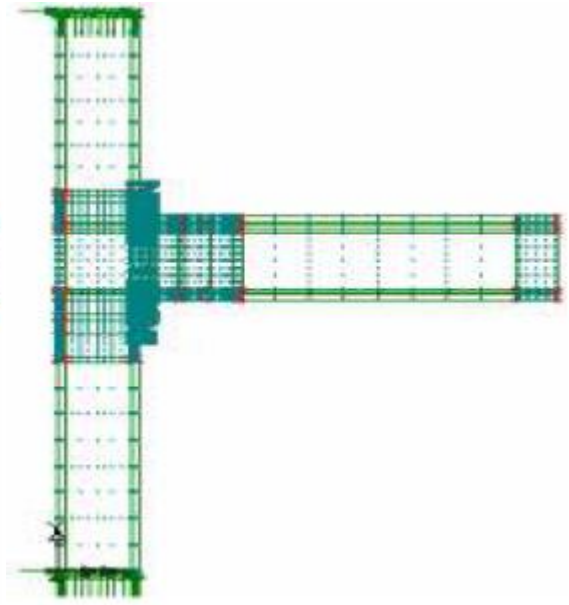

Figure 2.23 : New Connection Plate 10mm and Bolt 22mm

The corbel acts as a support for the beam and the whole connection strength depends on the corbel. This could be proven when shear cracks occur at the corbel. The experimental connection strength depends mainly on the interaction of the plate and bolt**.** The main reason was shear cracks happen at the plate and bolt area on top of the beam. Therefore, the new connection was modeled to fully utilize the bolt and concrete interaction. When the bolt was embedded in the concrete, it was pulled out by the beam which was loaded by a point load until yields.

Analysis and results:- The finite element models starts to crack when the tensile strength of the concrete was exceeded. In Figures 2.24 to 2.27 the cracks pattern are shown according to FE analysis, the red lines represent tensile cracks while the blue lines mean the compressive cracks.

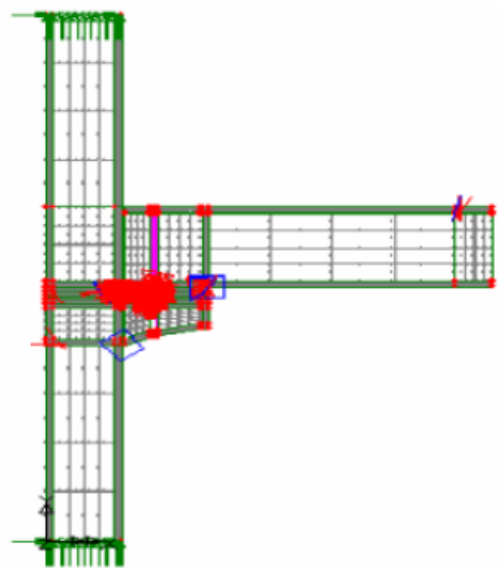

Figure 2.24 :- Crack Location for Corbel Only

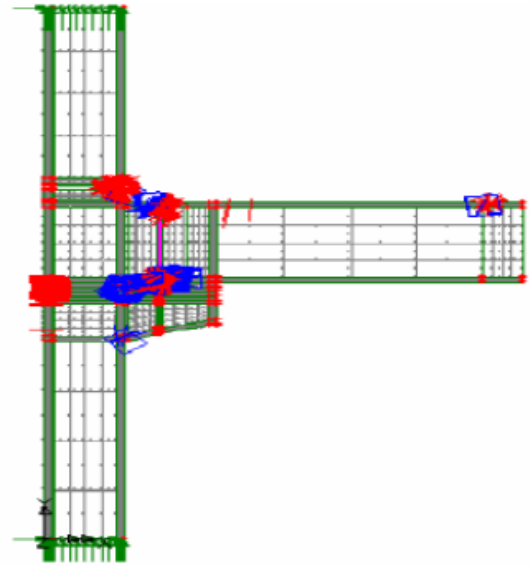

Figure 2.25 :- Crack Location for Corbel +Plate

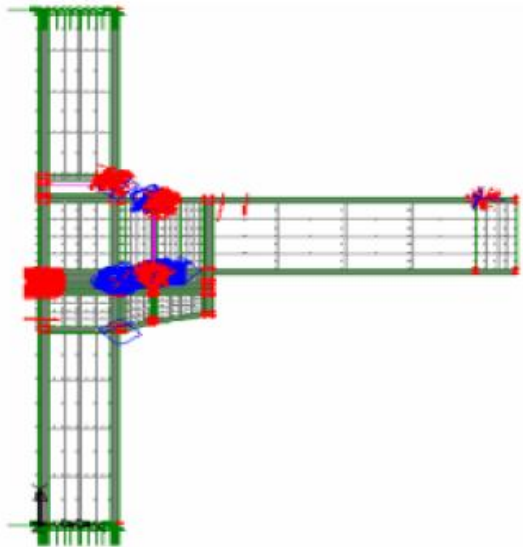

Figure 2.26 :- Crack Location for Corbel + Plate + Stiffener

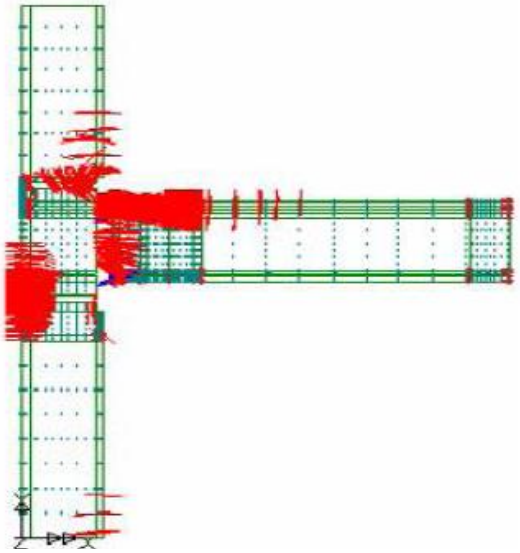

Figure 2.27 :- Crack Location for New Connection

Modal analysis results for seismic intensity loads 0.15g and 0.50g are shown in Table 3. The frequency for each model is almost the same with different load intensities. There were some discrepancies for the frequency because of the modeling error such as member size. Pinned connection frame has the lowest frequency and the value for 0.15g is 0.11 Hz. The highest frequency was for the fixed connection which is 0.40 Hz for 0.15g. In 0.50g, the lowest and highest frequency also happens in pinned and fixed connections respectively

Table 2.3: Modal Analysis Results for Seismic Intensity Load 0.15g and 0.5g

0.15g			.5g		
Connection	Period (s)	Frequency(Hz)	Connection	Period (s)	Frequency(Hz)
Pinned	*10.52*	*0.11*	Pinned	*12.90*	*0.09*
Semi-Rigid	*4.23*	*0.24*	Semi-Rigid	*4.37*	*0.23*
Rigid	*2.57*	*0.40*	Rigid	*2.25*	*0.39*
New Connection	*3.81*	*0.26*	New Connection	*3.92*	*0.22*

According to SAP2000 outputs the 0.50g seismic load intensity causes the highest moment in beam to column connections. The comparison between different types of connection in terms of maximum moment and shear is shown in Table 4.

Table 2.4: Maximum Moment and Shear according to Static and Seismic loading

Moment (kN.m)			Shear (kN)		
Connection	Static	Seismic	Connection	Static	Seismic
Pinned	*95.6*	*0*	Pinned	*63*	*0*
Semi-Rigid	*86.3*	*12.7*	Semi-Rigid	*63*	*5.2*
Rigid	*73.1*	*22.3*	Rigid	*63*	*9.3*
New Connection	*69.4*	*11.5*	New Connection	*63*	*4.4*

The frame analysis results show that the beam capacity was sufficient to sustain both shear and moment force for all types of connection stiffness. However, the column for fixed and pinned connections fails for both moment and shear forces. Also from the analysis results, the connection stiffness does have an effect on the moment and shear capacities of members. When the connection stiffness increases, the members such as columns and beams sustain heavier load that may lead to failure in the end. For pinned connection frames, the seismic forces were very low and do not tends to fail the structure. In reality, this type of connection may fail due to instability. From the frame analysis in this investigation it was found that, the connection stiffness does have a significant effect to the frame member for moment and shear forces under linear time history loading.

2.3.4 Performance of a precast concrete beam-to-beam connection subject to reversed cyclic loading (19)

Hasan Husnu Korkmaz. et, al (19) performed one phase of an extensive research program focusing on the seismic behaviour of precast connections carried out in Middle East Technical University. The primary objective of the research program was to observe and investigate the seismic behaviour of the connection detail proposed by the collaborating company and the specimens with improved details, in order to develop a "moment resisting precast concrete beam-to-beam connection". In this study, six beam–beam connection

subassemblies were tested under reversed cyclic loading simulating severe earthquake action. The first specimen was a monolithic specimen used as a reference specimen and tested to define the reference behaviour. The second specimen was a precast specimen, which was detailed by a company specializing in precast concrete production. The remaining specimens were modified according to the results of the formerly tested specimens. All of the specimens were identical in dimensions. All test specimens were 1⁄2.5 scaled models of the improved connection details used in the highly critical earthquake zones. The behaviour of the precast members was compared with that of the reference one and with the others.

Test specimens:- The study presented here was conducted to develop a moment-resisting precast concrete connection that can be used in seismic regions. The construction detail used for the investigation consisted of a middle precast beam, which was placed on the cantilever beams. These cantilever beams were extended from columns of the structure (Fig. 2.28). Within the connection region, the top reinforcement was continued by lap splicing. Bottom reinforcement was continued by welding the two steel plates together which were anchored to the bottom of the middle and cantilever beams. The first specimen (MR1), cast monolithically, was assigned as the reference specimen, designed for comparison purposes to figure out the reference behaviour. The second tested specimen (PO1) was the original precast specimen designed and detailed for this investigation. The other four specimens had several improvements as compared to the specimen PO1. These improvements were implemented with the observation of the deficiencies in each specimen at successive tests. Various modification alternatives have been carried out until the connection design attained almost the same capacity with the monolithic connection displaying a stable behaviour with sufficient ductility and energy dissipation rate.

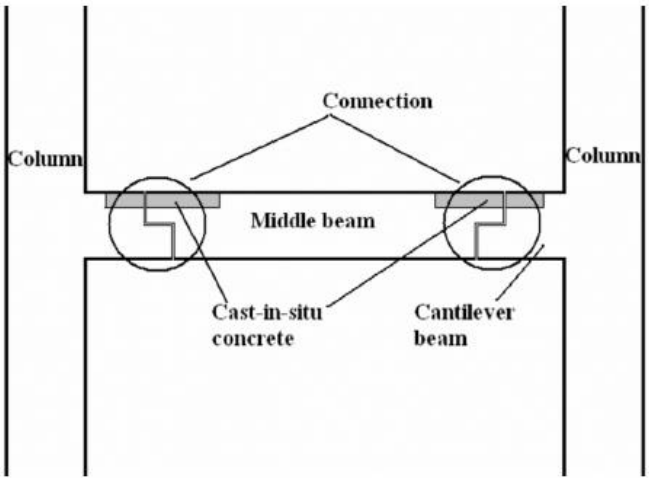

Fig. 2.28 Precast frame and connection under study.

The test specimens were manufactured so the beams would be terminated near the zero moment regions. The middle part of the beam was located on the cantilever beam, which was extending from the column. After connecting the middle beam and cantilever beam reinforcements together, cast-in-situ concrete was placed. For the top reinforcement connection, two alternatives were considered; (a) lap spliced and (b) welded. The precast members were prepared in the factory and connected to each other under the similar conditions experienced at the construction site. Since this connection type can be classified as a beam to beam connection, the test specimens did not contain a column. The test beam was extended from a central block which was rigidly fixed to the strong floor of the laboratory. The central blocks contained two model beams on either side. The test beams were a model of prototype members with a 1/2.5 scaling. The dimensions and reinforcement detail of the specimens is shown in Fig. 2.29.

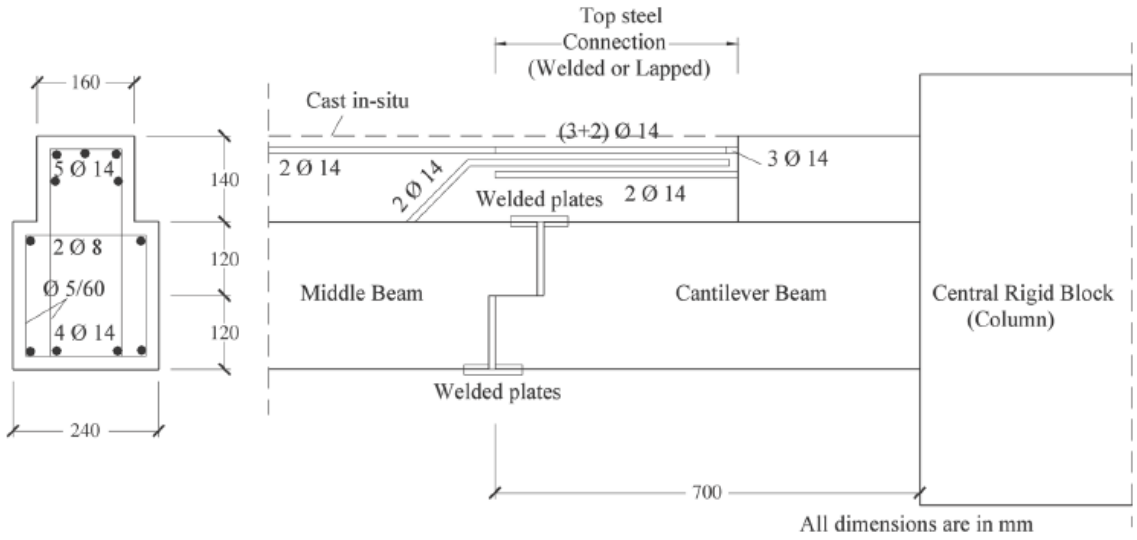

Fig. 2.29: Dimensions and reinforcement details of the specimen.

The precast middle beam and cantilever beam were 1 and 0.7 m long respectively. After placing the middle beam on the cantilever beam, the top and bottom reinforcement bars of both members were connected to each other. As mentioned before, the top reinforcement connections were made either by lap splicing or welding. So as to connect the bottom reinforcement bars, two rectangular steel plates were anchored at the bottom of both beam ends. Those plates were connected to each other by welding three steel bars. After connecting the beam reinforcement, cast-in-situ concrete was placed. This way, a section of 140 mm × 160 mm was added to the previous section.

Loading:- The cyclic loading was applied at the tip of the beam. The distance between the applied load and central block was chosen so that the shear force–bending moment relationship was the same as in the prototype. Various properties of the test specimens are listed in Table 2.5 in a manner suitable for comparison.

Table 2.5: Properties of test specimens

Specimen	Longitudinal steel		Top steel connection		Bottom steel connection		
	Top	Bottom	Type	Length	Bars	Weld length	Weld plate anchorage
MR1	4ϕ14 ($\rho \cong 0.015$)	2ϕ14	Continuos				
PO1	4ϕ14	2ϕ14	Lapped	390 mm (28ϕ)	3ϕ10	35 mm	3 × 2ϕ8 (L = 400 mm)
PM1	4ϕ14	2ϕ14	Welded		3ϕ10	60 mm	3 × 2ϕ8 (L = 400 mm)
PM2	4ϕ14	2ϕ14	Lapped	660 mm (47ϕ)	3ϕ10	60 mm	3 × 2ϕ8 (L = 400 mm)
PM3	4ϕ16 ($\rho \cong 0.020$)	2ϕ16	Welded		3ϕ16	60 mm	3 × 2ϕ12 (L = 500 mm)
PM4	4ϕ14	2ϕ14	Lapped	660 mm (47ϕ)	3ϕ14	60 mm	3 × 2ϕ10 (L = 400 mm)

1) Monolithic specimen (MR1) :- The monolithic specimen, MR1, was designed for comparison purposes and did not contain a precast connection.
2) Precast original specimen (PO1) :- The precast specimen, PO1, was designed with a purpose of investigating the behaviour initially. In specimen PO1, where the top bars were lap spliced, premature failure was observed due to rapid anchorage deterioration in the lap splice. Thus it is deduced that the lap splice length and the bottom beam-to-beam connection detail were unsatisfactory. Contrary to the expectations, significant deformation and hinging formed in the connection region rather than the root region where maximum moment values were foreseen.

Details of the other test specimens are shown in table 2.5.

Test procedure:-

Instrumentation:- The instrumentation consisted of five linear voltage differential transformers (LVDT) and seven electronic dial gauges of various ranges. A schematic illustration and entitling of instruments are given in Fig. 2.30 a, b & c.

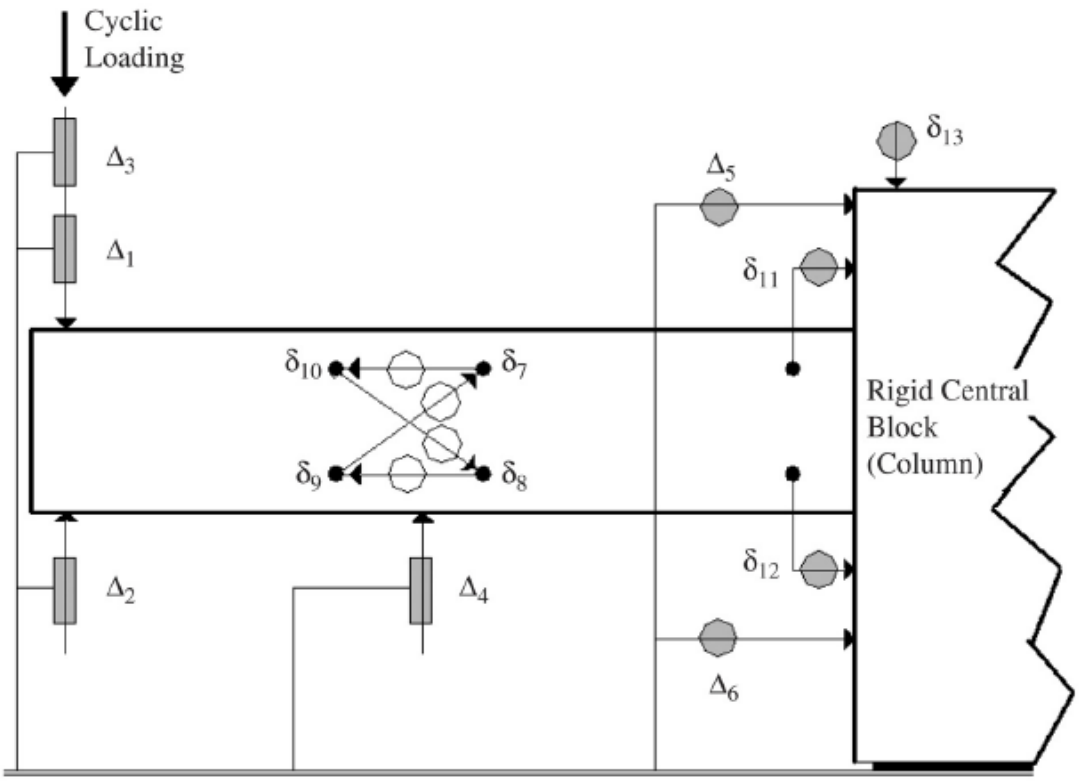

Fig. 2.30 (a) Schematic illustration and numbering of instruments.

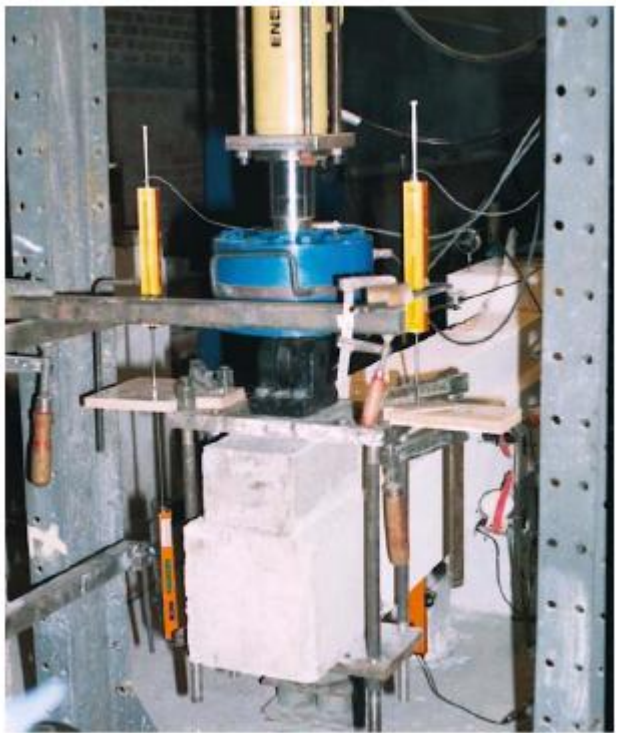

Fig. 2.30 (b) Loading system (18)

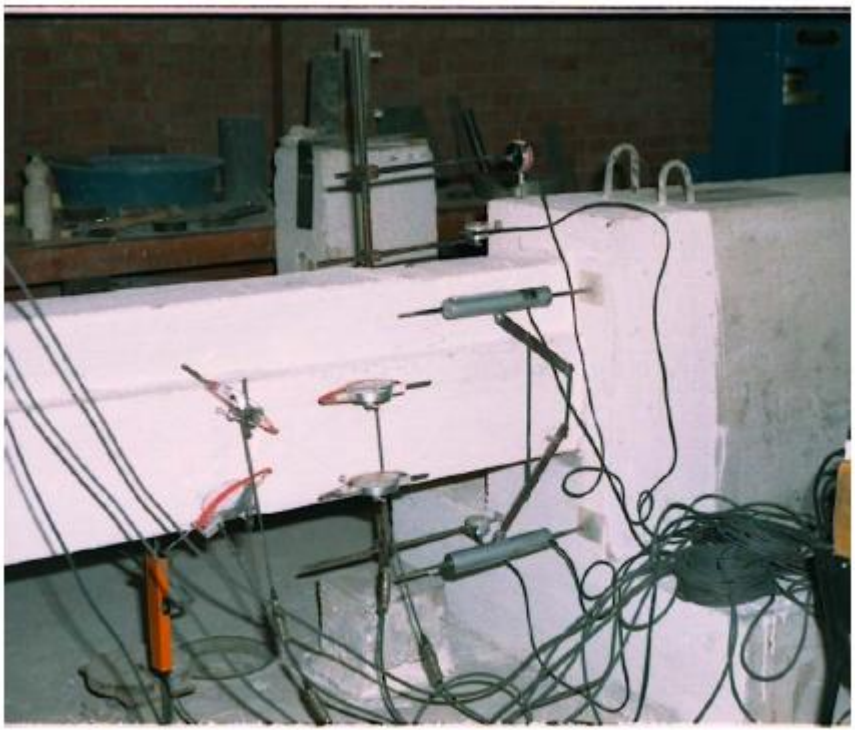

Fig. 2.30 (c) Strain gauges for radings at connection and root regions

The measured quantities throughout the experiments were the tip deflection of the beam, rotations of the beam root and the connection, shear deformations, and the rigid body rotation and translation. All of the measurement devices were connected to a digital data acquisition system, transmitting the outputs to a personal computer in digital form. The readings $\Delta 1$, $\Delta 2$ and $\Delta 3$ correspond to the measurements for tip deflection; $\Delta 5$ and $\Delta 6$ represent the measurements used to calculate the rigid body rotation. Also $\delta 13$ was used to calculate the rigid body translation. The readings $\delta 11$ and $\delta 12$ were used to determine the end rotations of the beam. The readings $\delta 9$, $\delta 10$ provided information about the shear deformation in the connection zone. Also flexural rotations and curvatures were computed by using the readings taken from $\delta 7$ and $\delta 8$.

The loading was applied according to the predefined loading history and displacement controlled. In the first cycle, loading was continuously applied in the elastic range and named the elastic cycle. In the second cycle, the specimen was loaded up to yield displacement. Estimation of the yield point necessitated some engineering judgement. Indicators of yielding in reinforcements followed by degradation in the stiffness are some clues for the designation of yielding point. The yield cycle was followed by inelastic cycles, imposing displacements that are multiples of the yield displacement.

Evaluation of test results :-In Fig. 2.31 the applied load versus net tip deflection curves and also in Fig 2.32 envelope load versus net tip deflection curves are presented. These envelope curves were obtained by connecting peak points of hysteresis curves of each cycle. From these curves one can see that the load carrying capacity of the monolithic reference specimen MR1 is the highest and that of the precast specimen with the original connection detail, PO1, is the lowest

The net tip deflection *(Δ*Net*)* consists of three components: namely the deflection due to shear *(Δ*shear*)*, deflection due to flexure *(Δ*flex*)*, and deflection due to the end rotation of the beam at the face of the column *(Δ*endrot*)*. These components were calculated by using Eqs. (1) and (2).

Δflex = ΔNet − Δendrot − Δshear **(equ. 1)**

$$\Delta_{\text{endrot}} = \left(\tan^{-1}\left(\frac{\delta_{11}+\delta_{12}}{H_{11,12}}\right)\right).L_{\text{beam}}$$

(equ. 2)

where δ_{11} and δ_{12} are the measurements obtained from dial gauges 11 and 12, $H_{11,12}$ is the distance between dial gauges 11 and 12. Obtained shear strain was assumed to be constant along the beam.

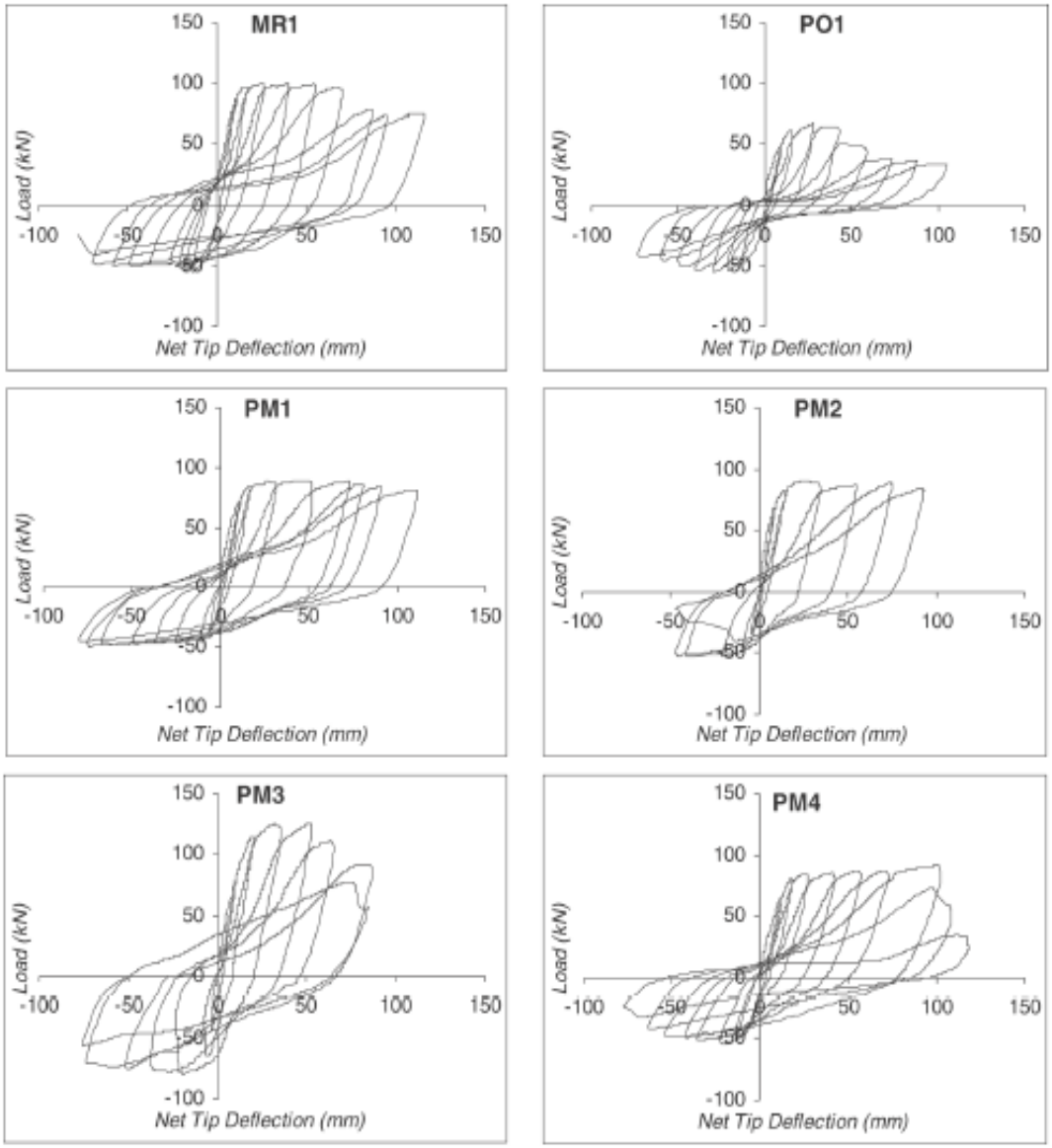

Figure: 2.31 Load–tip deflection curves of specimens.

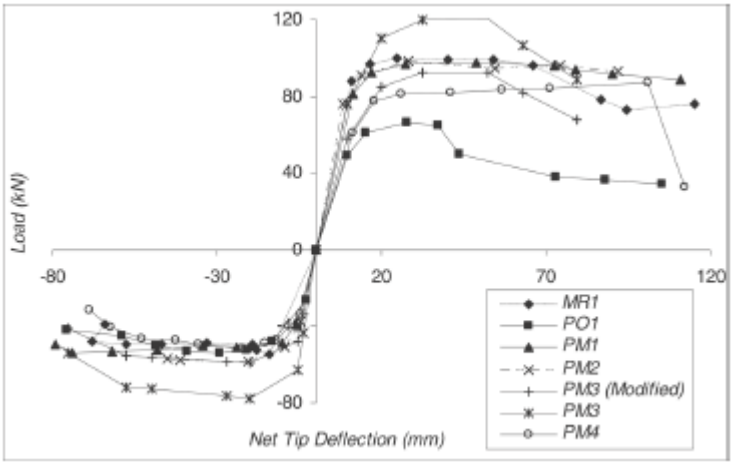

Figure: 2.32 Envelope load versus tip deflection (normalized) curves.

The obtained moment–curvature curves of the specimens for the connection region and the root region are shown in Figs.2.33 and 2.34, respectively. For specimen MR1 the major part of the deformation took place in the root region. On the other hand for specimen PO1 the major part of the deformation took place in the connection region. The ideal behaviour was seen in MR1. The behaviour of PO1 was the worst among the others. Since the maximum moment was observed in the root region, it is highly expected to form the most significant damage in this region.

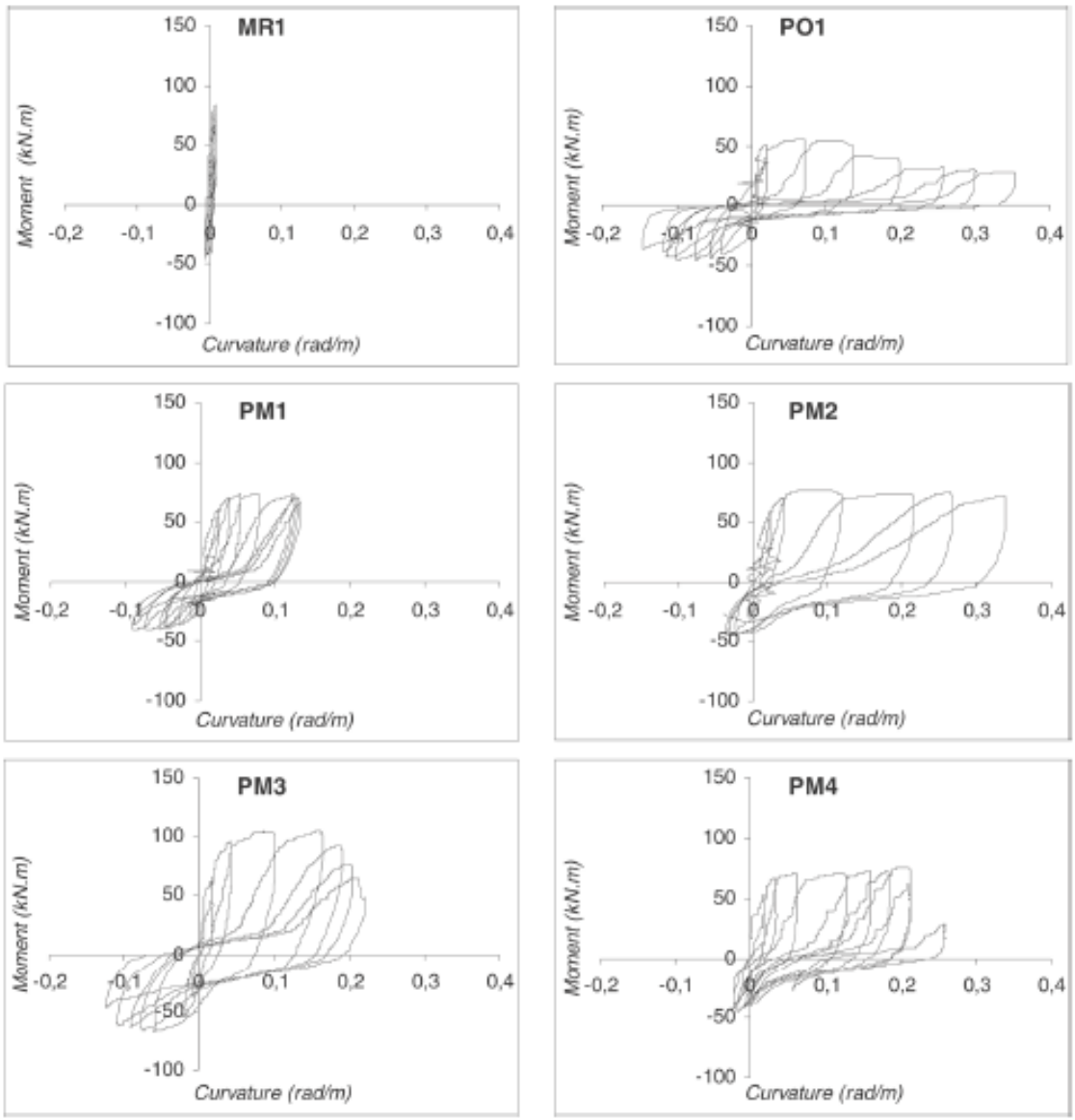

Fig. 2.33. Moment versus curvature curves of specimens for connection region.

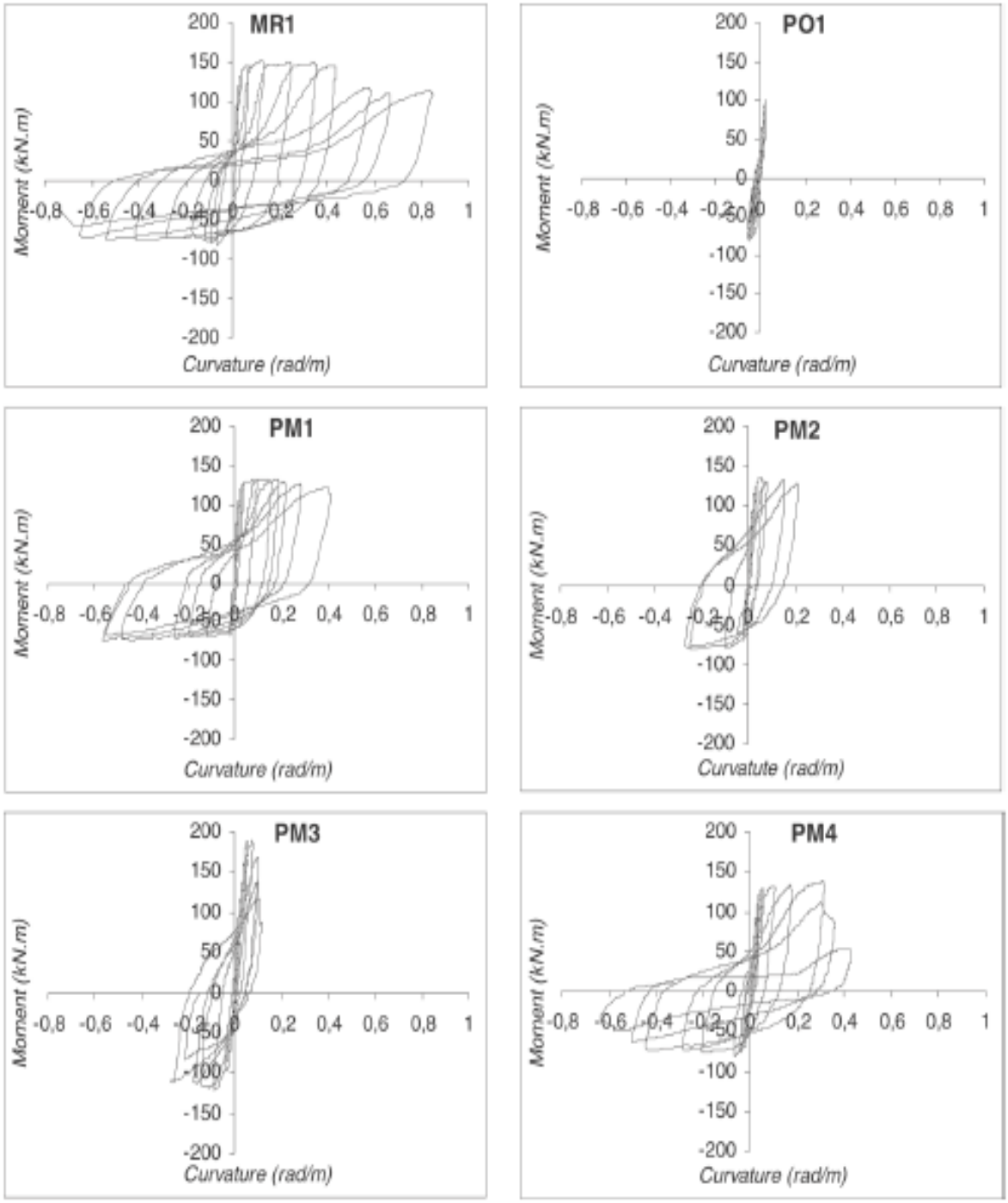

Fig. 2.34. Moment versus curvature curves of specimens for root region.

In Table 2.6, measured values of *P* and *U*, corresponding to first yielding and their ultimate values are summarized. In Table 2.6, the subscript '*y*' denotes the initial yielding, 'max' denotes the maximum value measured, '*R*' denotes the measured value for the reference specimen (MR1) and '85' denotes the value corresponding to 85% of the maximum load *(*0.85 × P_{max}*)*. In the table, '*P*' is the tip load and '*U*' is the measured tip deflection. The

deflection value U_{85} could not be determined for specimensMR1, PM1 and PM2, since those tests were truncated before 15% strength loss was exhibited. In order to refer to the ductility level of the specimens, which is defined as the ratio of U_{85} to yield deflection U_y, a term $\lambda_d = U_{85}/U_y$ is defined and notated as the "displacement ductility factor". The computed displacement ductility values are listed in Table 2.6 for all specimens. The generally accepted minimum value of ductility ratio is $\lambda_{d\text{-min}} = 4.0$. Specimens PM1, PM2 and PM4 exhibited satisfactory ductility levels while the displacement ductility factor of PO1 is the lowest $(\lambda_d . = 2.89 < 4.0)$ and was below the required minimum value.

Table 2.6 :-Measured values corresponding to yield and ultimate load

	Specimen	P_y (kN)	P_{max} (kN)	$\frac{P_{max}}{P_{max\,R}}$	U_y (mm)	U_{max} (mm)	U_{85} (mm)	$\lambda_d = \frac{U_{85}}{U_y}$	$\frac{\lambda_d}{\lambda_{dR}}$
Forward loading	MR1	99.3	102.1	1.00	12.01	24.61	>115	>9.58	1
	PO1	65.6	67.8	0.66	13.14	27.66	38.05	2.89	<0.30
	PM1	98.3	99.2	0.97	13.14	49.07	>118	>8.98	≈0.93
	PM2	100.4	100.5	0.98	11.40	28.03	>91	>7.98	≈0.83
	PM3	91.0	93.7	0.91	14.01	52.17	67.54	3.61	<0.38
	PM4	81.9	89.7	0.88	15.32	101.06	97.11	4.82	<0.50
Backward loading	MR1	49.2	55.9	1.00	7.66	14.12	70	9.13	1
	PO1	55.6	55.2	0.99	9.85	29.08	54.77	5.56	0.60
	PM1	50.8	55.0	0.98	9.85	74.10	>79	>8.02	>0.87
	PM2	60.4	59.1	1.06	9.65	20.35	>41	>4.24	>0.46
	PM3	60.3	59.9	1.07	6.58	20.06	61.40	9.33	1.02
	PM4	54.9	51.0	0.91	9.85	22.16	56.52	5.73	0.62

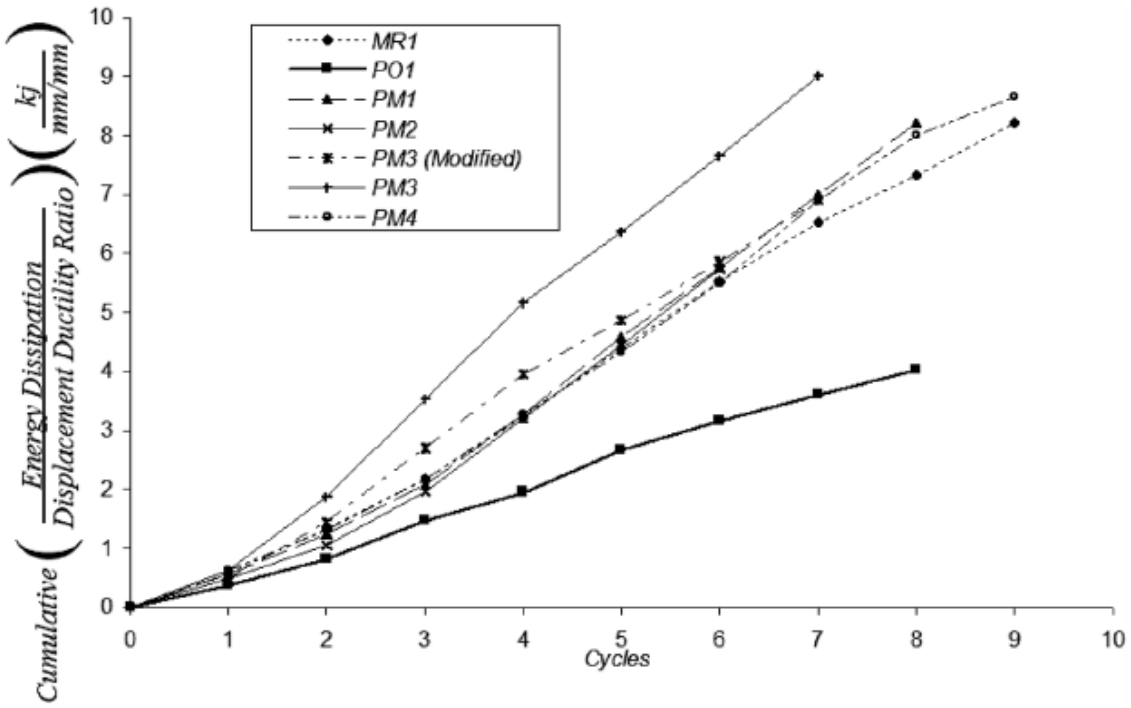

Fig. 2.35. Cumulative energy dissipation curves for all specimens.

Energy dissipation curves :- The energy dissipation capacity of a connection is a function of the area under the load–deflection curve and it indicates how effectively a connection withstands earthquake loadings. The typical way of comparing the energy dissipation is to plot the cumulative dissipated energy against the number of cycles applied. The cumulative energy dissipation versus number of cycle curves is represented in Fig. 2.35**.** The precast specimen with the original detailing displayed very poor energy dissipation capacity. The energy dissipation characteristics of all other specimens were quite alike.

Behaviour of test specimens:-

Behaviour of monolithic specimen MR1:- MR1 was the reference specimen and there was no precast connection in this specimen. The readings taken in the connection region were also used for comparison purposes. The behaviour of MR1 is the ideal behaviour. Though there were flexural cracks along the beam, the main deformation took place at the root region of the beam. At the concrete cover cracked and reinforcing bars and the stirrups were exposed. However, no damage was observed in the connection region (Fig. 2.36). This was an expected result since the largest moment forms in the root region.

Fig. 2.36. Test specimens MR1 at the end of the test and damage condition.

Behaviour of specimen PO1:- The second specimen PO1 was designed using the connection detail proposed for experimentation performed poorly. The lap length of PO1 was 28φ. Due to the in sufficient lap length, premature failure was observed. The load carrying capacity of PO1 was inadequate as well. Moreover, the ductility of specimen PO1 was poor (λ_d =2.89) and early strength degradation was observed. Energy dissipation capacity of PO1 was not satisfactory. The shear deformation in the connection region of PO1 was higher than the other specimens. Besides, from moment curvature curves of the connection and root regions,

one can easily interpret that while the connection region of PO1 was seriously deformed, the root region remained almost intact. That means the major part of the deformation took place in the connection instead of the root region. Again the stiffness of PO1 was quite poor compared with the others (Fig. 2.37).

Fig. 2.37. Test specimens PO1 at the end of the test and damage condition.

Behaviour of specimen PM1:- In PM1, the top longitudinal bars were connected by welding. For the bottom steel connection, the weld length was increased from 35 to 60 mm. The behaviour of PM1 seemed to be quite satisfactory. The following criterion was used while judging the behaviour as "satisfactory". The connection attained almost the same capacity as the monolithic connection (higher than 90% of monolithic ones). Also it displayed sufficient ductility *(λ_d > 4.0)* and energy dissipation with a stable behaviour. The load carrying capacity of PM1 was 97 percent (>90%) of that of MR1. The shear deformation envisioned in the connection region was very low. Proper plastic hinging took place at the root of the cantilever while only a slight damage occurred at the connection region which could be attributed to the weakness of the bottom plate connectors where indications of yielding were observed (Fig.2.38). The strength of PM1 is found to be satisfactory. The energy dissipation capacity of the PM1 was also quite satisfactory.

Fig. 2.38. Test specimens PM1 at the end of the test and damage condition.

Behaviour of specimen PM2:- For specimen PM2 the lap length of the top bars was increased to 47φ. At the end of the sixth cycle bottom steel connectors *(*3φ10*)* ruptured and it was concluded that they were insufficient. The increase in the top steel lap length led to a considerable improvement in the behaviour. However, the overall performance of this specimen was not as satisfactory as that of PM1. Combined failure was observed; namely, considerable damage took place both at the connection region and the root of the cantilever where hinging started but could not reach a pronounced level (Fig. 2.39). The load carrying capacity of PM2 was very close to that of MR1 (98 percent of that of MR1). Shear deformation in the connection region was not high enough. Both the connection and root of PM2 were deformed while the former was higher than the latter. The ductility of PM2 was satisfactory *(*λ_d > 7.98*)*. In addition, the energy dissipation capacity of PM2 was observed to be adequate (122 percent of that of MR1). The stiffness of PM2 decreased rapidly after the third cycle. This faster stiffness degradation was considered to be undesirable.

Fig. 2.39 Test specimens PM2 at the end of the test and damage condition.

Behaviour of specimen PM3:- For specimen PM3, φ16 bars were used as the longitudinal reinforcement, and 3φ16 were used for the bottom steel connection. The adjusted load carrying capacity of PM3 was 92 percent of that of MR1. The ductility of PM3 was not satisfactory *(λd = 3.61)*. The energy dissipation capacity of PM3 was nearly the same value as the capacity of PM1. A quite acceptable behaviour was observed despite the fact that the connection was subjected to higher shear forces and bending moments as a result of the increased beam reinforcement. A combined failure was attained. The major deformation took place in the connection region. At the end of the last cycle, the top reinforcement of PM3 ruptured near the welding region. In other words, considerable damage occurred both at the connection zone and the root of the cantilever, along with the cover crushing observed over the entire beam stub (Fig. 2.40). The rupture of one of the top bars was attributed to the complications caused by welding.

Fig. 2.40 Test specimens PM3 at the end of the test and damage condition.

Behaviour of specimen PM4:- For specimen PM4, 3φ14 bars were used at the bottom steel connection. Other reinforcement details were the same as the details of PM2. The load carrying capacity of PM4 was 88 percent of that of MR1. Once again, an acceptable behaviour was observed as a result of combined failure (in PM4 major deformation had been forced to occur in the root region). Considerable damage formed at both critical zones (Fig. 2.41). When compared with PM2, the performance of this specimen appeared to be somewhat inferior to that ofPM2.

Fig. 2.41. Test specimens PM4 at the end of the test and damage condition.

The various conclusions obtained from this work are:-

1) The original connection detail was not suitable for seismic use.

2) Significant improvements could be achieved by introducing the modifications proposed.

3) Connecting the top steel via welding solved the problem of anchorage, and the modified detail performed quite satisfactorily not only in the case where reasonable beam reinforcement *($\rho \sim = 0.015$)* had been used but also in the case of more heavily *($\rho \sim = 0.020$)* reinforced beams where the connection was subjected to higher shear forces and bending moments.

4) A longer (around 50φ) and better confined lap splice for the connection of the top steel may also be considered as a rather satisfactory alternative to welding, in the cases of moderate beam reinforcement. But this method is not recommended for the cases of heavily reinforced beams.

5) Stress flow in the bottom reinforcement was realized in the original detail through steel bars welded to plates anchored in the beams to be connected. The original bottom steel connectors appeared to be insufficient.

6) The bottom connectors were made stronger (strengthened) in the improved specimens, and a satisfactory result could be obtained in the cases where the connectors were stronger than the beam bottom steel itself and where connection plates were properly anchored.

2.3.5 Performance-Based Seismic Evaluation of Two Five-Story Precast Concrete Hybrid Frame Buildings (20)

Rahman, Ataur, M., et al.(20) developed a unique hybrid frame, which include minimum structural damage when subjected to earthquake loading and the recentering capability, which were the result of using a combination of mild steel reinforcement and unbonded prestressing to establish connections between precast beams and precast columns. Using acceptance criteria defined in terms of inter story frame drift and floor acceleration, their investigation presents a multiple-level performance-based seismic evaluation for two five-story precast concrete hybrid frame buildings. The design and analysis of these two buildings, established as the displacement-based and force-based design solutions for a prototype building used in the precast seismic structural system (PRESSS) program, were conducted at 60% scale so that the analysis models could be validated using the PRESSS test data. Despite a difference of 40% in the design base shear, the two buildings satisfied the acceptance criteria when subjected to input motions with intensities less than or equal to that of the design-level earthquake. For input motions, equal to 150% of the design-level earthquake, the building designed using the displacement-based principles did not satisfy the inter story drift limit, whereas the force-based solution provided acceptable performance.

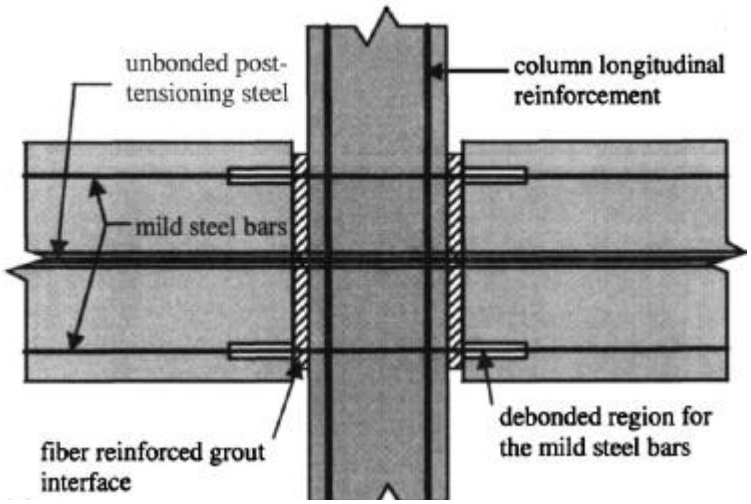

Figure 2.42 : Typical connection details of precast hybrid frame used in this study

Performance-Based Evaluation :- Seismic performance of the two hybrid frame buildings were evaluated under earthquake input motions corresponding to four intensity levels. At each intensity level, the damage state in the buildings was quantified using the maximum transient inter story drift, maximum residual inter story drift, the maximum floor acceleration, and maximum plastic rotation, where inter story drift is defined as the relative floor displacement divided by story height. Acceptable performance of the buildings was

arbitrated by comparing the maximum values of the inter story drift and floor acceleration against the limiting values. The seismic hazard corresponding to the four intensity levels and the limiting values for the transient inter story drifts were defined in accordance with the recommendations of the Seismology Committee(1999). The four earthquake intensity levels used in this study were identified as EQ-I, EQ-II, EQ-III, and EQ-IV. These four intensities correspond to 22, 50, 100, and 150%, respectively, of a design-level earthquake that is expected in a high seismic zone for soil type S_C without the influence of near source effects. Four levels of earthquakes were characterized as frequent, occasional, rare, and maximum considered events and have mean return periods of 25, 72, 250–800, and 800–2500 years, respectively.

Interstory Drift Limits :- The following inter story drift limits wsd used as acceptable limits to evaluate the building performances at the four earthquake intensity levels: maximum transient drifts of 0.5% (EQ-I), 1.5% (EQ-II), 2.5% (EQ-III), and 3.8% (EQ-IV); and maximum residual drifts of 0.1% (EQ-I), 0.3% (EQ-II), 0.5% (EQ-III), and 0.75% (EQ)IV. These limits were chosen based on the guidance given in the *SEAOC blue book* (Seismology Committee 1999) and considering the recentering nature of the hybrid frames.

Results and conclusions :- Following validation of the analytical modeling procedure, both buildings were subjected to several short- and long-duration earthquake input motions which were comparable with acceleration response spectra corresponding to four levels of earthquake intensities. Using the analysis results, the following conclusions were drawn:

1.) The seismic performance of the two buildings satisfied the performance limits under earthquake input motions with intensities similar to or below that of the design-level earthquake. Hence, the force-based methods described in design codes for monolithic concrete special moment frames and the direct displacement design are acceptable procedures for the design of the prototype five story precast hybrid frame building to produce acceptable performance at design-level earthquakes.

2.) At EQ-IV, the building based on the force-based method produced acceptable performance. However, the building designed according to the displacement-based method was unsatisfactory as it resulted in significantly higher maximum transient interstory drifts than the acceptable limit of 3.8% assumed in this study. The performance of the building based on the displacement-based design could be improved by designing for the EQ-IV spectrum at a target drift of 3.8%;

3.) Overall the hybrid building designed to the displacement based method experienced large plastic rotations. When these values obtained at the column bases and the end of first floor

beams were compared, the largest plastic rotations experienced by the building designed to the force-based method on average was about 70% of those recorded in the building designed to the displacement-base method

CHAPTER-3
RESEARCH METHODOLOGY

3.1 Introduction

This chapter discusses about the methodology to carry out this research. This research will be done by using computer modeling and it is a preliminary investigation on precast beam column joints & frames under seismic load.

In this work, a detailed three-dimensional (3D) nonlinear finite element model is developed to study the response and predict the behavior of precast beam–column exterior connection & frame for three type of precast beam – column connection detail subjected to cyclic loads.

3.2 General description of precast beam column joints investigated

In this work three types of beam – column joints detail used in precast constructions are investigated. An exterior beam - column joint of a four storied building frame is chosen for investigation purpose. The location of the exterior connection is as shown in fig.-3.1 :-

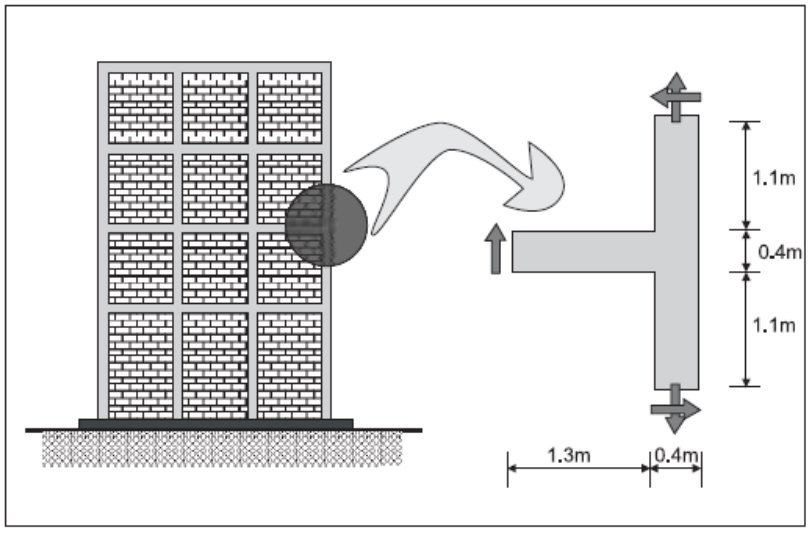

Fig. 3.1:- Exterior beam column sub. assemblage of an R.C. frame building, geometry and forces acting on it when it swings from right to left (17)

One of the connection details investigated in this work is taken from the connection details developed by B.G. Shirkey(22) for joining beam – column joints in precast structure under the name 3S system. This joint detail is labeled as joint **P.C.-1.**

The second connection detail is taken from one of the research work conducted by Manoj K. Joshi, C.V.R. Murty and M. P. Jaisingh (17) on precast beam–column connection. This joint detail is labeled as joint **P.C.-2.**

The third connection detail is taken from the research work conducted by R. Vidjeapriya and K.P. Jaya (13) on precast beam–column connection. This joint detail is labeled as joint **P.C.-3.**

The results from all of these joints are compared with a monolithic specimen labeled **M.C.-1** with same amount of reinforcement & material properties in order to compare the result of precast joint details with monolithic specimen.

3.2.1 Details of precast beam – column joint P.C.-1

3.2.1.1 Dimension of P.C. -1

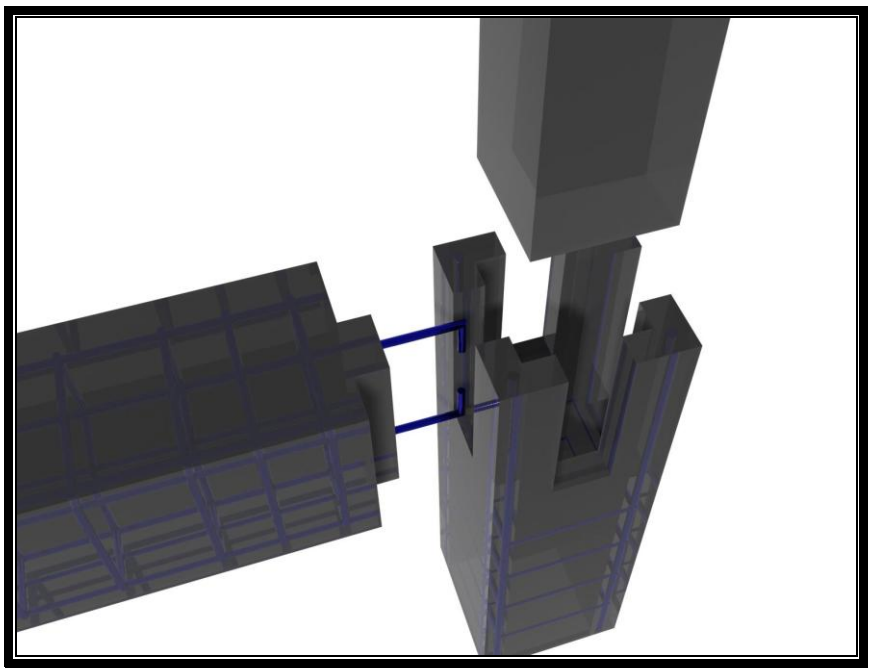

Fig.3.2- 3D view of precast joint P.C.1

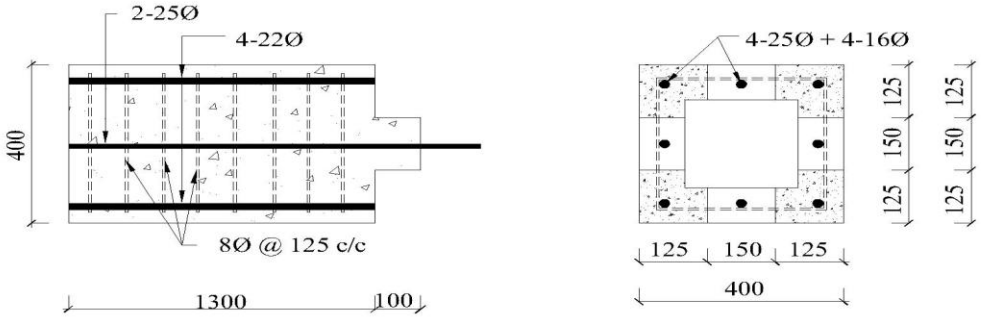

Fig. 3.3 - Plan of precast specimen P.C.-1

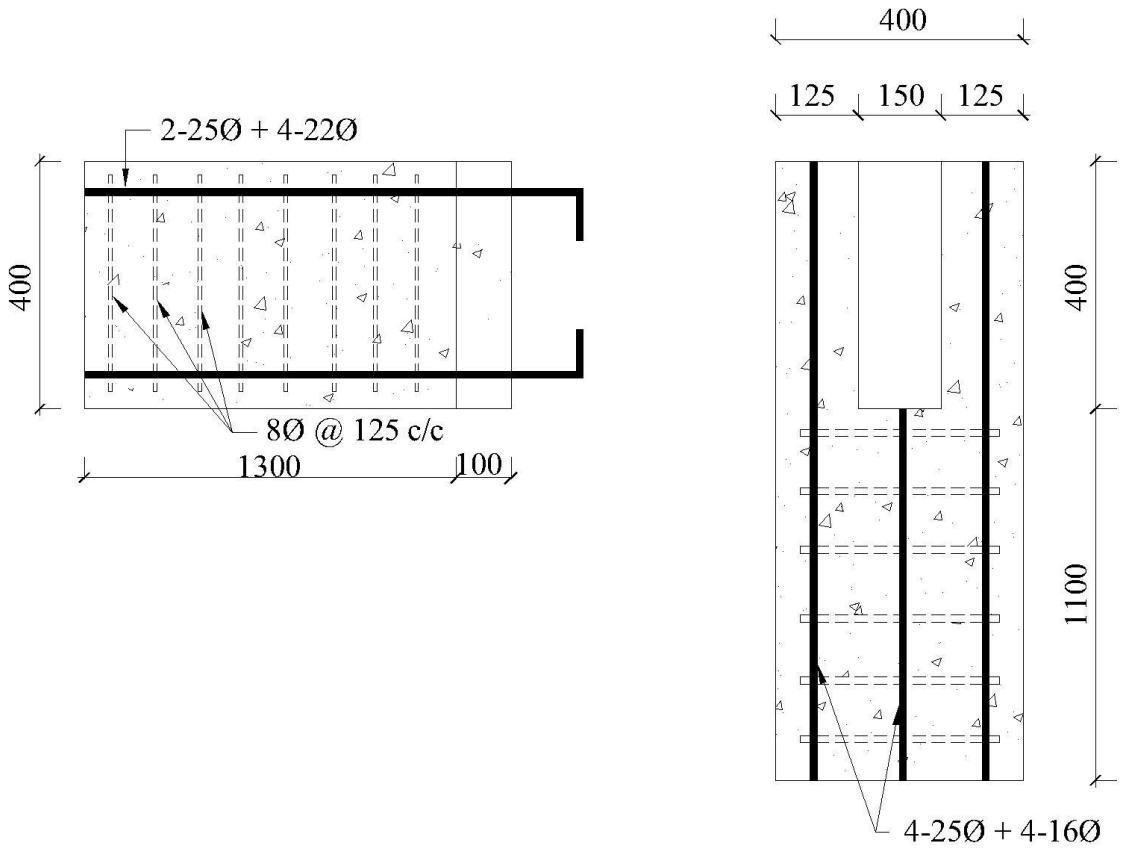

Fig. 3.4 - Elevation of precast specimen P.C.-1

3.2.1.2 Material properties of P.C.1

a) Modulus of Elasticity of steel, Es = 21,0000 MPa

b) MPa Modulus of Elasticity of concrete, EC = 22,360.68 MPa

c) Characteristic strength of concrete, f ck = 25MPa

d) Yield stress for steel, fy =415 MPa

e) Ultimate strain in bending, ε_{cu} =0.0035

The detailing of P.C.1 consists of a precast beam connected to a hollow core column by a key from beam that fits into a predesigned space left in the column. Two reinforcing bars from beam goes into hollow core of column which is then filled with cast in place conc. The key & reinforcing bars from beam fits into column & cast in place concrete is then filled into the hollow core of column to make the joint monolithic.

3.2.2 Details of precast beam – column joint P.C.-2

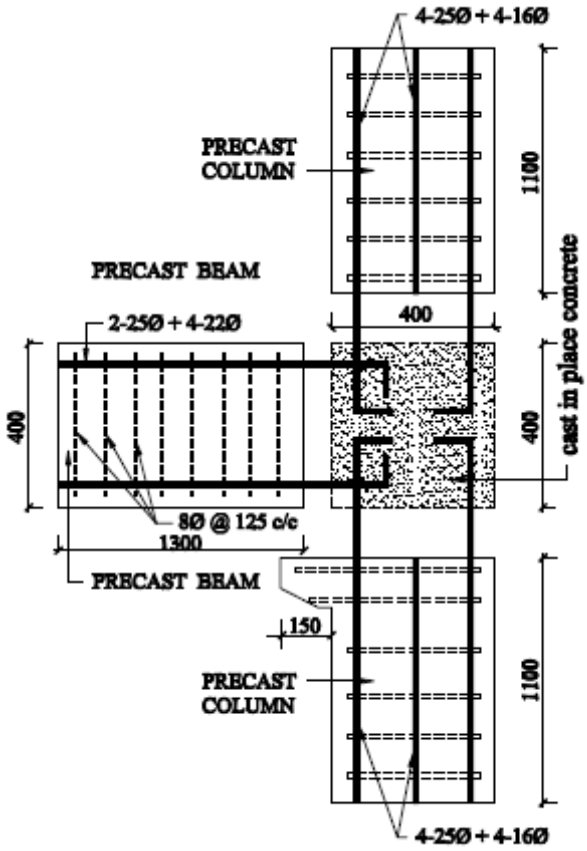

Fig. 3.5 – Side elevation of precast specimen P.C.-2

3.2.2.1 Material properties of P.C.2

a) Modulus of Elasticity of steel, Es = 21,0000 MPa

b) MPa Modulus of Elasticity of concrete, EC = 22,360.68 MPa

c) Characteristic strength of concrete, f ck = 25MPa

d) Yield stress for steel, fy =415 MPa

e) Ultimate strain in bending, Ɛcu =0.0035

The connection detail of P.C.2 consists of a precast beam resting on the corbel at the top of column. Protruding reinforcing bars from beam & column are filled with cast in situ concrete to form the joint as shown in fig. 3.5.

3.2.3 Details of precast beam – column joint P.C.-3

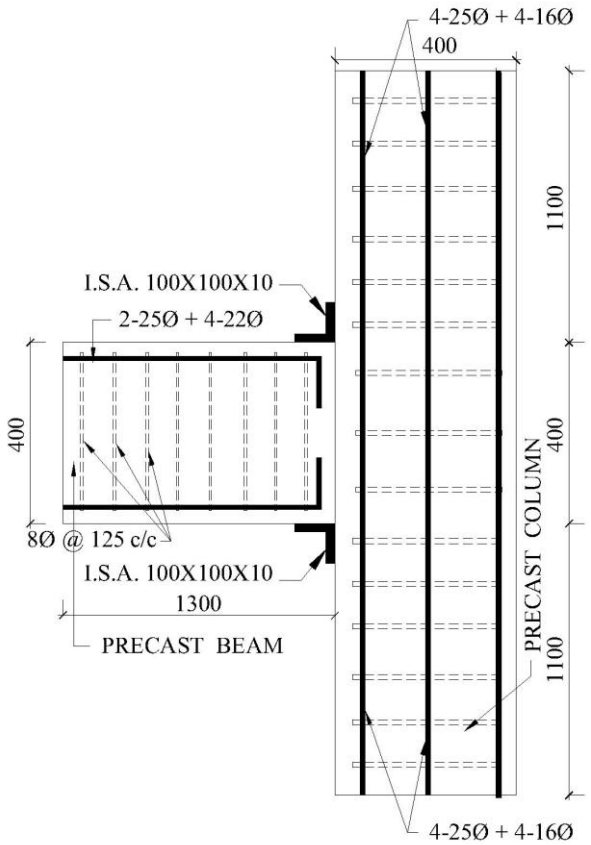

Fig. 3.6 – Side elevation of precast specimen P.C.-3

3.2.3.1 Material properties of P.C.1

a) Modulus of Elasticity of steel, Es = 21,0000 MPa

b) MPa Modulus of Elasticity of concrete, EC = 22,360.68 MPa

c) Characteristic strength of concrete, f ck = 25MPa

d) Yield stress for steel, fy =415 MPa

e) Ultimate strain in bending, ε_{cu} =0.0035

Joint P.C.3 is a mechanical connection as in this joint two independent members i.e. beam and column are connected to each other by M.S. angel section with the help of 10mm dia. bolts. Strength of this joint is governed by connectivity, size & strength of M.S. angel.

3.2.4 Details of monolithic beam – column joint M.C.-1

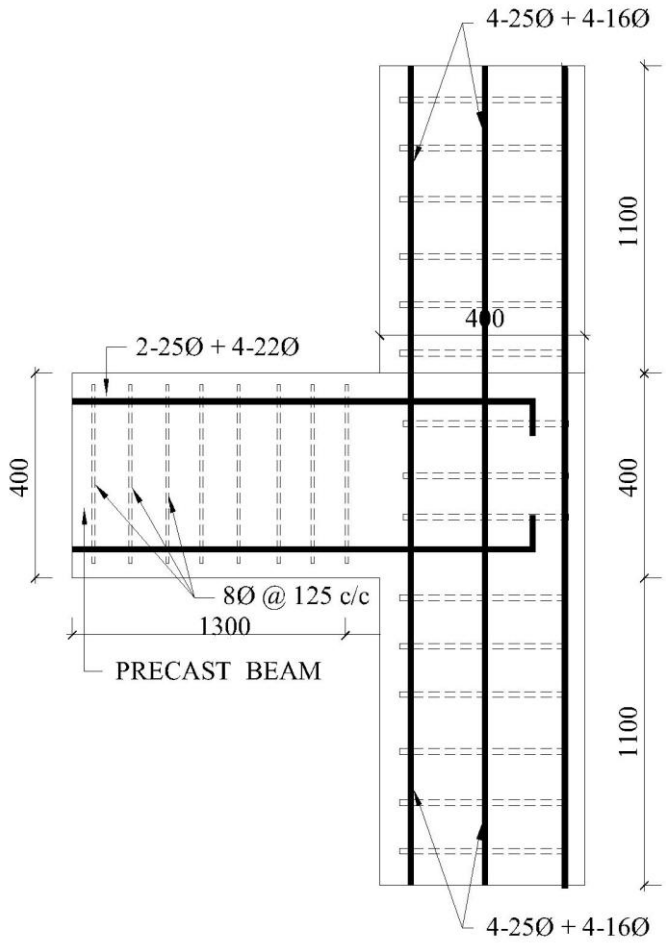

Fig. 3.7 – Side elevation of monolithic specimen M.C.-1

3.2.4.1 Material properties of M.C.1

a) Modulus of Elasticity of steel, Es = 21,0000

b) MPa Modulus of Elasticity of concrete, EC = 22,360.68 MPa

c) Characteristic strength of concrete, f ck = 25MPa

d) Yield stress for steel, fy =415 MPa

e) Ultimate strain in bending, Ɛcu =0.0035

3.3 Detail of the frame investigated

Four types of frames with joint configuration for beam – column already explained are modeled. These frames are labeled as P.C.F.-1, P.C.F.-2, P.C.F.-3 & M.C.F.-1

3.3.1 Dimension of frame investigated

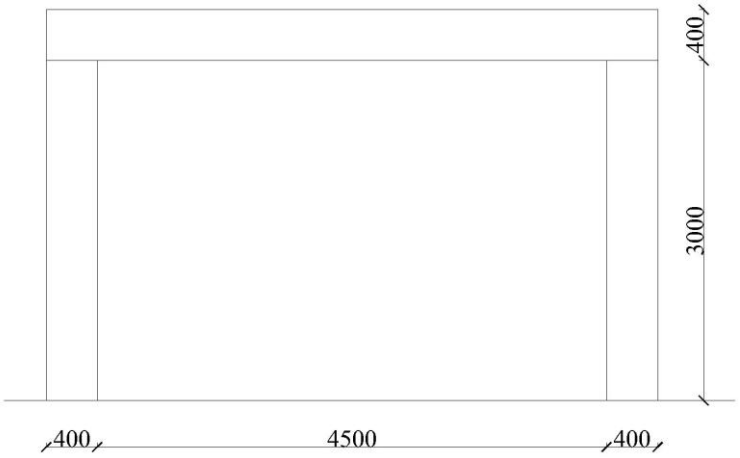

Fig. 3.8 – Side elevation of frame investigated

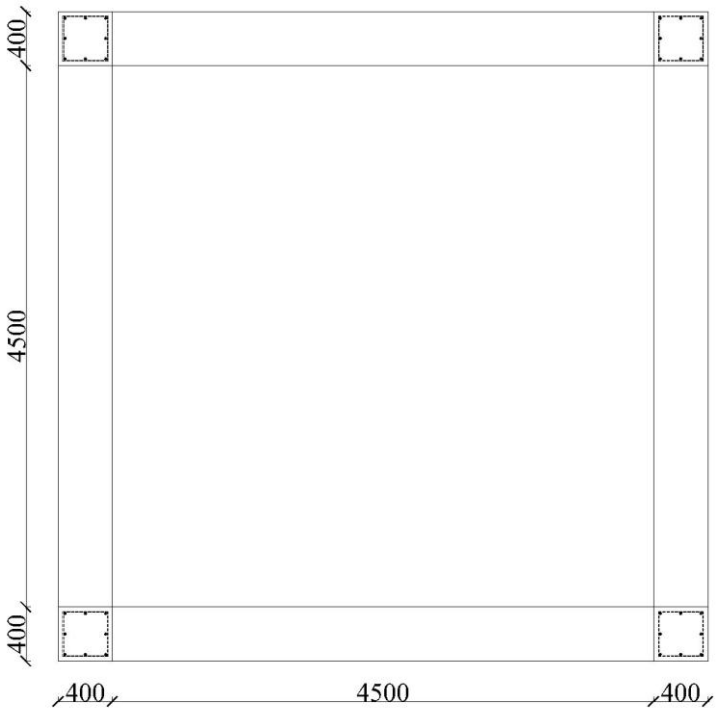

Fig. 3.9 – Plan of frame investigated

3.4 Loading

The sub-assemblage specimens are subjected to 2 types of displacement controlled loading.

1) First type of loading consist of uniformly increasing monotonic displacement. In this displacements on structure are increased with each load step with the uniform increment of 1mm up to the failure of structure

2) Second type of loading consist of cyclic displacement simulating the loading of an earthquake. The loading history used is taken from the research paper of Manoj K. Joshi, C.V.R. Murty and M. P. Jaisingh (17) & is shown in fig.3.8

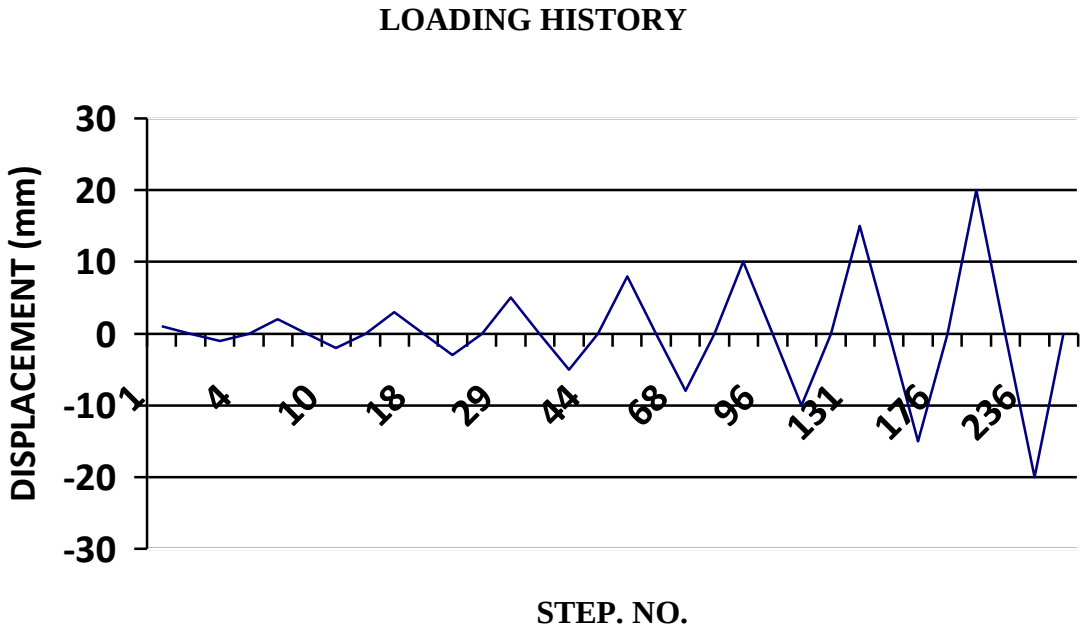

Fig. 3.10 – Loading history

Table -3.1 :- Loading history used in investigation

Step No.	1	2	3	4	6	8	10	12	15	18	21	24	29	34	39	44
Displacement(mm)	1	0	1	0	2	0	-2	0	3	0	-3	0	5	0	-5	0

Step No.	52	60	68	76	86	96	106	116	131	146	161	176	191	216	236
Displacement	8	0	-8	0	10	0	-10	0	15	0	-15	0	20	0	-20

3.5 INTRODUCTION TO FE MODELLING

For structural design and assessment of reinforced concrete members, the non-linear finite element (FE) analysis has become an important tool. Over the last one or two decade numerical simulation of reinforced concrete structures and structural elements has become a major research area. A successful numerical simulation demands choosing suitable elements, formulating proper material models and selecting proper solution method.

3.5.1 Finite Element Method

The finite element method (FEM) or finite element analysis is a numerical technique for finding approximate solutions of partial differential equations (PDE) as well as of

integral equations. The solution approach is based either on eliminating the differential equation completely (steady state problems), or rendering the PDE into an approximating system of ordinary differential equations, which are then numerically integrated using standard techniques.

In solving partial differential equations, the primary challenge is to create an equation that approximates the equation to be studied, but is numerically stable, meaning that errors in the input data and intermediate calculations do not accumulate and cause the resulting output to be meaningless. The Finite Element Method is a good choice for solving partial differential equations over complex domains. [21]

3.6 Principles of finite element analysis used in F.E.M. based software ATENA

The basic concept of FEM modeling is the subdivision of the mathematical model into disjoint (non-overlapping) components of simple geometry. The response of each element is expressed in terms of a finite number of degrees of freedom characterized as the value of an unknown function, or functions or at a set of nodal points. The response of the mathematical model is then considered to be the discrete model obtained by connecting or assembling the collection of all elements.

Within the framework of the finite element method reinforced concrete can be represented either by superimposition of the material models for the constituent parts (i.e., for concrete, for reinforcing steel and for FRP), or by a constitutive law for the composite concrete, embedded steel and composite FRP laminates considered as a continuum.

The finite element method is well suited for superimposition of the material models for the constituent parts of a composite material. Several constitutive models covering these effects are implemented in the computer code ATENA, which is a finite element package designed for computer simulation of concrete structures. The graphical user interface in ATENA provides an efficient and powerful environment for solving many anchoring problems. ATENA enables virtual testing of structures using computers, which is the present trend in the research and development world. Material models of this type can be employed for virtually all kinds of reinforced concrete structural members. Depending on the type of material modeling to be solved in ATENA, concrete can be represented by solid brick elements, the reinforcement is modeled by bar elements (discrete representation) Geometry

and shape of any mathematical element help in proper placement of the nodal points and materials properties helps in using proper modeling.

3.6.1 MATERIAL MODELS

The program system ATENA offers a variety of material models for different materials and purposes. The most important material models in ATENA for RCC structure are concrete and reinforcement. These advanced models take into account all the important aspects of real material behavior in tension and compression [21].

3.6.1.1 MODELLING OF CONCRETE

1) Geometry of the Concrete

Element geometric modeling of concrete has been done using 3D solid brick element with up to 20 nodes in ATENA, shown in **Figure 3.11**

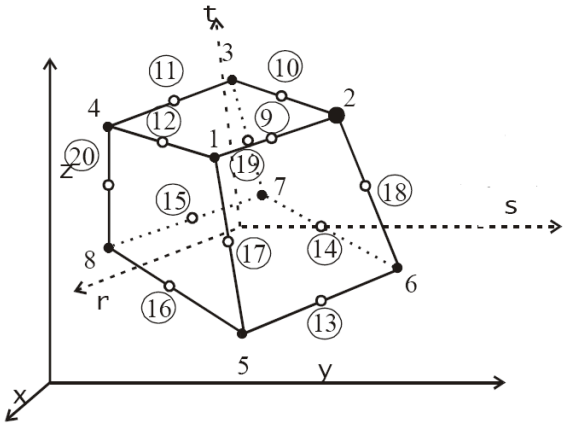

Figure 3.11 Geometry of Brick elements [21]

2) Element Properties

3D solid brick element having three degree of freedom at each node : translations in the nodal x, y and z directions. This is an isoparametric elements integrated by Gauss integration at integration points. This element is capable of plastic deformation, cracking in three orthogonal directions, and crushing. The most important aspect of this element is the treatment of non-linear material properties.

3) Element Interpolation function

3D solid brick element interpolation functions for all variants of the elements are given below:

N1= (1/8) (1+r) (1+s) (1+t) N2= (1/8) (1-r) (1+s) (1+t)

N3= (1/8) (1-r) (1-s) (1+t) N4= (1/8) (1+r) (1-s) (1+t)

N5= (1/8) (1+r) (1+s) (1-t) N6= (1/8) (1-r) (1+s) (1-t)

N7= (1/8) (1-r) (1-s) (1-t) N8= (1/8) (1+r) (1-s) (1-t)

3.6.1.2 MODELLING OF REINFORCEMENT

1) Geometry of the reinforcement

Reinforcement modeling could be discrete or smeared. In our work, a discrete modeling of reinforcement has been done. The reinforcement has been modeled using bar elements in ATENA.

2) Element Properties

Reinforcement steel is a 3D bar element, which has three degrees of freedom at each node; translations in the nodal x, y and z direction. Bar element is a uniaxial tension-compression element. The stress is assumed to be uniform over the entire element. Also plasticity, creep, swelling, large deflection and stress-stiffening capabilities are included in the element.

3) Element Shape Functions:

The shape functions in natural co-ordinate system for the three dimensional bar element without rotational degrees of freedom.

N1= (1/2) (1+s) N2= (1/2) (1-s)

3.7 STRESS-STRAIN RELATIONS FOR CONCRETE [21]

Concrete exhibits a large number of micro-cracks, especially, at the interface between coarser aggregates and mortar, even before subjected to any load. The presence of these micro-cracks has a great effect on the mechanical behavior of concrete, since their propagation during loading contributes to the nonlinear behavior at low stress levels and causes volume expansion near failure. Many of these micro-cracks are caused by segregation, shrinkage or thermal expansion of the mortar. Some micro-cracks may develop during loading because of the difference in stiffness between aggregates and mortar. Since the aggregate-mortar interface has a significantly lower tensile strength than mortar, it

constitutes the weakest link in the composite system. This is the primary reason for the low tensile strength of concrete.

The response of a structure under load depends to a large extent on the stress-strain relation of the constituent materials and the magnitude of stress. Since concrete is used mostly in compression, the stress-strain relation in compression is of primary interest **[21]**.

3.7.1 EQUIVALENT UNIAXIAL LAW

The nonlinear behavior of concrete in the biaxial stress state is described by means of the so called effective stress σcef, and the equivalent uni-axial strain εeq. The effective stress is in most cases a principal stress.

The equivalent uni-axial strain is introduced in order to eliminate the Poisson‟s effect in the plane stress state. **εeq = σci / Eci**

The equivalent uni-axial strain can be considered as the strain, that would be produced by the stress σci in a uni-axial test with modulus associated Eci with the direction *i*. Within this assumption, the nonlinearity representing damage is caused only by the governing stress σci. The complete equivalent uni-axial stress-strain diagram for concrete is shown in **Figure3.12**

The numbers of the diagram parts in **Figure 3.12**(material state numbers) are used in the results of the analysis to indicate the state of damage of concrete.

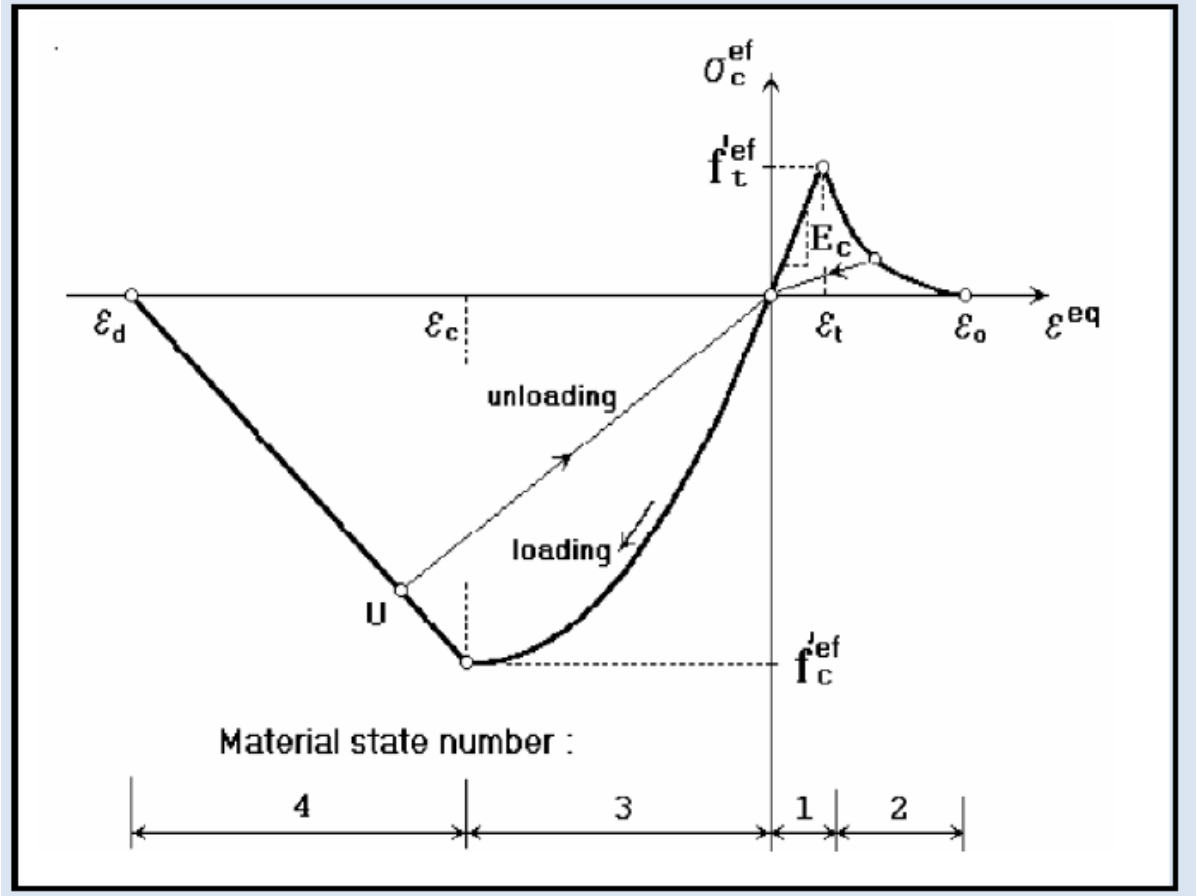

Figure 3.12 Uniaxial stress-strain law for concrete [21]

Unloading is a linear function to the origin. An example of the unloading point *U* is shown in **Figure 3.12**. Thus, the relation between stress σcef and strain εeq is not unique and depends on a load history. A change from loading to unloading occurs, when the increment of the effective strain changes the sign. If subsequent reloading occurs the linear unloading path is followed until the last loading point *U* is reached again. Then, the loading function is resumed.

The peak values of stress in compression fcef and in tension ftef are calculated according to the biaxial stress state. Thus, the equivalent uni-axial stress-strain law reflects the biaxial stress state

3.7.2 BIAXIAL STRESS FAILURE CRITERION OF CONCRETE

1) Compressive Failure

A biaxial stress failure criterion according to KUPFER et al. (1969) is used as shown in **Figure3.13**. In the compression-compression stress state the failure function is

fcef = [(1+3.65a)/(1+a)2]fc; a = (σc1/σc2) (3.1)

Where σc1, σc2 are the principal stresses in concrete and fc is the uni-axial cylinder strength. In the biaxial stress state, the strength of concrete is predicted under the assumption of a proportional stress path.

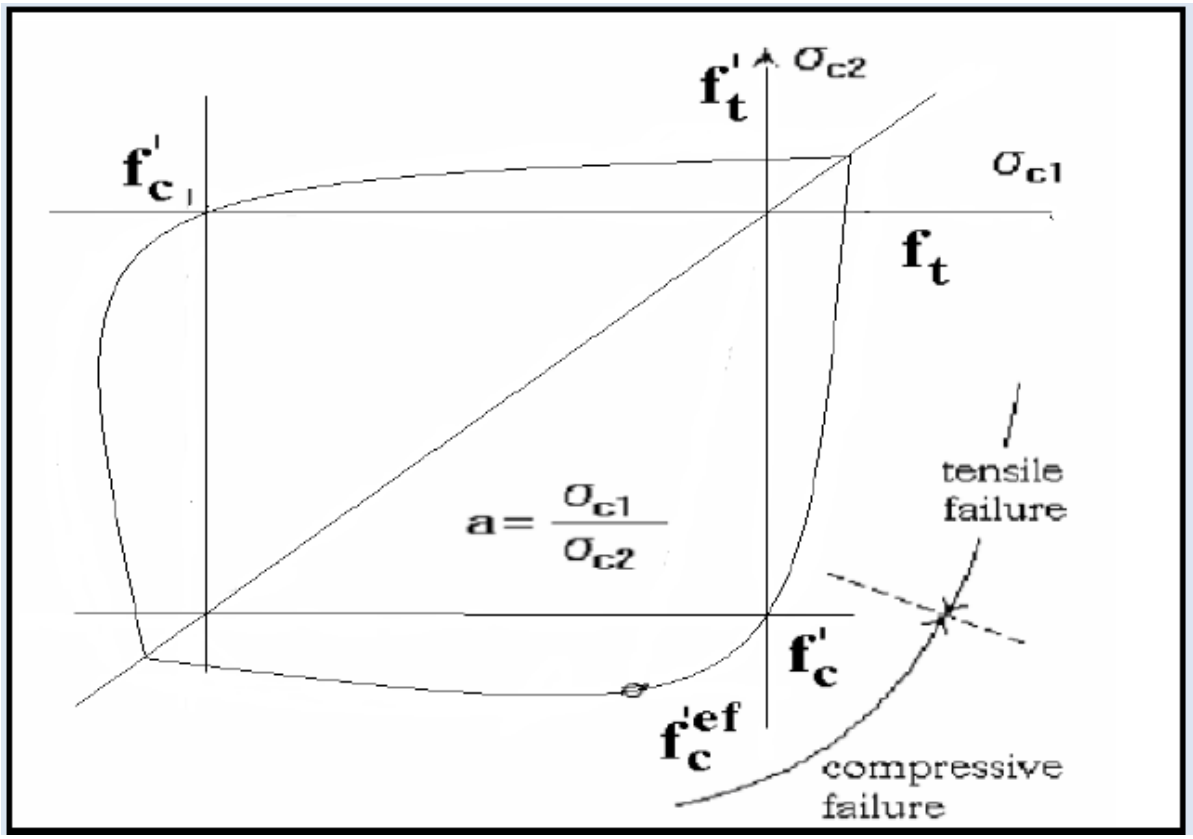

Figure 3.13 Biaxial failure functions for concrete [21]

In the tension-compression state, the failure function continues linearly from the point σc1 = 0, σc2 = fc, into the tension-compression region with the linearly decreasing strength:

fcef = fc rec, rec = [1+ 5.3278(σc1/ fc)] (3.2)

Where rec is the reduction factor of the compressive strength in the principal direction 2 due to the tensile stress in the principal direction 1.

2) Tensile failures

In the tension-tension state, the tensile strength is constant and equal to the uniaxial tensile strength f‟t. In the tension-compression state, the tensile strength is reduced by the relation:

$f_{tef} = f_t r_{et}$ (3.3)

Where ret is the reduction factor of the tensile strength in the direction 1 due to the compressive stress in the direction 2. The reduction function has one of the following forms.

ret = 1 – 0.8 (σc2/ fc) (3.4)

ret = [A + (A – 1) B]/ AB; B = Kx + A; x = σc2/ fc (3.5)

The relation in Eq. (3.4) is the linear decrease of the tensile strength and (3.5) is the hyperbolic decrease.

Two predefined shapes of the hyperbola are given by the position of an intermediate point *r*, *x*. Constants *K* and *A* define the shape of the hyperbola.

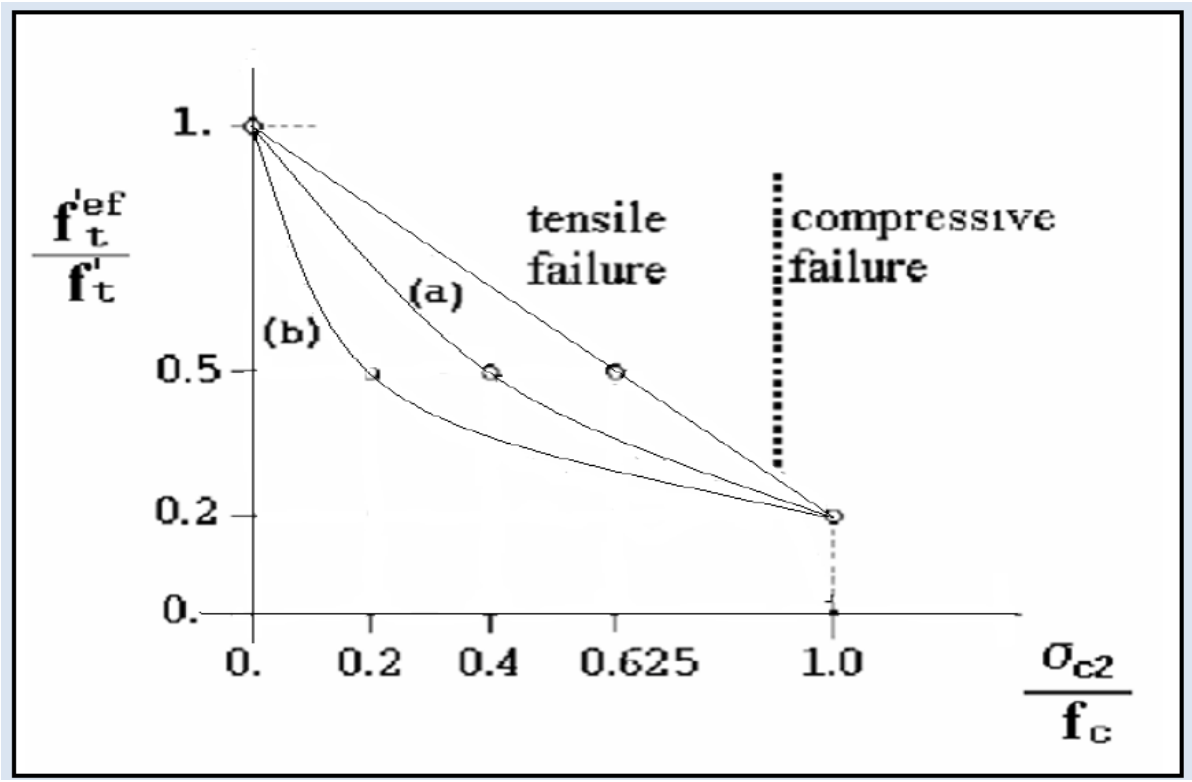

Figure 3.14 Tension-compression failure functions for concrete. **[21]**

3.7.3 TENSION BEFORE CRACKING

The behaviour of concrete in tension without cracks is assumed linear elastic. Ec *is* the initial elastic modulus of concrete, ftef is the effective tensile strength derived from the biaxial failure function already describe by **σcef = Ec εeq, 0 < σc < ftef**

3.7.4 TENSION AFTER CRACKING

A fictitious crack model is based on a crack-opening law and fracture energy. This formulation is suitable for modeling of crack propagation in concrete. It is used in

combination with the crack band. It is a region (band) of material, which represents a discrete failure plane in the finite element analysis. In tension it is a crack, in compression it is a plane of crushing. In reality these failure regions have some dimension. However, since according to the experiments, the dimensions of the failure regions are independent on the structural size, they are assumed as fictitious planes. In case of tensile cracks, this approach is known as rack the "crack band theory**", (*BAZANT OH 1983*).** Here is the same concept used also for the compression failure. The purpose of the failure band is to eliminate two deficiencies, which occur in connection with the application of the finite element model: element size effect and element orientation effect.

1) Element size effect.

The direction of the failure planes is assumed to be normal to the principal stresses in tension and compression, respectively. The failure bands (for tension Lt and for compression Lc) are defined as projections of the finite element dimensions on the failure planes.

2) Element Orientation Effect.

The element orientation effect is reduced, by further increasing of the failure band for skew meshes, by the following formula (proposed by (***CERVENKA et al. 1995*).**

$Lt = \gamma Lt$, $Lc = \gamma Lc$

$\gamma = 1 + (\gamma max - 1)\ (\theta / 45),\ \theta\ \varepsilon\ (0; 45)$ (3.6)

An angle θ is the minimal angle (min ($\theta 1$, $\theta 2$)) between the direction of the normal to the failure plane and element sides. In case of a general quadrilateral element the element sides" directions are calculated as average side directions for the two opposite edges. The above formula is a linear interpolation between the factor γ=1.0 for the direction parallel with element sides, and $\gamma = \gamma$ max, for the direction inclined at 45o. The recommended (and default) value of γ max =1.5.

3.8 BEHAVIOUR OF CRACKED CONCRETE [21]

3.8.1 DESCRIPTION OF A CRACKED SECTION

The nonlinear response of concrete is often dominated by progressive cracking which results in localized failure. The structural member has cracked at discrete locations where the concrete tensile strength is exceeded.

At the cracked section all tension is carried by the steel reinforcement. Tensile stresses are, however, present in the concrete between the cracks, since some tension is transferred from

steel to concrete through bond. The magnitude and distribution of bond stresses between the cracks determines the distribution of tensile stresses in the concrete and the reinforcing steel between the cracks.

Additional cracks can form between the initial cracks, if the tensile stress exceeds the concrete tensile strength between previously formed cracks. The final cracking state is reached when a tensile force of sufficient magnitude to form an additional crack between two existing cracks can no longer be transferred by bond from steel to concrete.

As the concrete reaches its tensile strength, primary cracks form. The number and the extent of cracks are controlled by the size and placement of the reinforcing steel. At the primary cracks the concrete stress drops to zero and the steel carries the entire tensile force. The concrete between the cracks, however, still carries some tensile stress, which decreases with increasing load magnitude. This drop in concrete tensile stress with increasing load is associated with the breakdown of bond between reinforcing steel and concrete. At this stage a secondary system of internal cracks, called bond cracks, develops around the reinforcing steel, which begins to slip relative to the surrounding concrete.

Since cracking is the major source of material nonlinearity in the serviceability range of reinforced concrete structures, realistic cracking models need to be developed in order to accurately predict the load-deformation behavior of reinforced concrete members. The selection of a cracking model depends on the purpose of the finite element analysis. If overall load-deflection behavior is of primary interest, without much concern for crack patterns and estimation of local stresses, the "smeared" crack model is probably the best choice. If detailed local behavior is of interest, the adoption of a "discrete" crack model might be necessary. Unless special connecting elements and double nodes are introduced in the finite element discretization of the structure, the well established smeared crack model results in perfect bond between steel and concrete, because of the inherent continuity of the displacement field.

3.8.2 MODELLING OF CRACKS IN CONCRETE

The process of crack formation can be divided into three stages, **Figure 3.15**. The un-cracked stage is before a tensile strength is reached. The crack formation takes place in the process zone of a potential crack with decreasing tensile stress on a crack face due to a bridging effect. Finally, after a complete release of the stress, the crack opening continues without the stress.

The tension failure of concrete is characterized by a gradual growth of cracks, which join together and eventually disconnect larger parts of the structure. It is usually assumed that cracking formation is a brittle process and that the strength in tension loading direction abruptly goes to zero after such cracks have formed.

Therefore, the formation of cracks is undoubtedly one of the most important non-linear phenomenon, which governs the behavior of the concrete structures. In the finite element analysis of concrete structures, two principally different approaches have been employed for crack modeling. These are (a) discrete crack modeling (b) smeared crack modeling

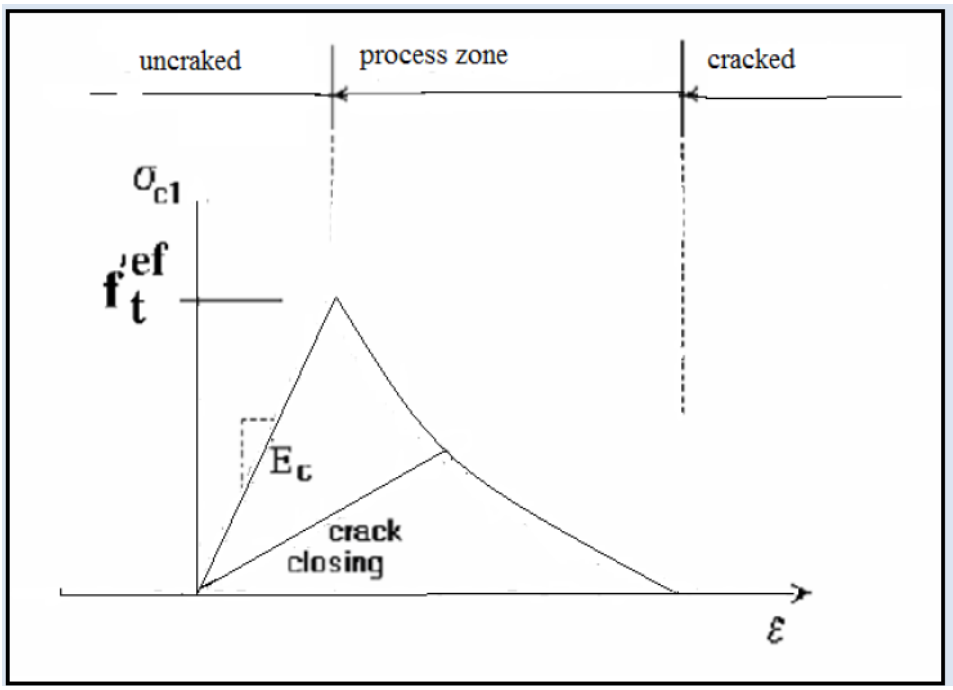

Fig.3.15 - Stages of Crack Opening [21]

The discrete approach is physically attractive but this approach suffers from few drawbacks, such as**,** it employs a continuous change in nodal connectivity, which does not fit in the nature of finite element displacement method; the crack is considered to follow a predefined path along the element edges and excessive computational efforts are required. The second approach is the smeared crack approach. In this approach the cracks are assumed to be smeared out in a continuous fashion.

Within the smeared concept two options are available for crack models: the fixed crack model and the rotated crack model. In both models the crack is formed when the principal stress exceeds the tensile strength. It is assumed that the cracks are uniformly

distributed within the material volume. This is reflected in the constitutive model by an introduction of orthotropy.

3.9 STRESS-STRAIN LAWS FOR REINFORCEMENT [21]

3.9.1 INTRODUCTION

Reinforcement can be modeled in two distinct forms: discrete and smeared. Discrete reinforcement is in form of reinforcing bars and is modeled by truss elements. The smeared reinforcement is a component of composite material and can be considered either as a single (only one-constituent) material in the element under consideration or as one of the more such constituents. The former case can be a special mesh element (layer), while the later can be an element with concrete containing one or more reinforcements. In both cases the state of uniaxial stress is assumed and the same formulation of stress-strain law is used in all types of reinforcement.

3.9.2 BILINEAR LAW

The bilinear law, elastic-perfectly plastic, is assumed as shown in **Figure 3.16**

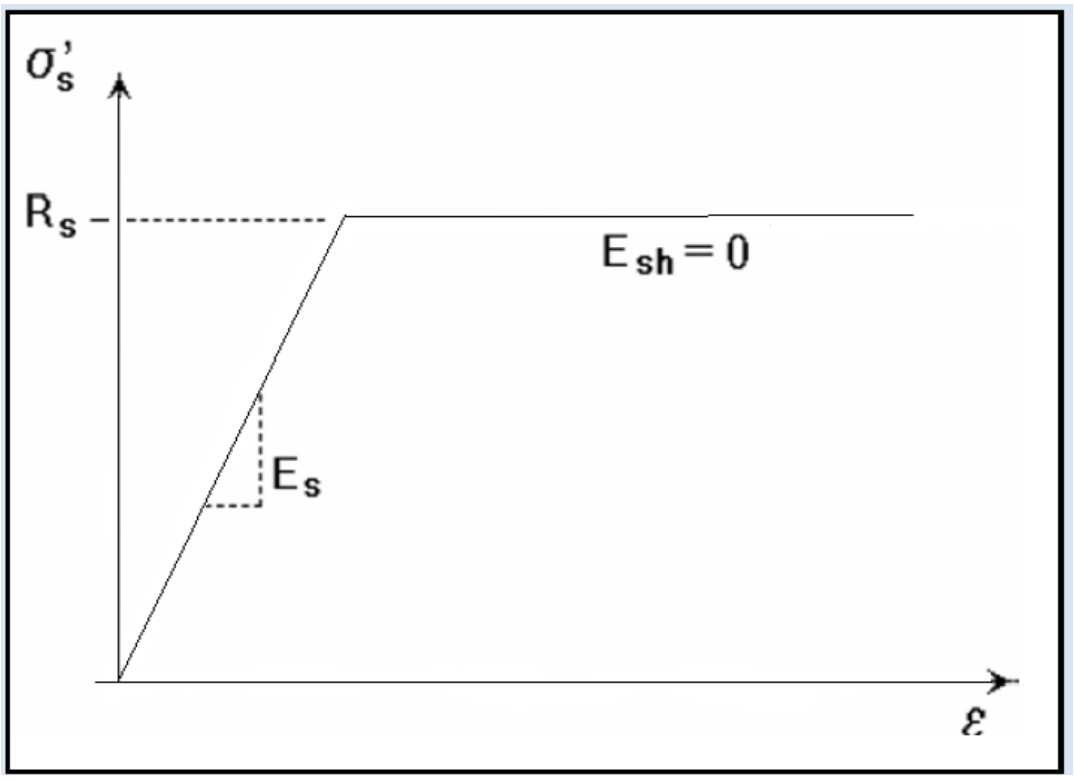

Figure 3.16 - The bilinear stress-strain law for reinforcement [21]

The initial elastic part has the elastic modulus of steel *E*s. The second line represents the plasticity of the steel with hardening and its slope is the hardening modulus *E*sh. In case of perfect plasticity *E*sh =0. Limit strain ε*L* represents limited ductility of steel.

3.9.3 MULTI-LINEAR LAW

The multi-linear law consists of four lines as shown in **Figure 3.17.** This law allows modeling of all four stages of steel behavior :- elastic state, yield plateau, hardening and fracture. The multi-line is defined by four points, which can be specified by input.

The above described stress-strain laws can be used for the discrete as well as the smeared reinforcement. The smeared reinforcement requires two additional parameters: the reinforcing ratio *p* and the direction angle β as shown in **Figure. 3.18.**

Where ρ = (Area of steel/ Area of concrete)

The spacing *s* of the smeared reinforcement is assumed infinitely small. The stress in the smeared reinforcement is evaluated in the cracks; therefore it should include also a part of stress due to tension stiffening. **σ scr =σs +σ*ts***

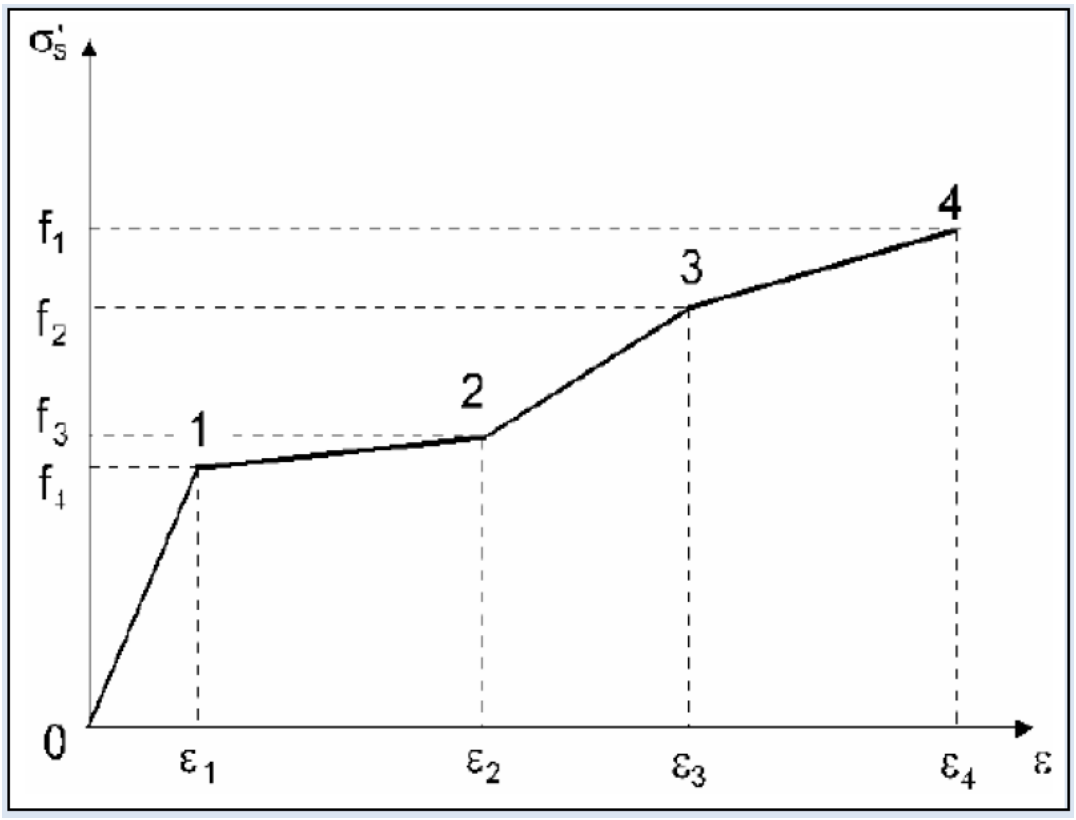

Figure 3.17 - The multi-linear stress-strain law for reinforcement [21]

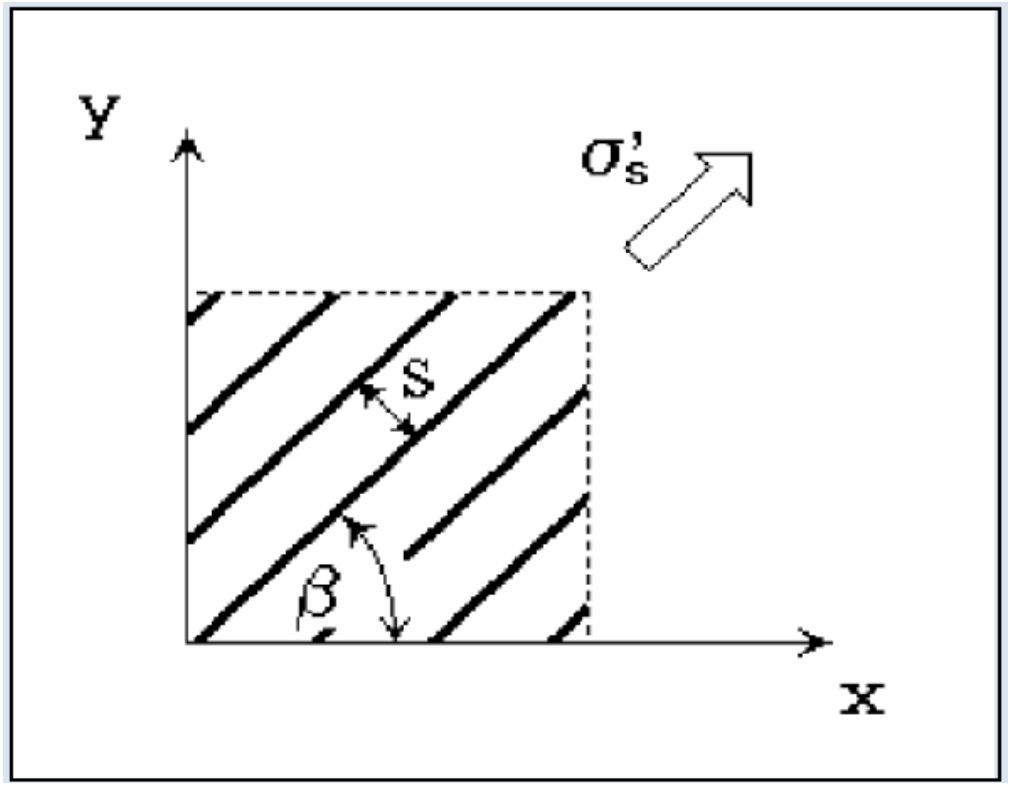

Figure 3.18 - Smeared reinforcement [21]

where σs is the steel stress between the cracks (the steel stress in smeared reinforcement), σscr is the steel stress in a crack. If no tension stiffening is specified σts = 0 and σscr = σs. In case of the discrete reinforcement the steel stress is always σs.

Once we understand the finite element modeling, the next step is the analytical programming. The main objective of this analytical program is to get the result of under reinforced concrete frame and compare with the experimental results. In the analytical programming, first we select the materials and its properties and create geometry of the frame.

3.10 F.E. analysis using ATENA

Once we understand the finite element modeling, the next step is the analytical programming. The main objective of this analytical program is to get the result of precast joints & frame and compare with the results of monolithical joint. In the analytical programming, first we select the materials and its properties and create geometry of the structure. The frame is tested by subjecting it to the loading pattern as described earlier & load deflection values are plotted as graphs.

3.10.1 MATERIAL PROPERTIES

Concrete, reinforcement steel, steel plates, & contact element have been used to model the precast RCC joins & frame. The specification and the properties of these materials are as under:

Table -3.2 :- Material properties of concrete

Properties	Value
Elastic Modulus (Fresh concrete)	9.426E+03 MPa
Poisson Ratio	0.200
Tensile strength	4.421E-01 Mpa
Compressive strength	-2.125E+00 Mpa
Specific fracture energy	1.105E-05 MN/m
Critical Compressive Displacement	-5.000E-04
Plastic Strain at Compressive Strength	-2.255E-04
Reduction of Compressive Strength	0.8
Specific Material weight	2.300E-02 MN/mE+3
Coefficient of Thermal Expansion	1.200E-05 1/k
Fixed Crack Model Coefficient	1.000

Table -3.3 :- Material properties of reinforcement

Properties	Value
Elastic Modulus	2.100E+05 MPA
Yield strength	415.000 MPA
Specific material weight	7.850E-02 MN/mE+3
Coefficient of thermal expansion	1.200E-05 1/K

3.10.2 Step wise procedure for F.E. modeling with ATENA

Modeling in ATENA is divided into three parts.

Preprocessing :- This window allows the definition of various material properties, shape, dimensions, supporting conditions, monitoring points & loads on structure.

Analysis :- After defining the various material properties, geometry, supports & loading conditions of structure, F.E. analysis are preformed in analysis window.

Post processing :- After the F.E. analysis of structure is completed, results are shown in post processing window.

Procedure: In pre-processing window following steps are performed :-

Step1: Geometry of F.E. model is created .

Step2: Material properties are assigned to the various elements of F.E. model.

Step3: Supports and various constraints, loadings and monitoring points are defined.

Step4: Finite element meshing parameters are given and meshing of the model is generated accordingly.

Step5: Various analysis steps are defined. The definition of analysis steps includes loading increments & type of solution parameter to be used.

F.E. model of the different joints & frame created in ATENA is shown in following figures :

F.E. models of joint P.C.1

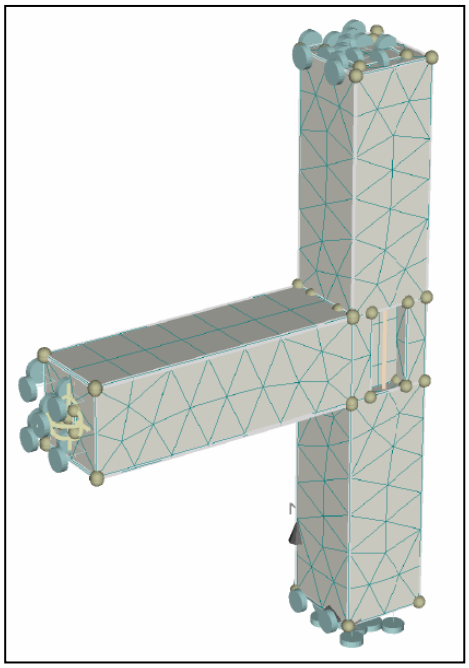

Figure 3.19a – F.E. model of P.C.1 (With surface)

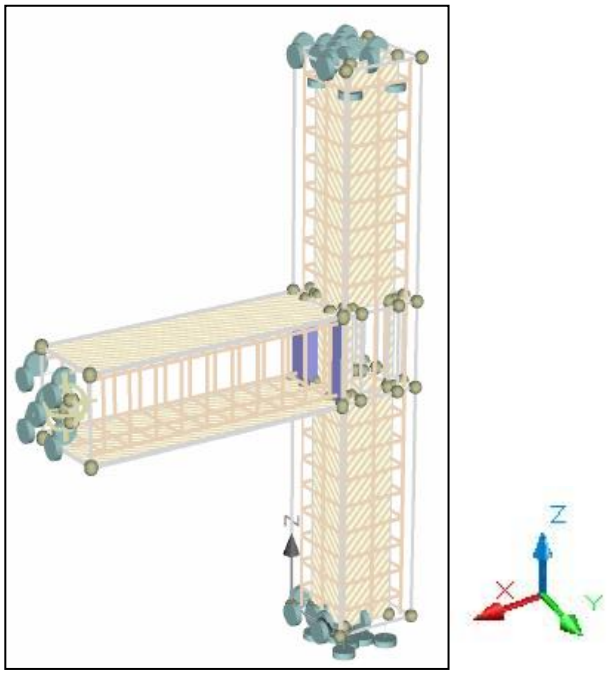

Figure 3.19b – F.E. model of P.C.1 (Without surface)

Shaded area in **Fig. 3.19b** represents contact between surfaces. At the interface of beam & column, contact surface has been edited to no connection as per the configuration of joint. Top & bottom surface of the column has been restrained in all 3 directions i.e. in X, Y & Z direction. End surface of the beam has been restrained in X & Y direction & is free in Z direction. Deformations has been applied in the center of beam at the free surface in Z direction (downward direction). Monitoring point is also placed at this point to monitor the reactions which the beam will give against the deformations applied.10mm thick steel plate has been added at the top & bottom of beam surface in order to avoid local failure of beam & to bring the joint action in place against deformations applied.

F.E. models of joint P.C.2

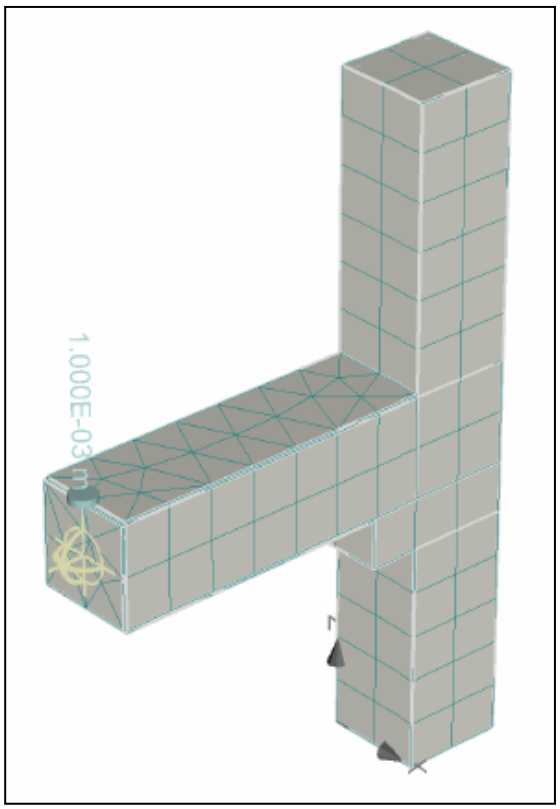

Figure 3.20a – F.E. model of P.C.2 (With surface)

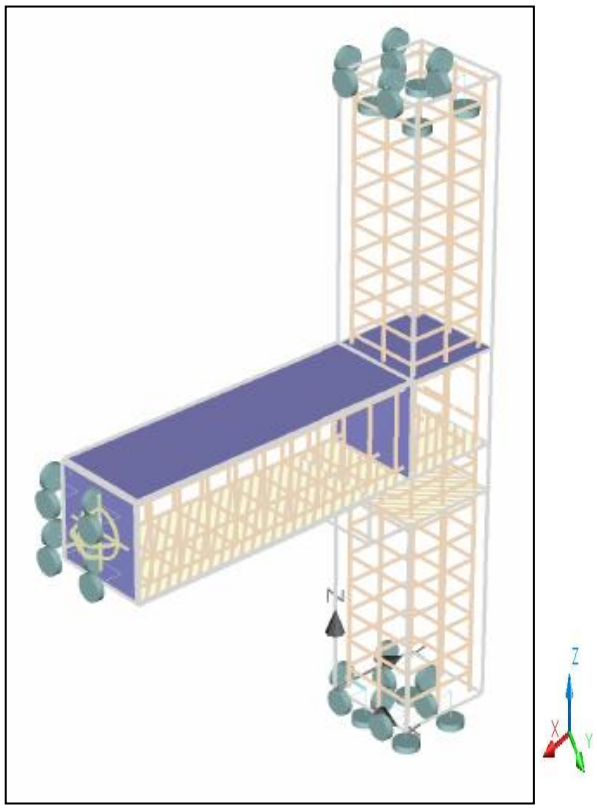

Figure 3.20b – F.E. model of P.C.2 (Without surface)

Shaded area in **Fig. 3.20b** represents contact between surfaces. At the interface of beam & column i.e. at the junction of precast & cast in situ concrete contact surface has been edited to no connection as per the configuration of joint. Top & bottom surface of the column has been restrained in all 3 directions i.e. in X, Y & Z direction. End surface of the beam has been restrained in X & Y direction & is free in Z direction. Deformation has been applied at the center of beam at free surface in Z direction. Monitoring point is also placed at this point to monitor the reactions which the beam will give against the deformations applied. 10mm thick steel plate has been added at the top & bottom of beam surface in order to avoid local failure of beam & to bring the joint action in place against deformations applied.

F.E. models of joint P.C.3

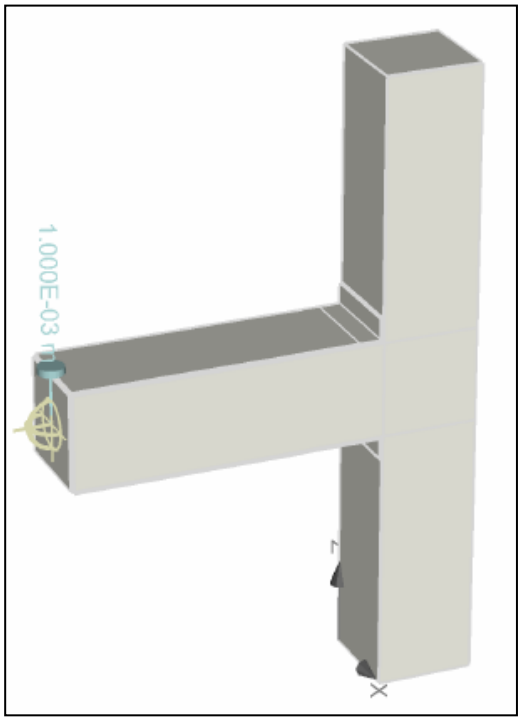

Figure 3.21a – F.E. model of P.C.3 (With surface)

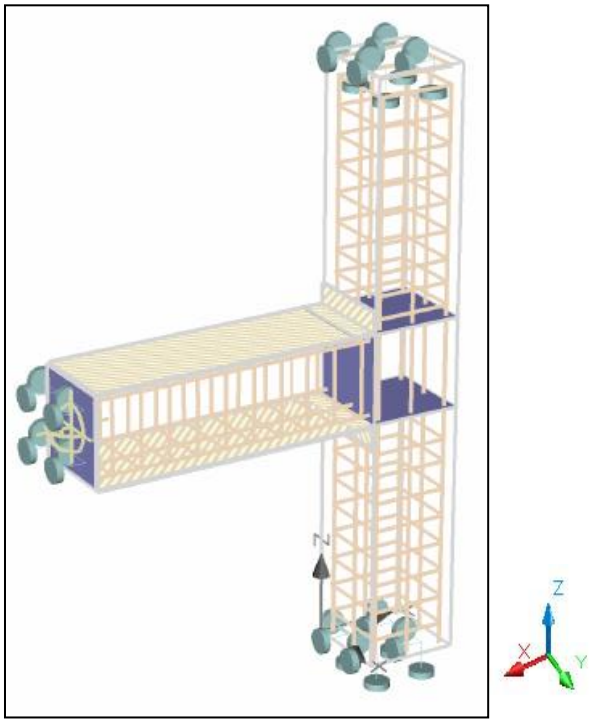

Figure 3.21b – F.E. model of P.C.3 (Without surface)

Shaded area in **Fig. 3.21b** represents contact between surfaces. At the interface of beam & column contact surface has been edited to no connection as per the configuration of joint .Top & bottom surface of the column has been restrained in all 3 directions i.e. in X, Y & Z direction. End surface of the beam has been restrained in X & Y direction & is free in Z direction. At the interface of beam & column cleat angels are modeled using elastic isotropic materials which are used to form the joint. Contact surface between cleat angles & concrete has been given as perfect connection so as to transfer forces to the cleat angles. Deformation has been applied at the center of beam at free surface in Z direction. Monitoring point is also placed at this point to monitor the reactions which the beam will give against the deformations applied.10mm thick steel plate has been added at the top & bottom of beam surface in order to avoid local failure of beam & to bring the joint action in place against deformations applied.

F.E. models of a frame :-

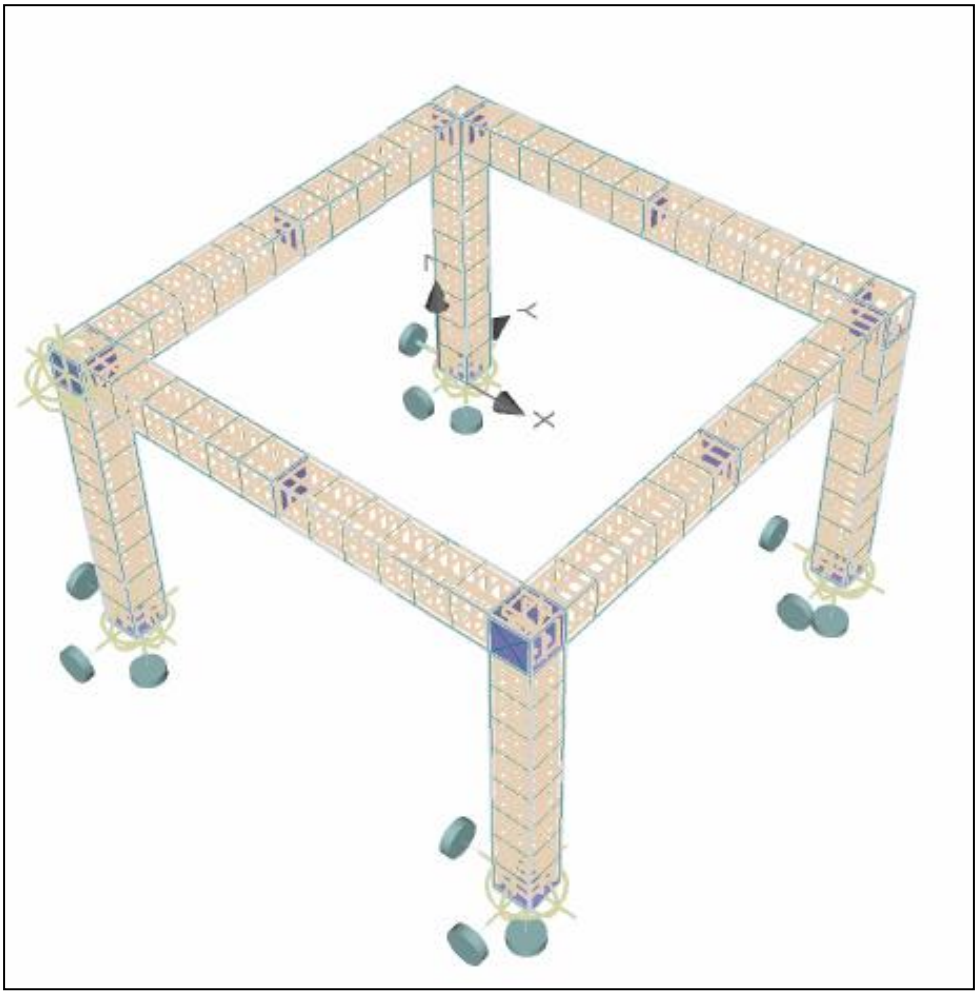

Figure 3.22 – F.E. model of Frame (Without surface)

F.E. model for a typical frame is shown in figure 3.22. Base of the column is restrained in all three directions Deformation are given at the end of beam column joint in Y direction. Reactions are monitored at the base of the column

Step6: After creating the geometry of structure & defining other parameters for F.E. modeling such as meshing , definition of loads & supports etc the analysis of structure are then started. In this work the F.E. meshing of the structure is done by using brick element. The element size used in this work is taken as 200mmx200mm as this size was sufficient to easily mesh the structure with sufficient finite elements to achieve reliable results with available computational power. The FE non-linear analysis is done in Run window. The FE non-linear static analysis calculates the effects of steady loading conditions on a structure, while ignoring inertia and damping effects, such as those caused by time-varying loads. A

static analysis can, however, include steady inertia loads (such as gravity and rotational velocity), and time-varying loads that can be approximated as static equivalent loads (such as the static equivalent wind and seismic loads commonly defined in many building codes).
Static analysis is used to determine the displacements, stresses, strains, and forces in structures or components by loads that do not induce significant inertia and damping effects.

Step7: When the FE non linear static analysis is completed the, the results are shown in third part of the ATENA i.e. Post processing. The stress- strain values at every step, crack pattern and cracks propagation at every step shown help in to analyze the behavior of the elements at every step of load deflection.

3.11 METHODS FOR NON-LINEAR SOLUTION [21]

The best part of the ATENA is the simpler way of solving the non-linear structural behavior through finite element method and its incremental loading criteria. Different methods are available in ATENA for solving non-linear equations such as, linear method, Newton-Raphson Method, Modified Newton-Raphson method, Arc Length methods are used in ATENA.
Among these the Newton-Raphson Method and Modified Newton-Raphson Method are more commonly used methods. In our present study, Newton-Raphson method is used for solving the simultaneous equations. It is an iterative process of solving the non-linear equations.
One approach to non-linear solutions is to break the load into a series of load increments. The load increments can be applied either over several load steps or over several sub steps within a load step. At the completion of each incremental solution, the program adjusts the stiffness matrix to reflect the nonlinear changes in structural stiffness before proceeding to the next load increment. .
The ATENA program overcomes this difficulty by using Full Newton-Raphson method, or Modified Newton-Raphson method, which drive the solution to equilibrium convergence (within some tolerance limit) at the end of each load increment. In Full Newton-Raphson method, it obtains the following set of non-linear equations:

$K(p)\,\Delta p = q - f(p)$

where: q is the vector of total applied joint loads,

$f(p)$is the vector of internal joint forces,

Δp is the deformation increment due to loading increment,

p are the deformations of structure prior to load increment, $\boldsymbol{K}(p)$ is the stiffness matrix, relating loading increments to deformation increments.

Figure 3.23 illustrates the use of Newton-Raphson equilibrium iterations in nonlinear analysis. Before each solution, the Newton-Raphson method evaluates the out-of -balance load vector, which is the difference between the restoring, forces (the loads corresponding to the element stresses) and the applied loads. The program then performs a linear solution, using the out-of -balance loads, and checks for convergence. If convergence criteria are not satisfied, the out-of-balance load vector is re-evaluated, the stiffness matrix is updated, and a new solution is obtained. This iterative procedure continues until the problem converges. But sometimes, the most time consuming part of the Full Newton-Raphson method solution is the re-calculation of the stiffness matrix $\boldsymbol{K}$ ($pi-1$) at each iteration. In many cases this is not necessary and we can use matrix $\boldsymbol{K}$ ($p0$) from the first iteration of the step. This is the basic idea of the so-called Modified Newton-Raphson method. It produces very significant time saving, but on the other hand, it also exhibits worse convergence of the solution procedure. The simplification adopted in the Modified Newton-Raphson method can be mathematically expressed by: $K(pi-1) = K(p0)$

The modified Newton-Raphson method is shown in **Figure 3.23** Comparing **Figure3.23** and **Figure3.24** it is apparent that the Modified Newton-Raphson method converges more slowly than the original Full Newton-Raphson method. On the other hand a single iteration costs less computing time, because it is necessary to assemble and eliminate the stiffness matrix only once. In practice a careful balance of the two methods is usually adopted in order to produce the best performance for a particular case. Usually, it is recommended to start a solution with the original Newton-Raphson method and later, i.e. near extreme points, switch to the modified procedure to avoid divergence.

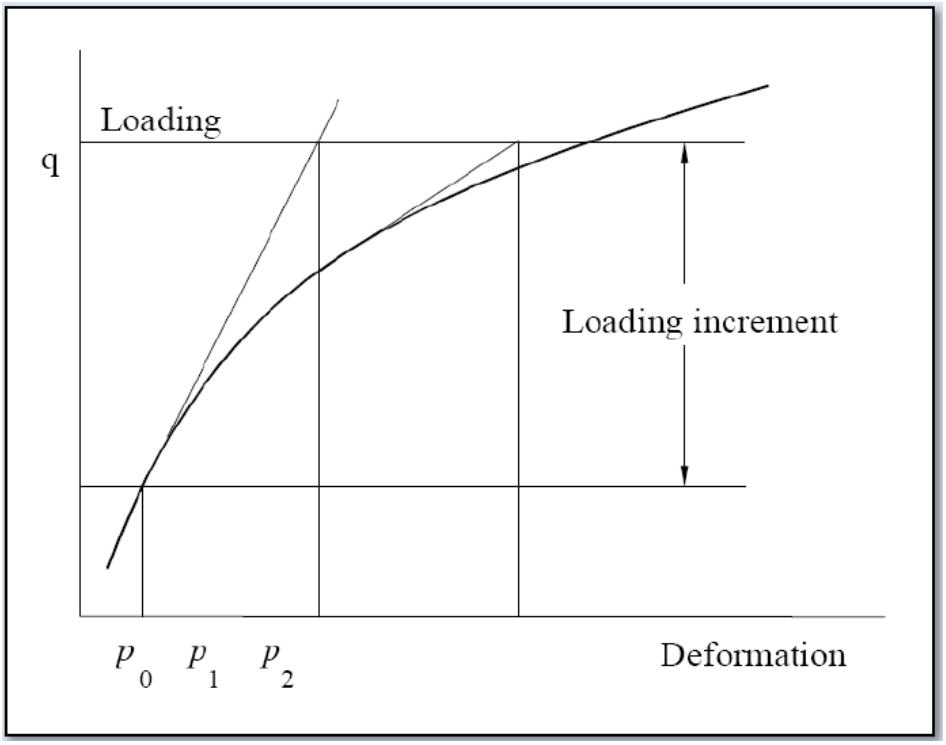

Figure 3.23 Full Newton-Raphson Method [21]

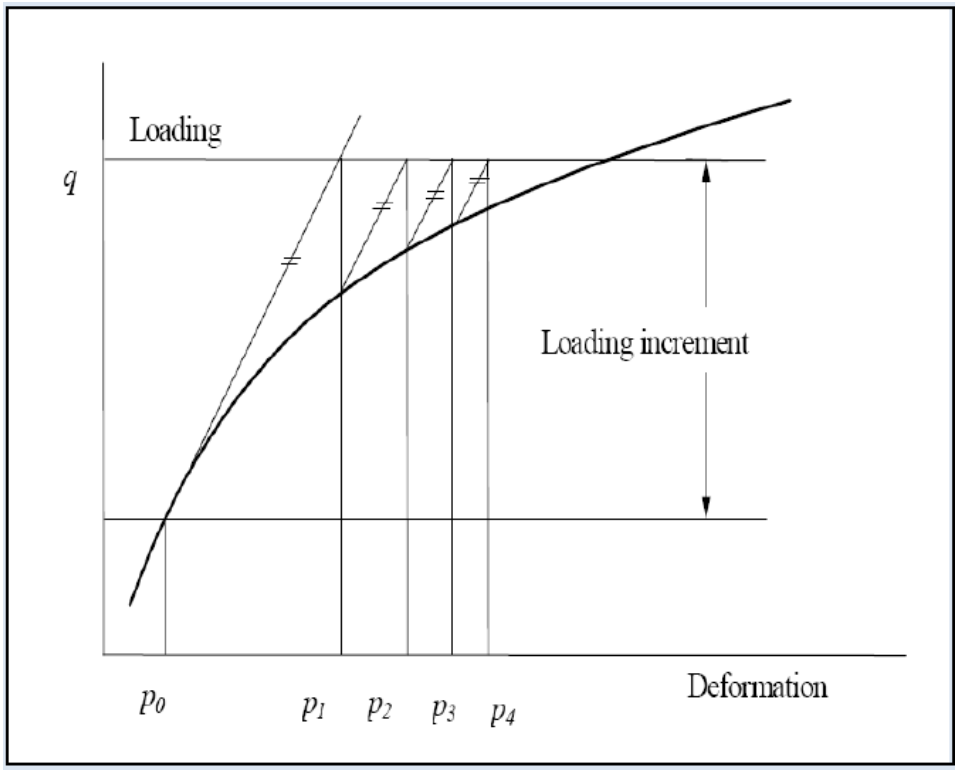

Figure 3.24 Modified Newton-Raphson Method [21]

CHAPTER-4
RESULTS & DISCUSSIONS

This chapter presents the results of finite element analysis of precast beam - column joints & frame under deformation controlled loading pattern previously discussed using ATENA software. The various results discussed includes load deflection curve for investigated joints, cracks development pattern, deformed shape under different loads & stress contours.

4.1 Finite element analysis results of beam – column joint under monotonic loading

The geometry, location of point of application of displacement & location of monitoring points for recording reactions against deformation for all joints are described in previous chapter.

4.1.1 Load displacement relations for beam – column joint M.C.1 under monotonic displacements.

The graph showing load-displacement relationship for control specimen M.C.1 is shown in fig 4.1. & its deformed shapes with crack development at various stages is shown in fig 4.2 to 4.5. From this graph it can be seen that peak reaction of 139 K.N. in M.C.1 occurs at the deformation of 3mm at its free end. After this there is a change in stiffness of joint due to cracking of concrete in joint region & stiffness of joint decreases thus at the displacement of 6mm at free end the recorded reaction at monitoring point falls to 83 K.N. From the displacement of 6mm up to the displacement of 12mm the yielding of steel occurs & reactions recorded are having almost same value. After the yielding of steel there is a sharp decrease in the stiffness of joint & deformation starts to increase rapidly with lesser restraint from joint. Beyond the displacement of 30mm the value of recorded reactions gets stable with increase in displacement indicating the failure of joint. The result from this joints are taken as reference for accessing the behavior of precast joints in comparison to monolithic joint.

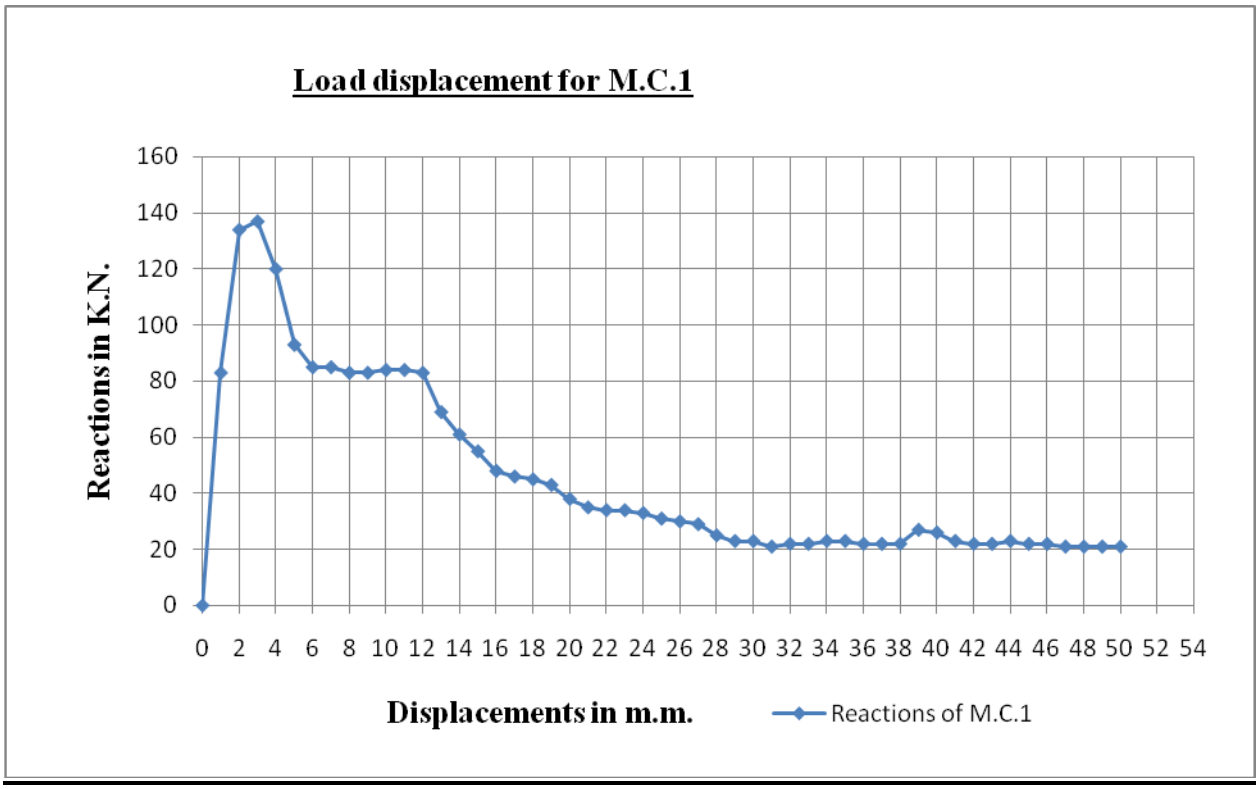

Figure 4.1 - Load displacement for M.C.1 under monotonic loading

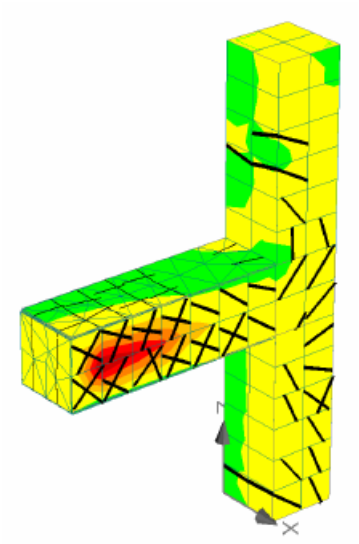

Fig 4.2 :- Deformed shape at 3mm displacement.

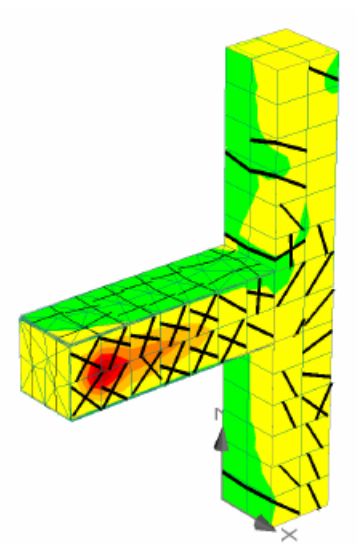

Fig 4.3 :- Deformed shape at 4mm displacement.

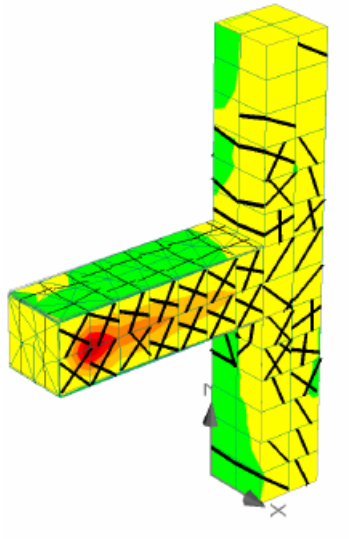

Fig 4.4 :- Deformed shape at 11mm displacement.

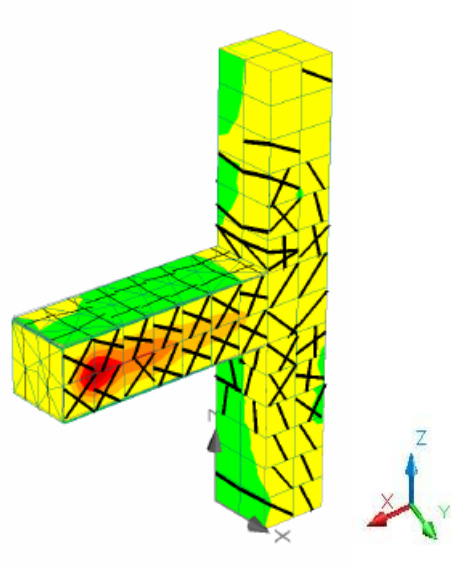

Fig 4.5 :- Deformed shape at 12mm displacement.

4.1.2 Load displacement relations for beam – column joint P.C.1 under monotonic displacement increments.

The graph showing load-displacement relationship for joint P.C.1 is shown in fig 4.6. & its deformed shapes with crack development at various stages are shown in fig 4.7 to 4.8. From this graph it can be seen that peak reaction of 137 K.N. in P.C.1 occurs at the deformation of 5mm at its free end. After this there is a uniform decrease in stiffness of joint partially due to cracking of concrete around precast key joint, partially due to beginning of yielding of steel & also due to slipping of steel that comes from precast beam & fits into precast column core filled with cast in situ concrete. After achieving the highest reactions against deformations, this joint configurations is not able to give much resistance to deformation with sharp decrease in load carrying capacity of joint. At the displacement of 22mm recorded reactions at monitoring points falls to 60 K.N. The recorded reactions at monitoring point remains almost stable further indicating the high yielding and formation of plastic hinges thus it can be said that joint has failed. The behavior of joint P.C.1 is satisfactory as it gives higher reactions against deformations applied at free ends & also have sufficient ductility to giving alarming deformations before failure.

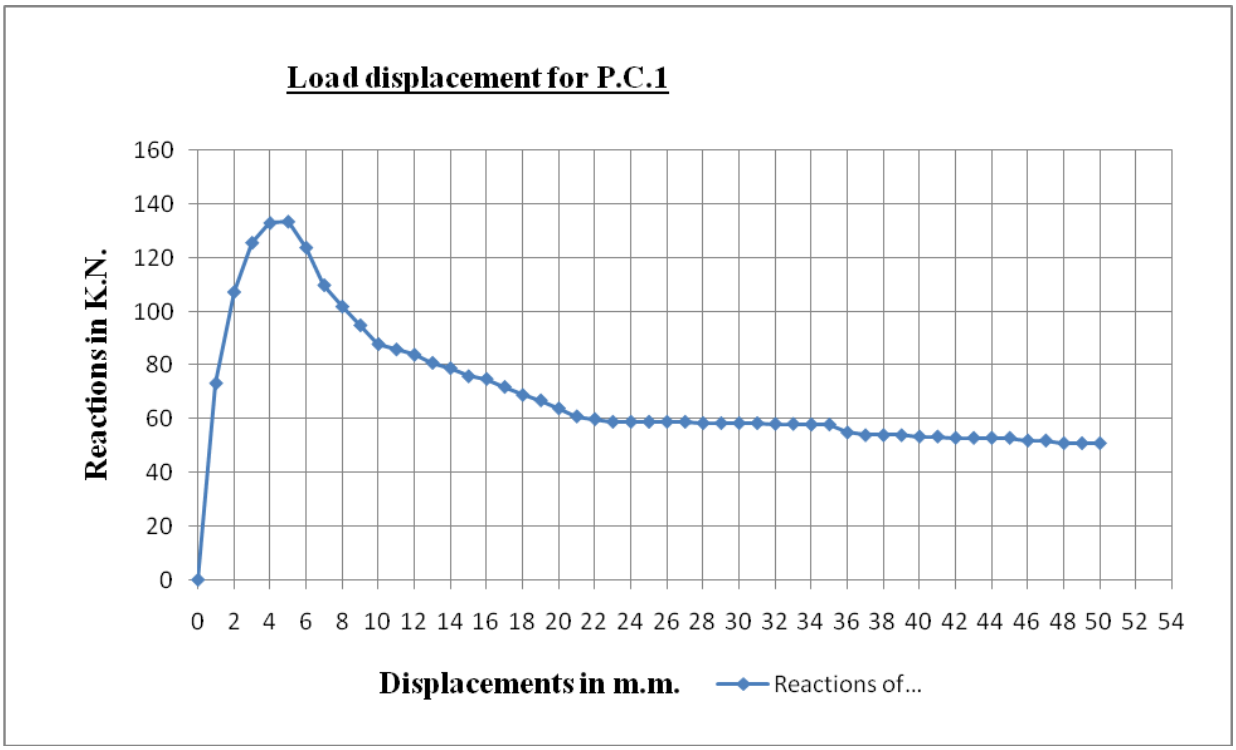

Figure 4.6 - Load displacement for P.C.1 under monotonic loading

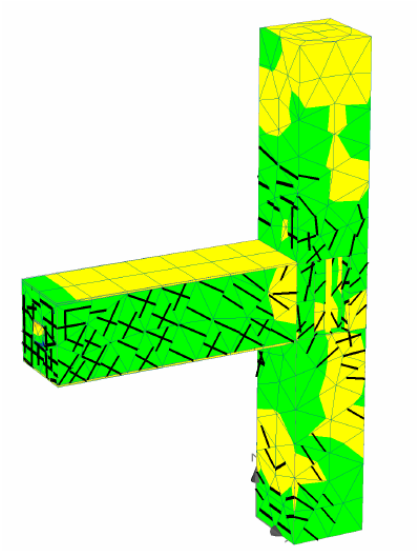

Fig 4.7 :- Deformed shape at 5mm displacement.

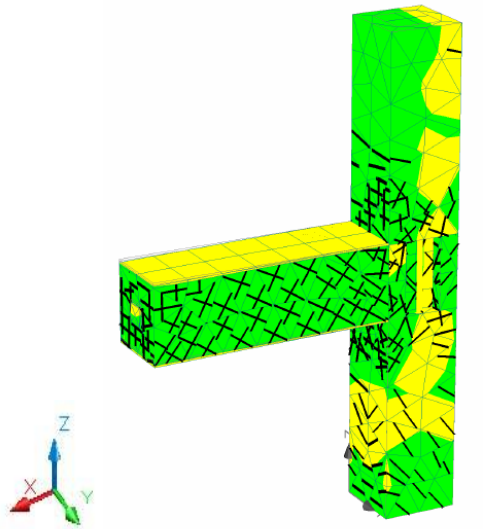

Fig 4.8 :- Deformed shape at 12mm displacement.

4.1.3 Load displacement relations for beam – column joint P.C.2 under monotonic displacements.

The load-displacement relationship graph for joint P.C.2 is shown in fig 4.9. & its deformed shapes are shown in fig 4.10 to 4.13. From this graph it can be seen that peak reaction of 117 K.N. in P.C.2 occurs at the deformation of 2mm at its free end. After this there is a sharp decrease in the load carrying capacity of joint as the recorded reactions at monitoring point falls to 30 K.N. at the displacement of 12mm at free end. This abrupt decrease in the stiffness of the joint is due to configuration of joint. As in this joint precast beam rests upon corbel protruding from column & joint is made by placing cast in place concrete in joint region, once the slipping of steel in joint region starts & crushing of concrete in corbel takes place there is an immediate decrease in stiffness of joint & it behaves in brittle manner. As the reactions against applied deformation are quite less after the displacement of 12mm & their as a continuous increase in displacements after this without change in recorded reactions, the joint can be said to be failed.S

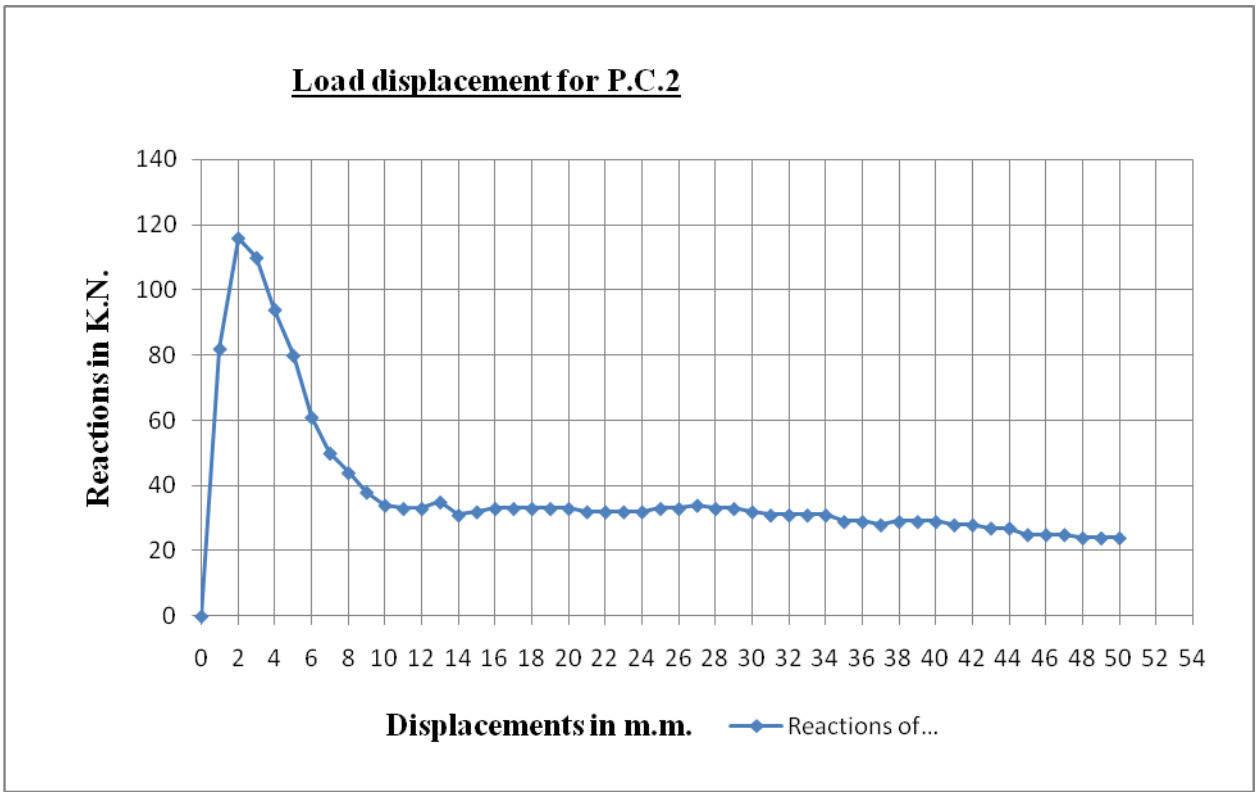

Figure 4.9 - Load displacement for P.C.2 under monotonic loading

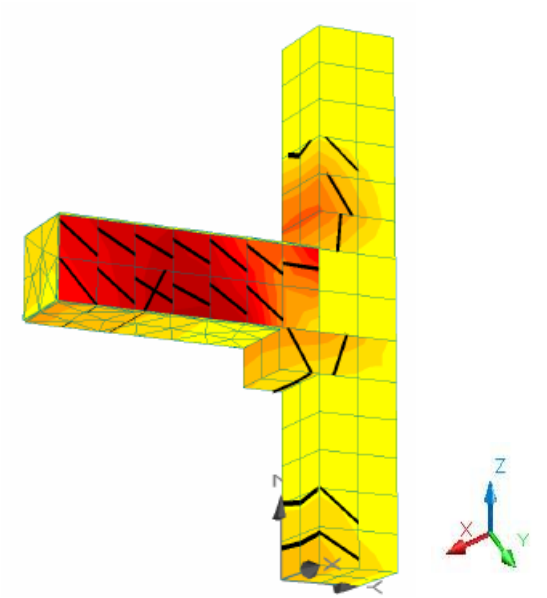

Fig 4.10 :- Deformed shape at 2mm displacement.

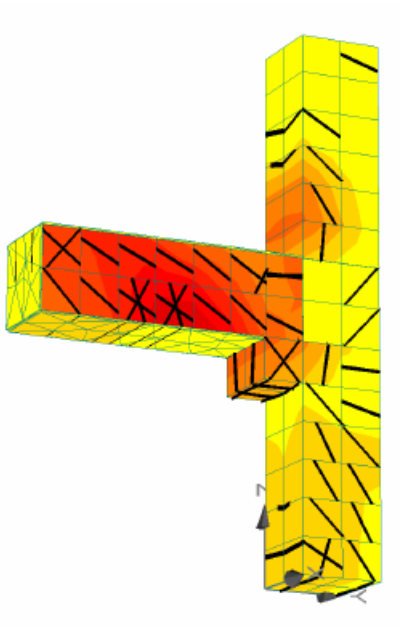

Fig 4.11 :- Deformed shape at 3mm displacement.

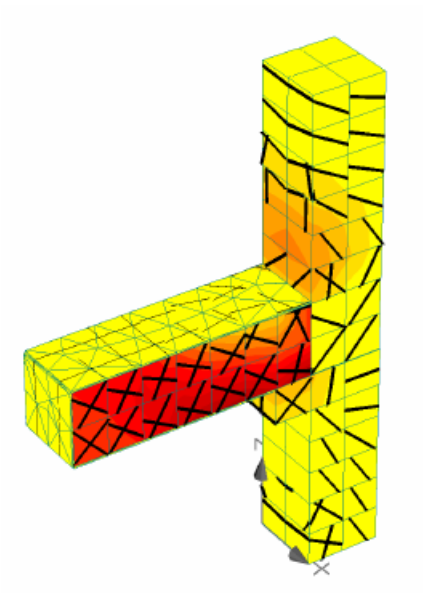

Fig 4.12 :- Deformed shape at 5mm displacement.

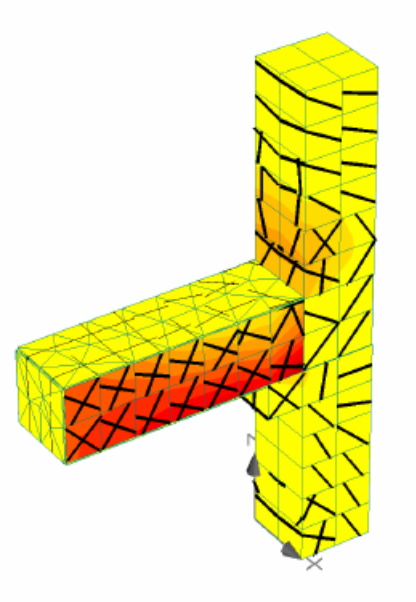

Fig 4.13 :- Deformed shape at 12mm displacement.

4.1.4 Load displacement relations for beam – column joint P.C.3 under monotonic displacements.

The load-displacement relationship graph for P.C.3 is shown in fig 4.14. & its deformed shapes are shown in fig 4.15 to 4.16. The maximum recorded reaction of 135 K.N. in this joint occurs at the displacement of 3mm at its free end. As most of the resistance to applied deformations in this joint is given by cleat angels, once the connecting cleat angels looses their grip with the joint their resistance to deformation decreases and thus recorded value of reactions at monitoring points also decreases. The strength of this joint depends upon connecting cleat angels & mode of their connection with structural elements. The result from the analysis can be used to find the best suitable size of connecting angels for desirable strength of joint.

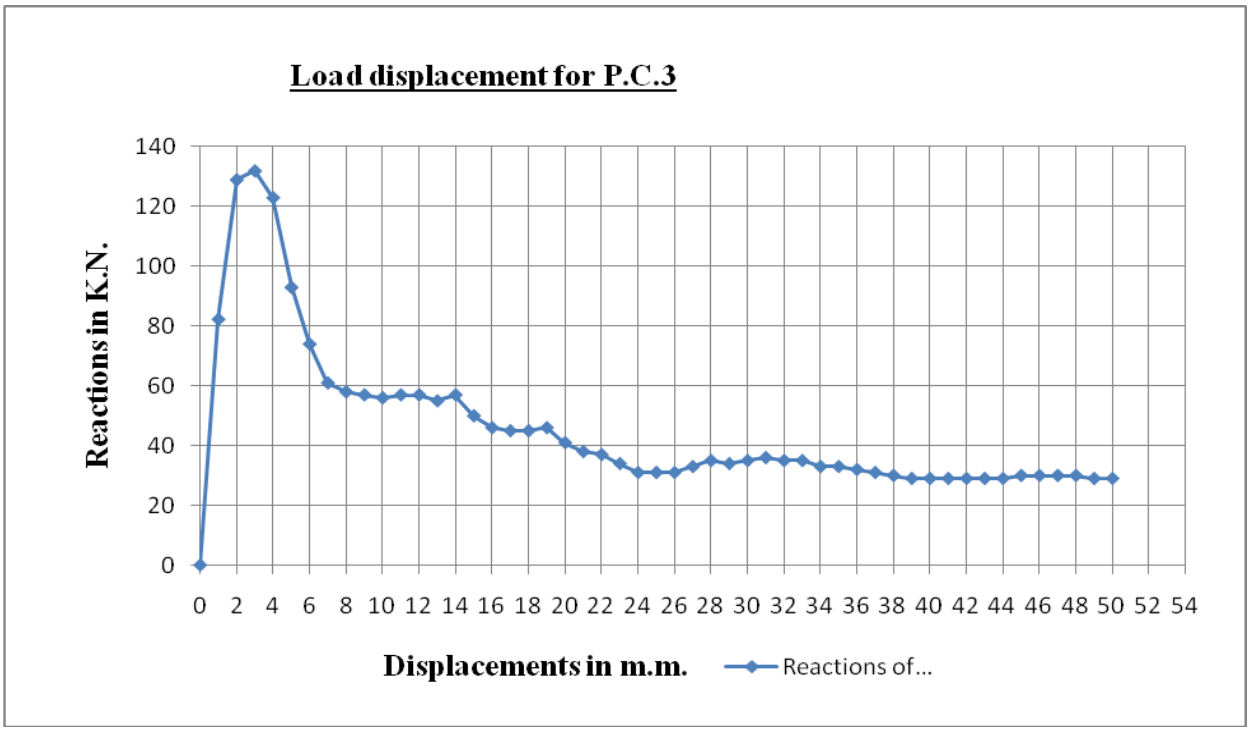

Figure 4.14 :- Load displacement for P.C.3 under monotonic loading

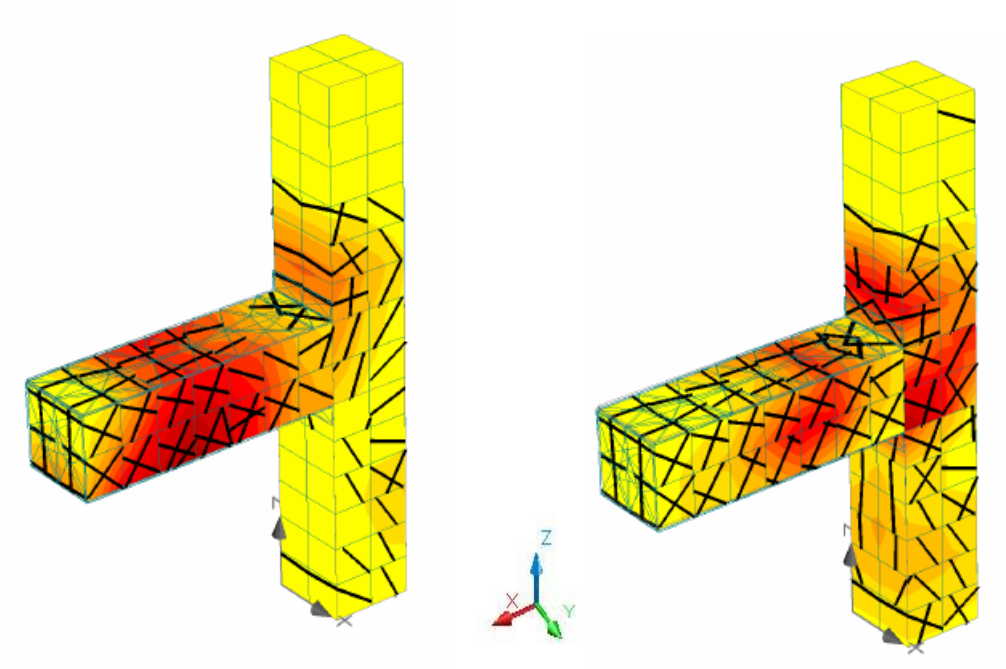

Fig 4.15 :- Deformed shape at 4mm displacement.

Fig 4.16 :- Deformed shape at 8mm displacement.

4.2 Comparison of load displacement relations of all joints under monotonic displacements.

The combined displacement V/S reaction graph for all joints is shown in fig. 4.9

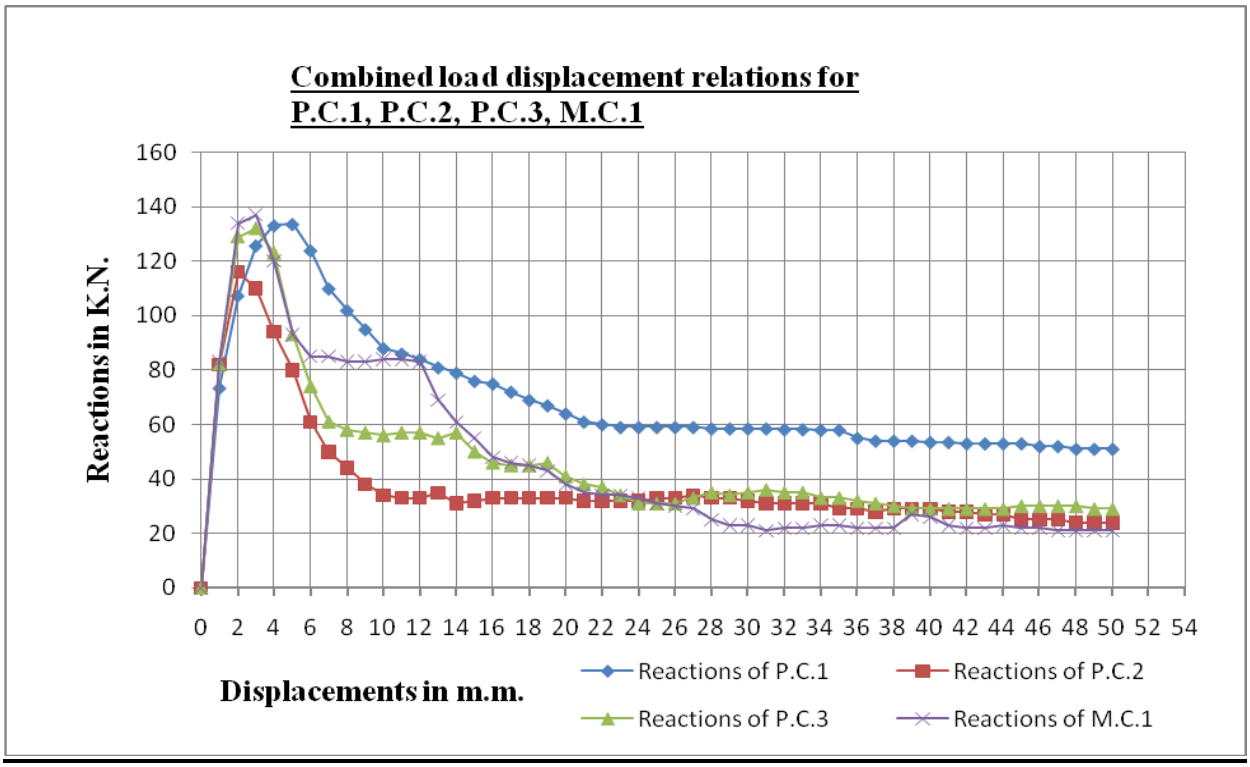

Figure 4.17 :- Load displacement relations for all joints under monotonic loading

Table 4.1 - Load displacement results for P.C.1, P.C.2, P.C.3 & M.C.1 under monotonic loading

Displacement in M.M.	Reactions of P.C.1 (K.N.)	Reactions of P.C.2 (K.N.)	Reactions of P.C.3(K.N.)	Reactions of M.C.1 (K.N.)
0	0	0	0	0
1	73.4	82	82.3	83
2	107.4	**116**	129	134
3	125.8	110	**132**	**137**
4	133.2	94	123	120
5	**133.7**	80	93	93
6	124	61	74	85
7	110	50	61	85
8	102	44	58	83
9	95	38	57	83
10	88	34	56	84
11	86	33	57	84
12	84	33	57	83
13	81	35	55	69
14	79	31	57	61
15	76	32	50	55
16	75	33	46	48
17	72	33	45	46
18	69	33	45	45
19	67	33	46	43
20	64	33	41	38
21	61	32	38	35
22	60	32	37	34
23	59	32	34	34
24	59	32	31	33
25	59	33	31	31
26	59	33	31	30
27	59	34	33	29
28	58.5	33	35	25
29	58.5	33	34	23
30	58.5	32	35	23
31	58.5	31	36	21
32	58.2	31	35	22
33	58.2	31	35	22
34	58	31	33	23
35	58	29	33	23
36	55	29	32	22
37	54	28	31	22
38	54	29	30	22
39	54	29	29	27

40	53.5	29	29	26
41	53.5	28	29	23
42	53	28	29	22
43	53	27	29	22
44	53	27	29	23
45	53	25	30	22
46	52	25	30	22
47	52	25	30	21
48	51	24	30	21
49	51	24	29	21
50	51	24	29	21

4.2.1 Comparison of results of joints P.C.1 with M.C.1 under monotonic displacements

1) The maximum reaction of P.C.1 is 133.7 K.N. that occurs at the displacement lvl. of 5mm, in comparison to M.C.1 whose maximum reaction is 137 K.N. at the displacement of 3mm.
2) Thus joint P.C.1. behaved satisfactory in comparison to monolithic specimen M.C.1.
3) The joint P.C.1 can be considered more ductile in comparison to M.C.1 under gravitational loads as yielding in joint occur at higher displacements.
4) The joint P.C.1 continues to give higher reaction even after yielding of steel in joint, this can be attributed to better configuration of joint
5) Cracks development pattren of P.C.1 shows that joint fully utalise the concrete around it during deformation as cracks are uniformely distributed all around the joint

4.2.2 Comparison of results of joints P.C.2 with M.C.1 under monotonic displacements

1) The maximum reaction of P.C.2 is 116 K.N. that occurs at the displacement lvl. of 2mm, in comparison to M.C.1 whose maximum reaction is 137 K.N. at the displacement of 3mm.
2) The performane of joint P.C.2 is less then in comparison to monolithic specimen
3) The joint P.C.2 is less ductile in comparison to M.C.1 under gravitational loads as the joint yields at less displacements
4) Cracks development pattren of P.C.2 shows that joint does not properly tranfer reactions to the column during deformation and most of the cracks develops in the

corbel on which beam is resting. Failure of corbel may cause the failure of whole connection

4.2.3 Comparison of results of joints P.C.3 with M.C.1 under monotonic displacements

1) The maximum reaction of P.C.3 is 132 K.N. that occurs at the displacement lvl. of 4mm, in comparison to M.C.1 whose maximum reaction is 137 K.N. at the displacement of 3mm.
2) The load carrying capacity & ductility of joint P.C.3 depends upon the strength, yield capacity , size & connectivity I.S.A. with beam & column. The connection angle used in this investigation gives satisfactory results in comparison to M.C.1

Of all the three precast joints the behaviour of joint P.C.1 is most satisfactory under gravitational loads, owing to its better joint configuration & anchoraging with column. The behaviour of joint P.C.2 is least satisfactory as it is connected with column only by reinforcement bars & is supported by corbel prtuding from column face . Once the corbel fail it may cause imegiate failure of joint.

4.3 Finite element analysis results of beam – column joint under cyclic loading

4.3.1 :- Load displacement relations for beam – column joint M.C.1 under cyclic loading

The deformed shapes with cracks of joint M.C.1 after cyclic displacements at various cycles are shown in fig 4.18 to 4.21 & graph showing hysteretic loop or recorded reaction at monitoring point against cyclic displacements for control specimen M.C.1 is shown in fig 4.22. Table 4.2 shows total energy dissipated at completion of each cycle up to cyclic displacements of +/-20mm. The results of cyclic displacement of this joint reveals that the maximum total reaction recorded at monitoring point is at cycle of +/-2mm. After this there is degradation in strength of joint due to cracking of concrete & initial yield of steel. At the higher value of cyclic displacements this joint still shows sufficient stiffness as higher value of reactions are recorded at monitoring points. From the displacement cycle of +/-15mm to +/- 20mm the recorded reactions for this joint reduces from 88.67 K.N. to 43.71 K.N. indicating the loss of stiffness in joint.

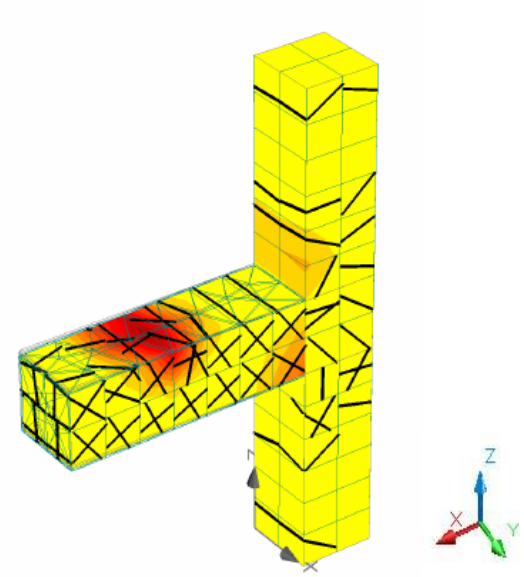

Figure 4.18 :– Deformed shape of M.C.1 under cyclic loading (+/-2 mm)

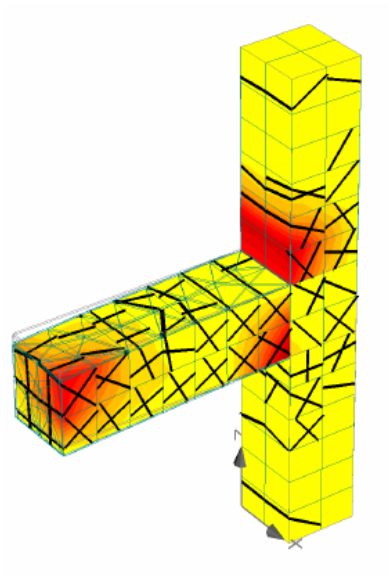

Figure 4.19 :– Deformed shape of M.C1 under cyclic loading (+/-5mm)

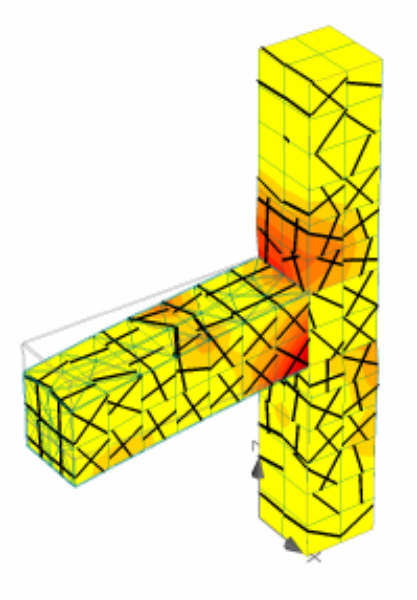

Figure 4.20 :– Deformed shape of M.C.1 under cyclic loading (+/-15 mm)

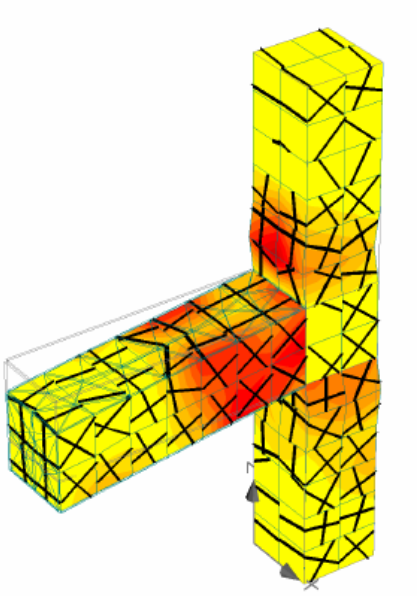

Figure 4.21 :– Deformed shape of M.C.1 under cyclic loading (+/-20mm)

Table 4.2 :- Total energy dissipated at the completion of each cycle by M.C.1 under cyclic loading

Cyclic Displacements (MM)	Total energy dissipated by M.C.1 (K.N.)
+1 ,-1	140.51
+2,-2	188.96
+3,-3	136.7
+5,-5	92.07
+8,-8	122.54
+10,-10	85.25
+15,-15	88.67
+20,-20	43.71

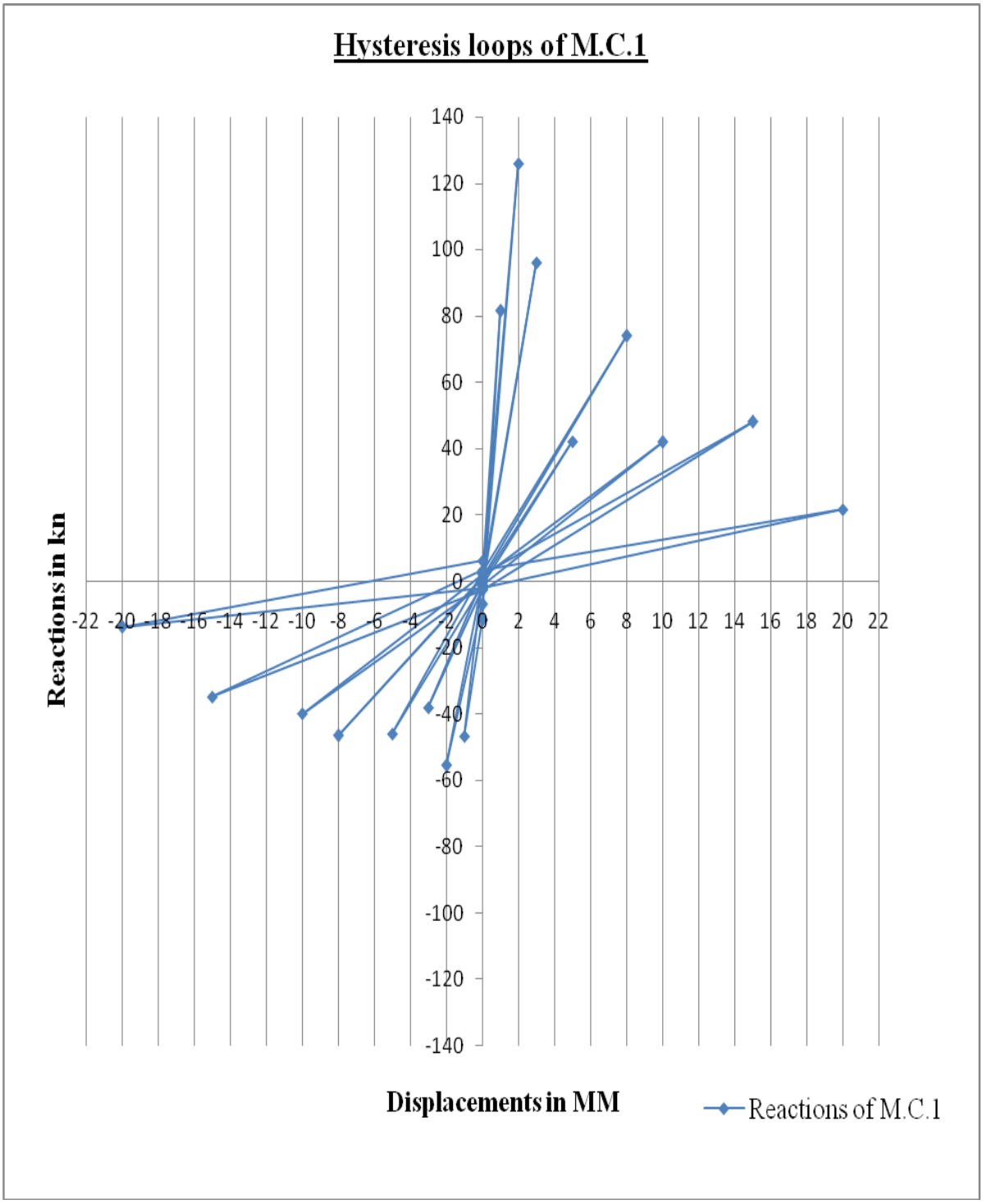

Figure 4.22 - Hysteresis loops of M.C.1

4.3.2 :- Load displacement relations for beam – column joint P.C.1 under cyclic loading

The deformed shapes with cracks of joint P.C.1 after various cyclic displacements are shown in fig 4.23 to 4.26 & graph showing hysteretic loop or recorded reaction at monitoring point against cyclic displacements for joint P.C.1 is shown in fig 4.27. Table 4.3 shows total energy dissipated at completion of each cycle up to cyclic displacements of +/-20mm. The results of cyclic displacement of this joint reveals that the maximum total reaction recorded at monitoring point is at cycle of +/-2mm. The degradation of total energy after this cycle is not to large indicating that this joint has sufficient stiffness even after larger cyclic displacements. At the higher value of cyclic displacements i.e. at cycles of +/-10mm to +/-15mm the total reactions recorded are 90.5 K.N. & 115.71 K.N. showing that the behavior of this joint is satisfactory even at higher cyclic displacement. At the cyclic displacement of +/-20mm the total energy dissipated is 66 K.N. showing the joint still has got sufficient strength. This can be attributed to the better configuration of joint. The crack pattern in the joint region shows that cracks are uniformly distributed in joint region indicating that complete joint region takes part for developing stiffness against applied cyclic deformations.

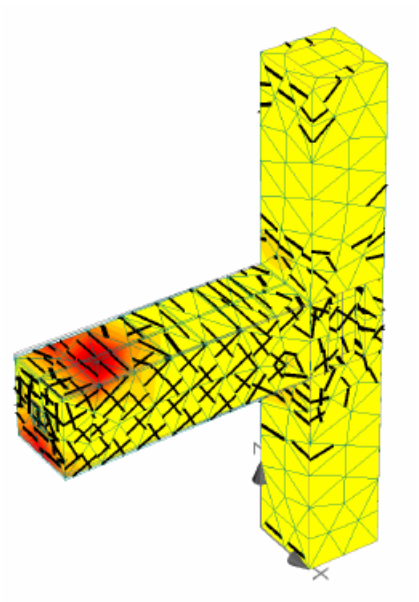

Figure 4.23 :– Deformed shape of P.C.1 under cyclic loading (+/-2 mm)

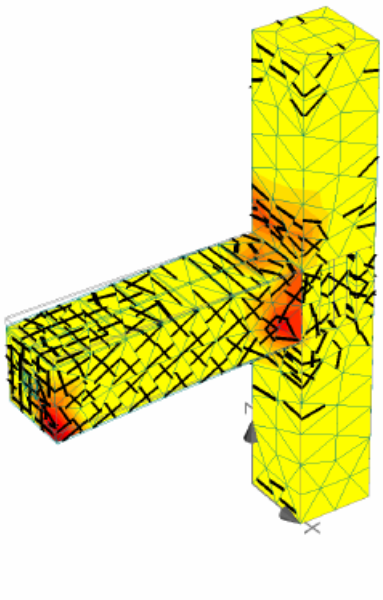

Figure 4.24 :– Deformed shape of P.C.1 under cyclic loading (+/-5mm)

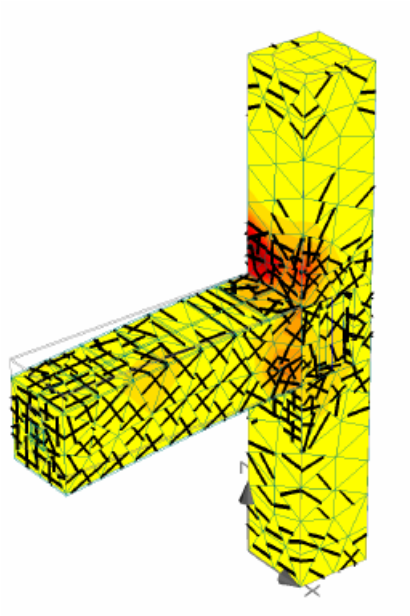

Figure 4.25 :– Deformed shape of P.C.1 under cyclic loading (+/-15 mm)

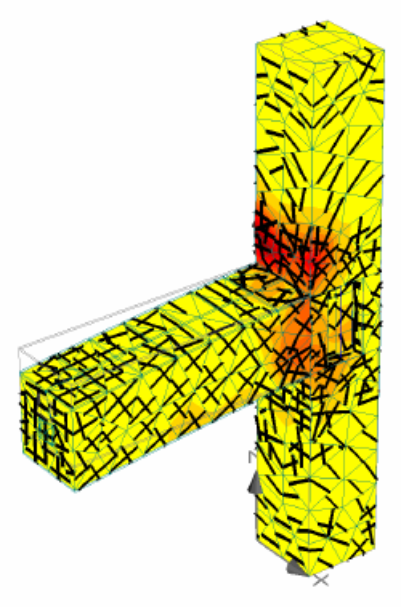

Figure 4.26 :– Deformed shape of P.C.1 under cyclic loading (+/-20mm)

Table 4.3 :- Total energy dissipated at the completion of each cycle by P.C.1 under cyclic loading

Cyclic Displacements (MM)	Total energy dissipated by P.C.1 (K.N)	Total energy dissipated by M.C.1 (K.N.)
+1 ,-1	137.1	140.51
+2,-2	171.5	188.96
+3,-3	140.8	136.7
+5,-5	95.5	92.07
+8,-8	139.5	122.54
+10,-10	90.5	85.25
+15,-15	115.71	88.67
+20,-20	66	43.71

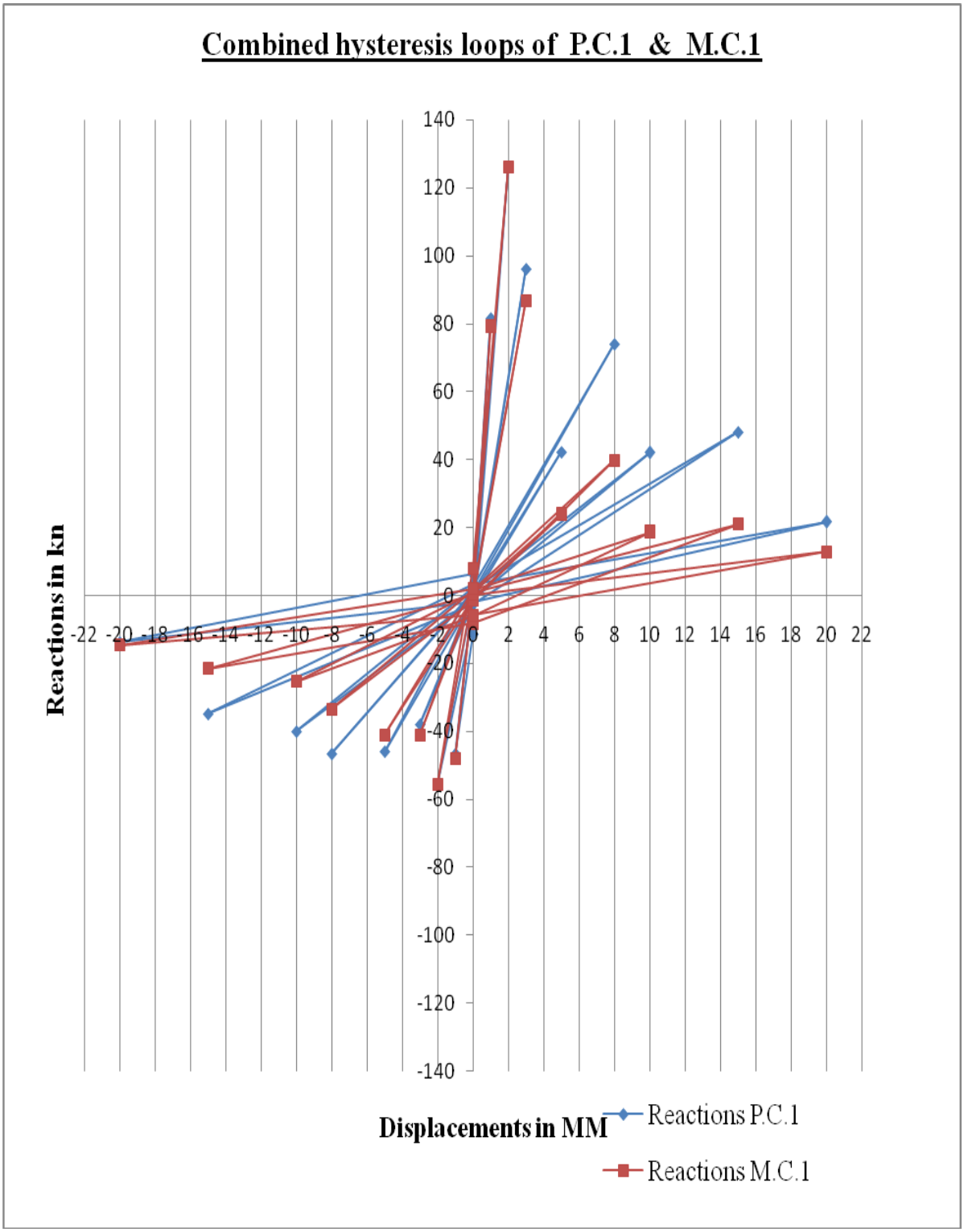

Figure 4.27 – Hysteretic loops of P.C.1 & M.C.1

4.3.3 :- Load displacement relations for beam – column joint P.C.2 under cyclic loading

The deformed shapes with cracks of joint P.C.2 after various cyclic displacements are shown in fig 4.28 to 4.31 & graph showing hysteretic loop or recorded reaction at monitoring point against cyclic displacements for joint P.C.2 is shown in fig 4.32. Table 4.4 shows total energy dissipated at completion of each cycle up to cyclic displacements of +/- 20mm. The results of cyclic displacement of this joint reveals that the maximum total reaction recorded of 189.92 K.N. at monitoring point is at cycle of +/-2mm. After this with each increasing displacement cycle the force required for resistance against displacement get reduced significantly. As the configuration of this joint is such that the resistance to displacement is given by supporting corbel from column & cast in place concrete in joint region once the displacements exceeds & cause cracking in concrete , joint is not able to give significant resistance to further cyclic displacements. At the displacement cycle of +/- 10mm to +/-15mm the total energy dissipated have almost the same value of 50 K.N. and at cycle of +/- 20mm the value is 35.35 K.N. indicating that joint has less resistance to deformation at higher value of cyclic displacements.

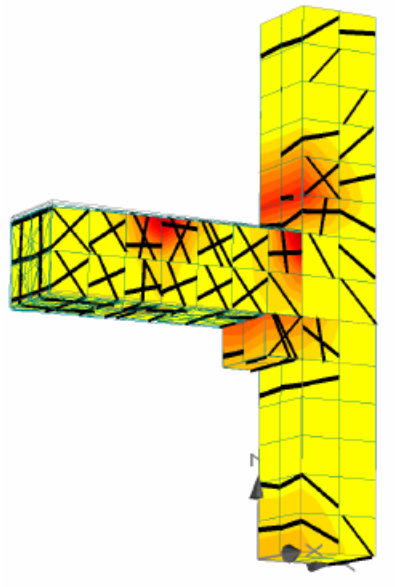

Figure 4.28 :– Deformed shape of P.C.2 under cyclic loading (+/-2 mm)

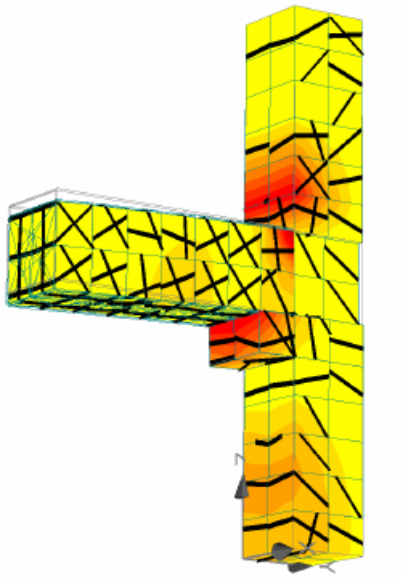

Figure 4.29 :– Deformed shape of P.C.2 under cyclic loading (+/-5mm)

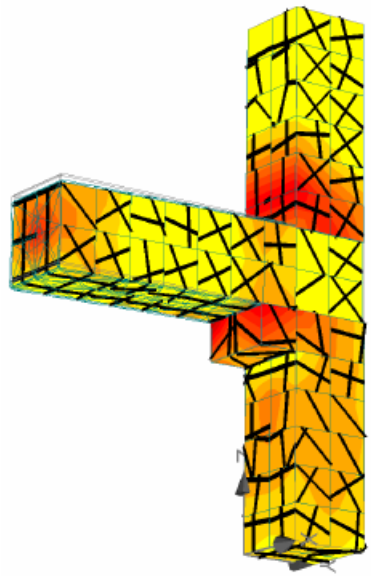

Figure 4.30 :– Deformed shape of P.C.2 under cyclic loading (+/-15 mm)

Figure 4.31 :– Deformed shape of P.C.2 under cyclic loading (+/-20mm)

Table 4.4 :- Total energy dissipated at the completion of each cycle by P.C.2 under cyclic loading

Cyclic Displacements (MM)	Total energy dissipated by P.C.2 (K.N)	Total energy dissipated by M.C.1 (K.N.)
+1 ,-1	127.85	140.51
+2,-2	189.92	188.96
+3,-3	128.79	136.7
+5,-5	66.97	92.07
+8,-8	76.17	122.54
+10,-10	50.68	85.25
+15,-15	50.91	88.67
+20,-20	35.25	43.71

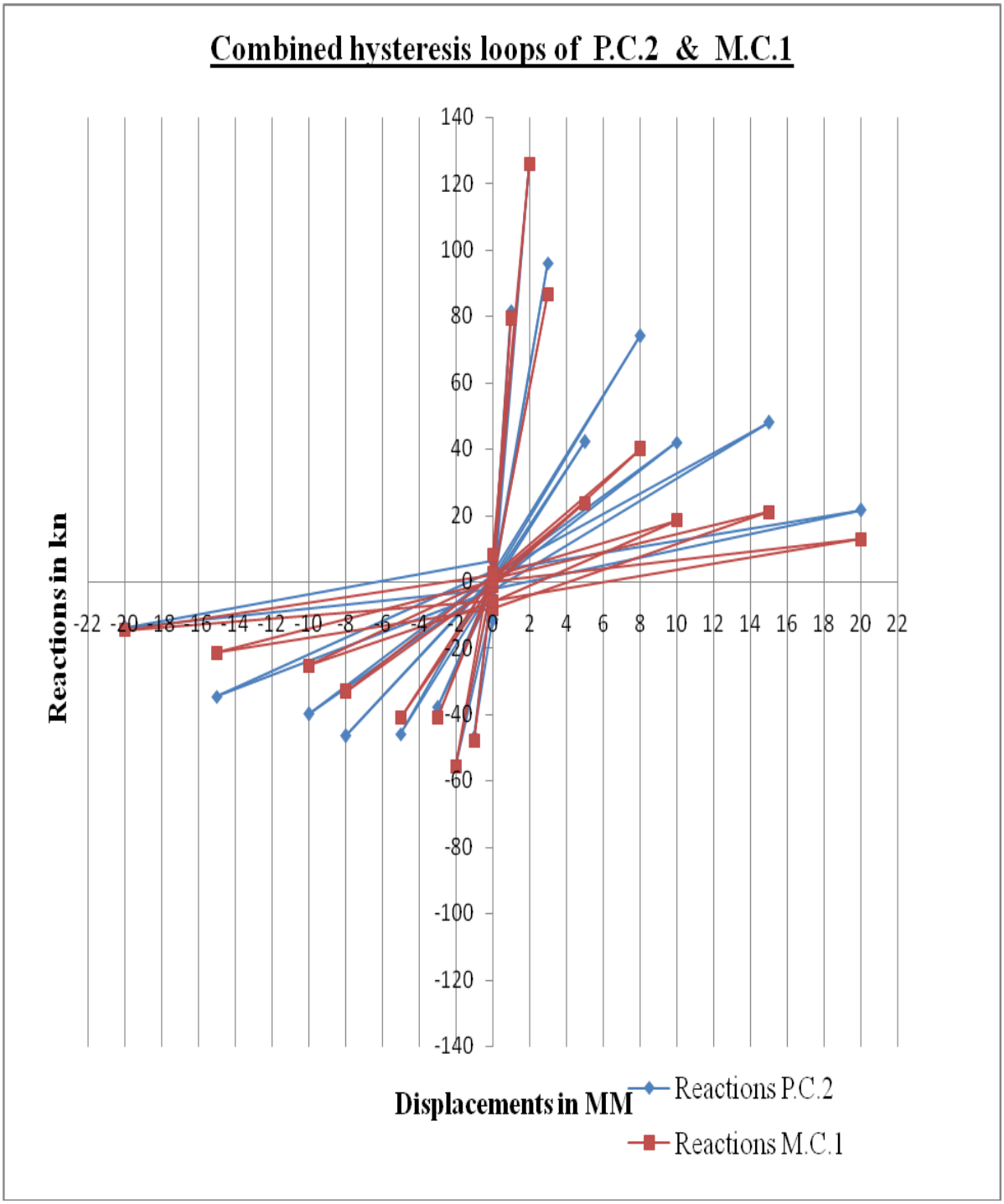

Figure 4.32- Hysteretic loops of P.C.2 & M.C.1

4.3.4 :- Load displacement relations for beam – column joint P.C.3 under cyclic loading

The deformed shapes with cracks of joint P.C.3 after various cyclic displacements are shown in fig 4.33 to 4.36 & graph showing hysteretic loop or recorded reaction at monitoring point against cyclic displacements for joint P.C.3 is shown in fig 4.37. Table 4.5 shows total energy dissipated at completion of each cycle up to cyclic displacements of +/- 20mm. The maximum energy dissipated of 190.44 K.N. in this joint is at the cyclic displacement of +/- 2mm. After the increase in displacement cycles this joint consisting of cleat angel bolted to beam & column to make a connection shows reduction in stiffness due to deformation of steel plates. At the displacement cycle of +/-8 MM the total energy dissipated is 133.83 K.N. which shows that this joint has got sufficient stiffness at this value of cyclic displacements. When the cyclic displacement are increased to +/-10mm their is a significant decrease in the stiffness of joint as the total energy dissipated at this cycle is 75.98 K.N. This decrease in resistance is due to deformation of cleat angels. With continuing increase in displacement cycles there is a continuous decrease in stiffness due to reduction in strength of cleat angels as well as separation of bond between cleat angel and joint. The behavior of this joint is satisfactory under cyclic loading.

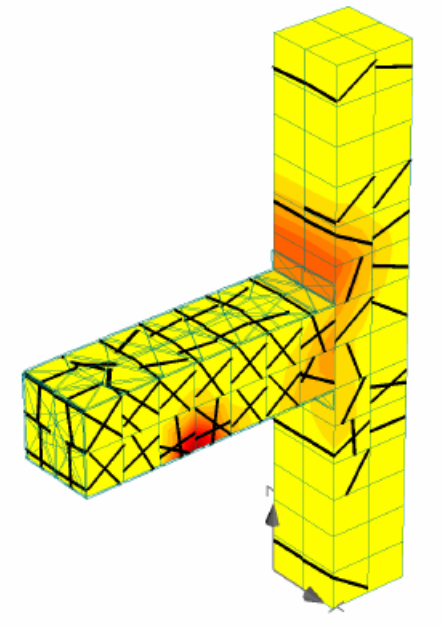

Figure 4.33 :– Deformed shape of P.C.3 under cyclic loading (+/-2 mm)

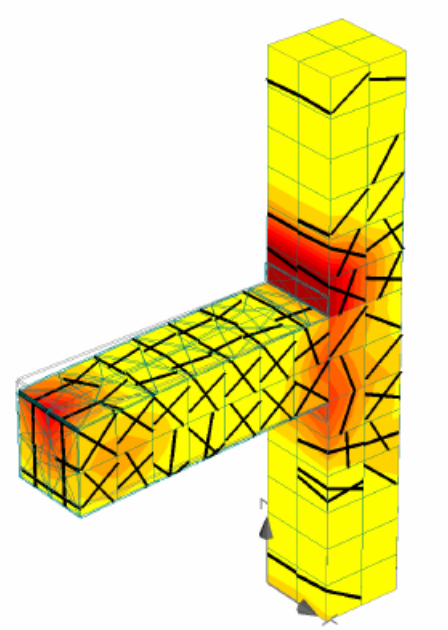

Figure 4.34 :– Deformed shape of P.C.3 under cyclic loading (+/-5mm)

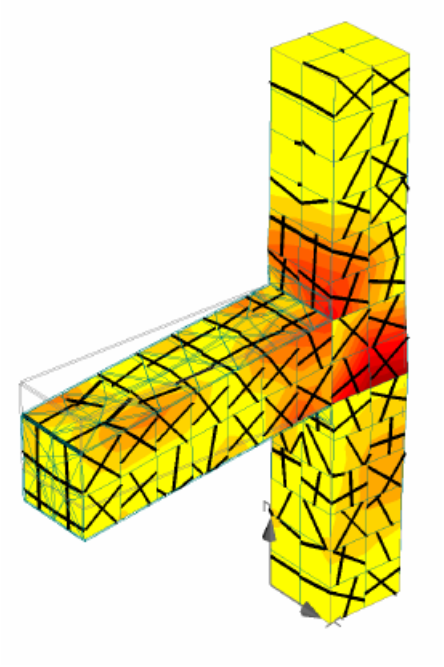

Figure 4.35 :– Deformed shape of P.C.3 under cyclic loading (+/-15 mm)

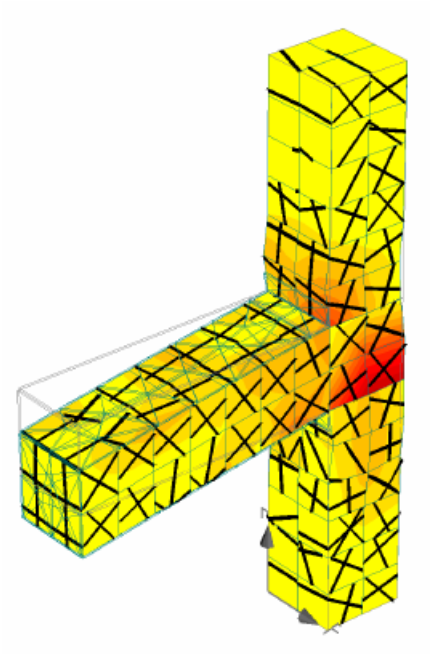

Figure 4.36 :– Deformed shape of P.C.3 under cyclic loading (+/-20mm)

Table 4.5 :- Total energy dissipated at the completion of each cycle by P.C.3 under cyclic loading

Cyclic Displacements (MM)	Total energy dissipated by P.C.3 (K.N)	Total energy dissipated by M.C.1 (K.N.)
+1 ,-1	132.53	140.51
+2,-2	190.44	188.96
+3,-3	155.72	136.7
+5,-5	99.8	92.07
+8,-8	133.83	122.54
+10,-10	75.98	85.25
+15,-15	61.61	88.67
+20,-20	51.31	43.71

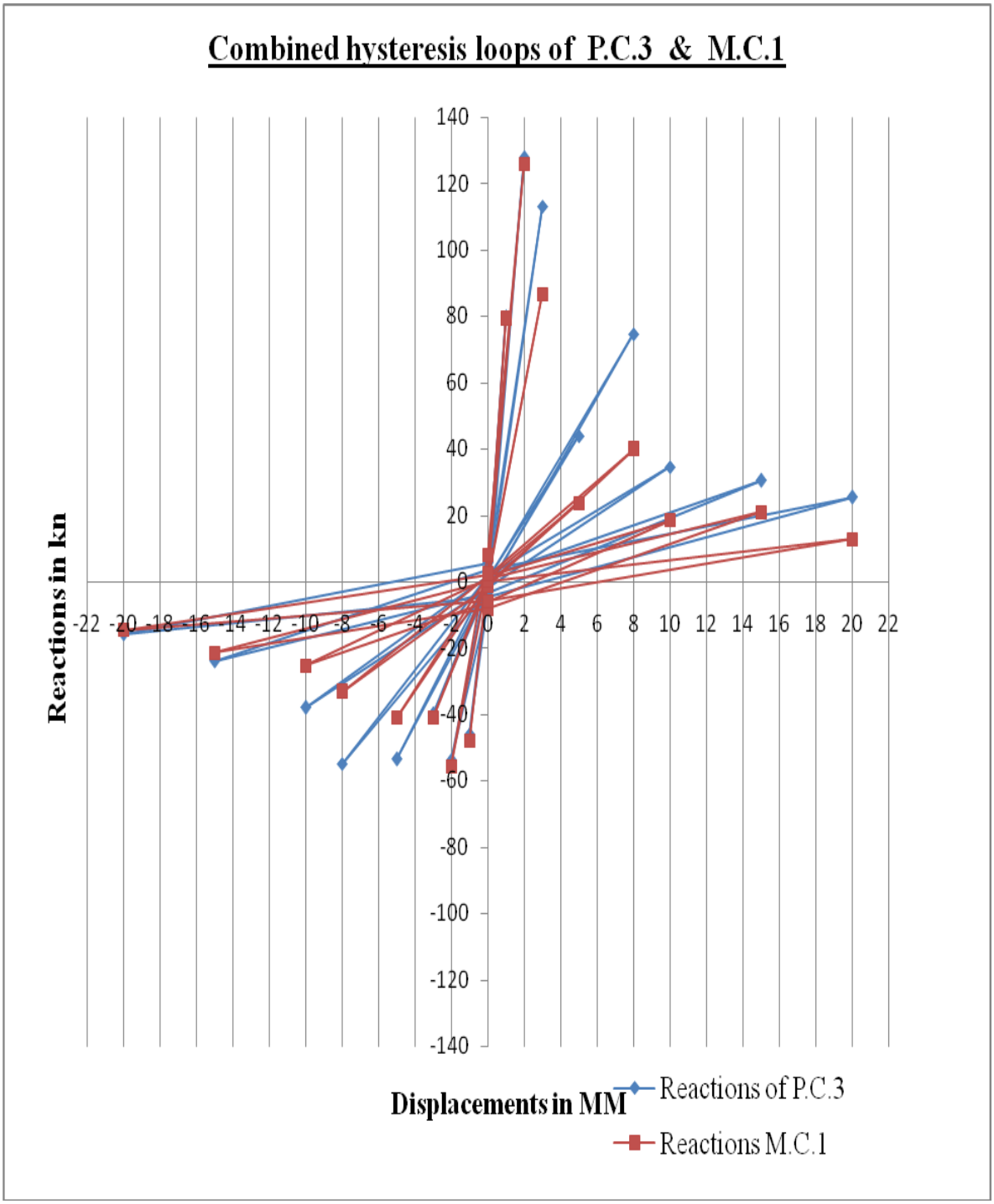

Figure 4.37- Hysteretic loops of P.C.3 & M.C.1

4.4 :- Comparison of load displacement relations of all joints under cyclic loading.

Table 4.6 :- Load displacement results for P.C.1, P.C.2, P.C.3 & M.C.1 under cyclic loading

Cyclic Displacements (MM)	Reactions of P.C.1 (K.N)	Reactions of P.C.2 (K.N.)	Reactions of P.C.3 (K.N.)	Reactions of M.C.1 (K.N.)
0	0	0	0	0
1	73	79	80	81.56
0	-9.6	0.838	-6.2	-11.6
-1	-50	-48	-46	-46.7
0	4.5	0.02	0.33	0.65
2	110	126	127.7	126
0	-11	8	-6.5	-7
-2	-45	-55.6	-54	-55.6
0	5.5	0.32	2.24	-0.36
3	92	86.67	113	96
0	-6.6	-0.42	-1.8	-2.5
-3	-41	-41	-40	-38
0	1.2	0.7	0.92	0.2
5	45.5	23.64	43.9	42.17
0	-5	-0.83	-1.8	-1.4
-5	-42	-41	-53.6	-46
0	3	1.5	0.5	2.5
8	70	39.71	74.54	74
0	-4	-1.5	-2.8	0.9
-8	-61	-33.4	-55	-46.51
0	4.5	1.56	1.49	1.13
10	40	18.5	34.45	42
0	-5	-6.2	-2	-1.2
-10	-41	-25.27	-38	-40
0	3.5	0.71	1.53	2.05
15	52.5	21	30.47	48
0	-6.11	-8.3	-3.44	-2.6
-15	-52	-21.47	-24	-34.77
0	5.1	0.14	3.7	3.3
20	39	12.77	25.35	21.55
0	-7	-5.9	-4.5	-2.11
-20	-18	-14.58	-15.91	-13.85
0	-2	2	5.55	6.2

Table 4.7 :- Total energy dissipated at the completion of each cycle by P.C.1, P.C.2, P.C.3 & M.C.1 under cyclic loading

Cyclic Displacements (MM)	Reactions of P.C.1 (K.N)	Reactions of P.C.2 (K.N.)	Reactions of P.C.3 (K.N.)	Reactions of M.C.1 (K.N.)
+1 ,-1	137.1	127.85	132.53	140.51
+2,-2	171.5	189.92	190.44	188.96
+3,-3	140.8	128.79	155.72	136.7
+5,-5	95.5	66.97	99.8	92.07
+8,-8	139.5	76.17	133.83	122.54
+10,-10	90.5	50.68	75.98	85.25
+15,-15	115.71	50.91	61.61	88.67
+20,-20	66	35.25	51.31	43.71

4.4.1 Analysis of load – displacement results of joints P.C.1 in comparison to M.C.1 under cyclic loading :-

1) The total energy dessipated by P.C.1 at the completion of ist cycle of +1,-1mm is 137.1 K.N. & that by M.C.1 is 140.51 K.N.
2) Reactions recorded during postive displacement of 2mm is 110 K.N. & that during negative dispalacement of 2mm is -45 K.N. This difference of reaction during same cycle is due to dvelopment of small micro cracks in concrete during initial displacements which give higher resistance to deformation. Once these cracks are developed, resistance to deformations are decresed, thus less reactions are recorded during opposite displacenent.
3) Once the micro cracks in concrete are fully developed & load is transferred to reinforcing bars , the difference between the reactions between same positive & negative cycle gets reduced
4) At the cyclic displacement of +5,-5mm the total energy dessipated by P.C.1 is 95.5 K.N. & that by M.C.1 is 92.07 K.N.
5) At the cyclic displacement of +20,-20mm the total energy dessipated by P.C.1 is 66 KN. & that by M.C.1 is 43.71 K.N.

From the data of energy dessipation at each cycle of P.C.1 in comparison to M.C.1 it can be seen that deterioration of strength of P.C.1 is at same rate as those of monolithic connection with increasing cyclic displacements & thus this type of joint may behave satisfactarely during cyclic deformations in strucure

4.4.2 Analysis of load – displacement results of joints P.C.2 in comparison to M.C.1 under cyclic loading :-

1) The total energy dessipated by P.C.2 at the completion of ist cycle of +1,-1mm is 127.85 K.N. & that by M.C.1 is 140.51 K.N.
2) At the cyclic displacement of +5,-5mm the total energy dessipated by P.C.2 is 66.97 K.N. & that by M.C.1 is 92.07 K.N.
3) At the cyclic displacement of +15,-15mm the total energy dessipated by P.C.2 is 50.91KN. & that by M.C.1 is 88.67 K.N.

From the data of energy dessipation at each cycle of P.C.2 in comparison to M.C.1 it can be seen that deterioration of strength of P.C.2 is much larger with increasing cyclic displacements & thus this type of joint may not behave satisfactarely during cyclic deformations in strucure. The reason behind this is that once the steel from beam fitting into the column losses its anchorage this joint is not abel to give much resistance to cyclic displacements.

4.4.3 Analysis of load – displacement results of joints P.C.3 in comparison to M.C.1 under cyclic loading :-

1) The total energy dessipated by P.C.3 at the completion of ist cycle of +1,-1mm is 132.53 K.N. & that by M.C.1 is 140.51 K.N.
2) At the cyclic displacement of +5,-5mm the total energy dessipated by P.C.3 is 99.8 K.N. & that by M.C.1 is 92.07 K.N.
3) At the cyclic displacement of +20,-20mm the total energy dessipated by P.C.3 is 51.31KN. & that by M.C.1 is 43.71 K.N.

The behaviour of P.C.3 is governed by the strength, yield capacity , size & connection strength of I.S.A. with beam & column. The connection angle used in this investigation gives satisfactory results in comparison to M.C.1 under cyclic displacements upto 20mm

Thus of all the three precast connections the connection behaviour of P.C.1 & P.C.3 is satisfactory in comparison to monolithic connection M.C.1 . The connection detail of P.C.1 gives it better anchorage with column under cyclic loading. In connection P.C.2 as it is supported in down ward direction by corbel, once the steel from beam fitting into the

column losses its anchorage this joint is not abel to give much resistance to cyclic displacements, thus this connection behaved unsatisfactory under cyclic loading.

4.5 Finite element analysis results of single storey frame during erection stage (without slab been placed) under cyclic loading.

The F.E. analysis results of a precast single storey frame during its erection stage constructed with connection details already investigated are presented here.

A precast concrete structure is an assemblage of precast elements which, when suitably connected together, form a 3D framework capable of resisting gravitation and wind (or even earthquake) loads. In precast construction various elements of frame such as beams, columns etc are precast & they are then assembled and connected at site as per design. During assembling of the frame a precast structure is most venerable because a precast structure achieves its full strength after completion of assemblage because all elements contributes to its strength & stiffness. Loads occurring on structure during erection stage of a precast structure such as of assembling machinery, shuttering, fast winds during erection stage or even seismic forces occurring during erection may be critical some time. Hence it is important to access the behavior of frame during erection stage because a precast fame may remain in uncompleted stage for large period of time because connections made during erection may be to have left ideal for some time so that cast in place concrete used in connection can gain required strength.

4.5.1 Finite element analysis results of single storey frame F.P.C.1.

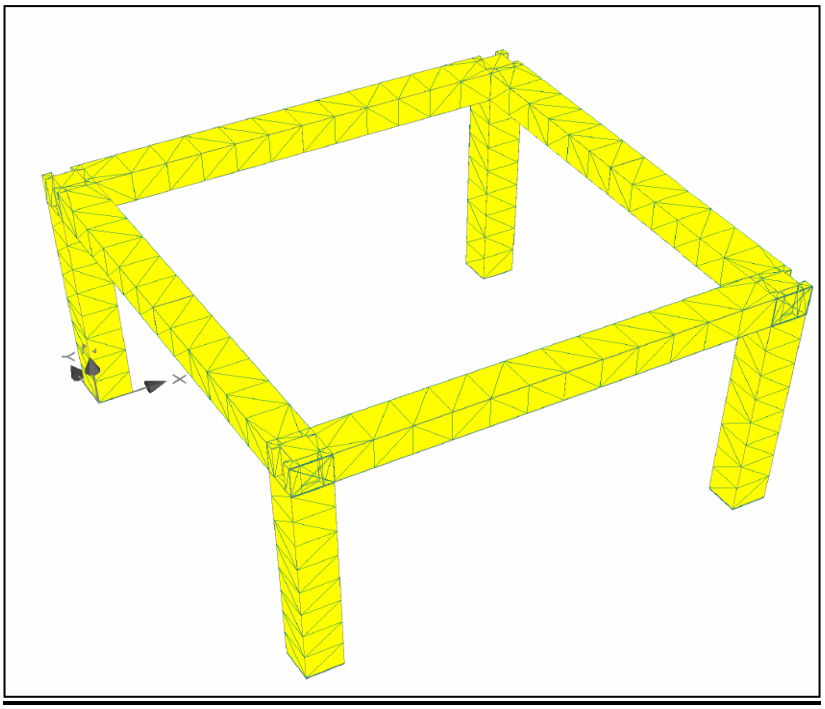

Figure 4.38 :– F.E. model of frame F.P.C.1

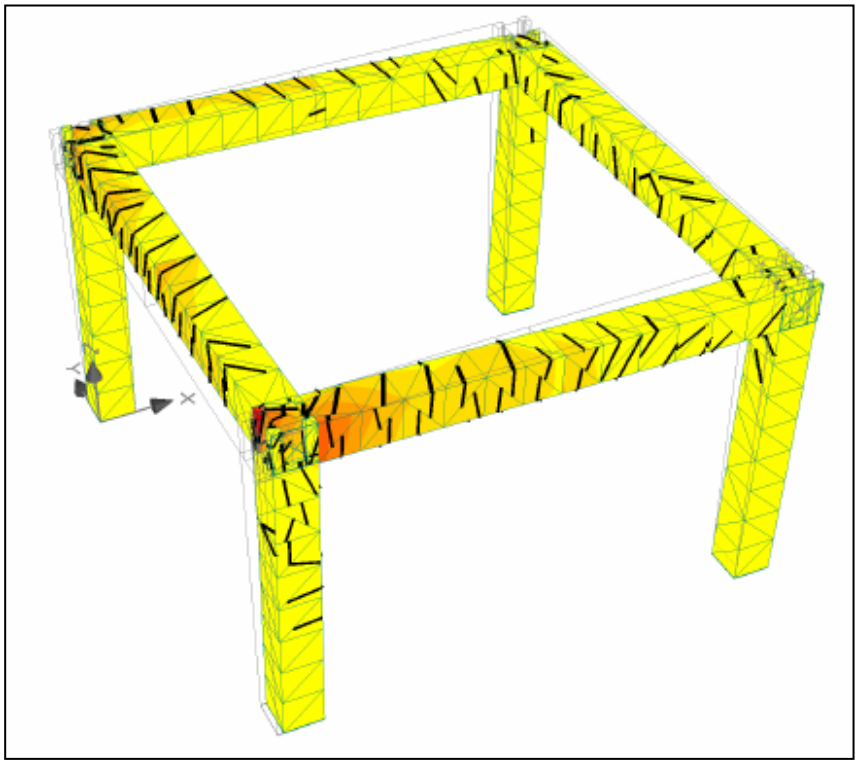

Figure 4.39 :– Deformed shape of frame F.P.C.1 at displacement cycle of +5,-5mm

Deformed shape of Frame F.P.C.1 after cyclic displacements of +5,-5mm revels that behavior of this frame is unsatisfactory during even small lateral displacements levels during erection stage. This results shows that joint P.C.1. is not able to withstand even small cyclic displacements & is not able to transfer lateral loads to frame members owing to its detail. Once the anchoraging steel in joint yields the structure may even collapse at small lateral displacements levels. Thus the frame constructed using joint P.C.1 needs special supporting mechanism at the stage of erection to prevent any sudden collapse of frame due to any accidental loading during erection stage.

4.5.2 Finite element analysis results of single storey frame F.P.C.2.

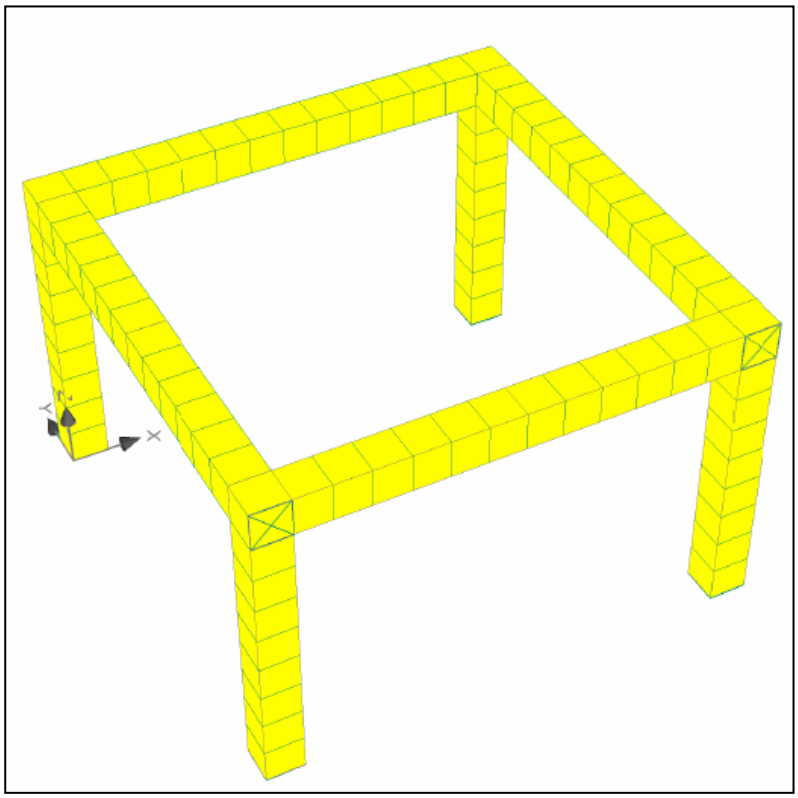

Figure 4.40 :– F.E. model of frame F.P.C.2

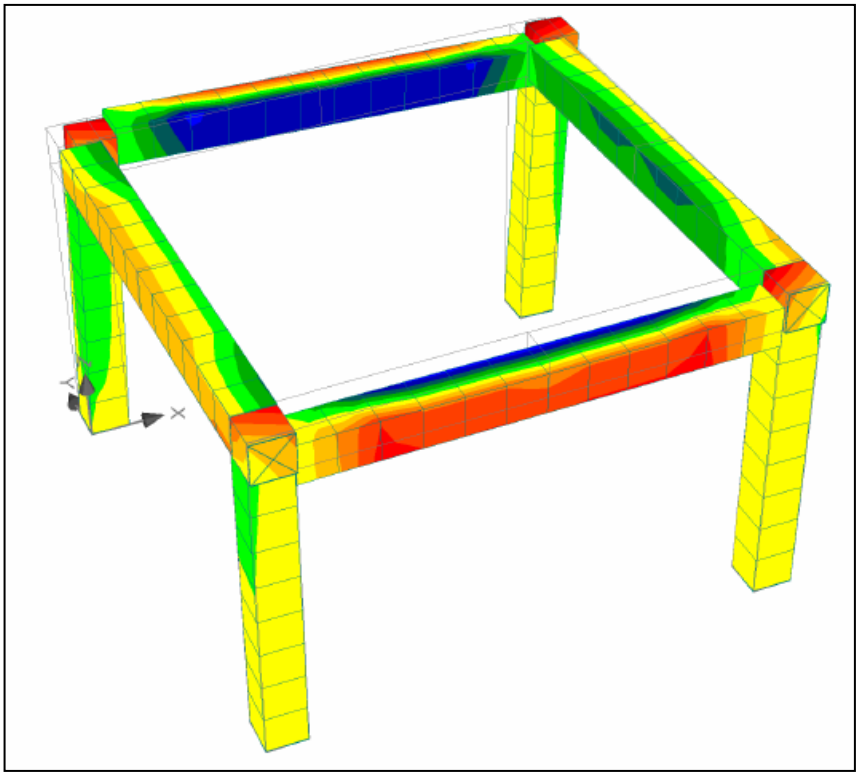

Figure 4.41 :– Deformed shape of frame F.P.C.1 at displacement cycle of +5,-5mm

The results of frame F.P.C.2. are similar to those of F.P.C.1. The deformed shape shows that joint P.C.2. is not able to withstand even small cyclic displacements & is not able to transfer lateral loads to frame members owing to its detail. Once the anchoraging steel in joint yields the structure may even collapse at small lateral displacements levels. Thus the frame constructed using joint P.C.2 needs special supporting mechanism at the stage of erection to prevent any sudden collapse of frame.

CHAPTER-5
CONCLUSIONS & RECOMMENDATIONS

5.1 General

In the present study, behavior of different types of beam column connection details used in precast construction under monotonic as well as inelastic cyclic displacements are investigated using finite element based software ATENA. The main aim of this investigation is to evaluate the structural characteristics of different beam- column joint details used in precast structure under seismic loading so as to comment on the structural safety of these joints in comparison to monolithic construction. Three type of beam – column connection details taken from the research work of different researchers are modeled and analyzed by using F.E.M. based software ATENA

5.2 Conclusions :-

The main observations and conclusions drawn are summarized below:-

5.2.1 Ease in erection :-

The selection of any joint in precast structure mainly depends upon the ease of constructing the joint. The connection detail which is easy & quickly to construct is more adopted in comparison to more complicated detailing.

1) The connection detail of P.C.1 is more complicated & requires strict quality control in dimensions & shape of structure.
2) The amount of form work reqired for P.C.1 is less
3) The connection detail of P.C.2 is simple & easy to construct & requires less quality control .
4) The amount of form work required for casting of P.C.2 is more.
5) Connection P.C.3 is a mechanical joint in which steel section is used to make the joint. This type of connection detail is also easy to construct depending upon the availability of skilled persons for making steel connections.

5.2.2 Strength of beam column joints under monotonic loads :-

1) Of the three connection details investigated in comparison to monolithic connection the behavior of all the three connections were satisfactory under gravitational loads.
2) The maximum reaction of P.C.1 is 133.7 K.N. that occurs at the displacement lvl. of 5mm, in comparison to M.C.1 whose maximum reaction is 137 K.N. at the displacement of 3mm.
3) The maximum reaction of P.C.2 is 116 K.N. that occurs at the displacement lvl. of 2mm, in comparison to M.C.1 whose maximum reaction is 137 K.N. at the displacement of 3mm
4) The maximum reaction of P.C.3 is 132 K.N. that occurs at the displacement lvl. of 4mm, in comparison to M.C.1 whose maximum reaction is 137 K.N. at the displacement of 3mm.

From these results this can be concluded that the strength of all the three joints are satisfactory under gravitational loads.

5.2.3 Cracks development & energy dissipation properties :-

1) The joint P.C.1 can be considered more ductile in comparison to M.C.1 under gravitational loads as yielding in joint occur at higher displacements.
2) The joint P.C.1 continues to give higher reaction even after yielding of steel in joint, this can be attributed to better configuration of joint
3) Cracks development pattren of P.C.1 shows that joint fully utalise the concrete around it during deformation as cracks are uniformely distributed all around the joint
4) The joint P.C.2 is less ductile in comparison to M.C.1 under gravitational loads as the joint yields at less displacements
5) Cracks development pattren of P.C.2 shows that joint does not properly tranfer reactions to the column during deformation and most of the cracks develops in the corbel on which beam is resting. Failure of corbel may cause the failure of whole connection
6) The load carrying capacity & ductility of joint P.C.3 depends upon the strength, yield capacity , size & connectivity I.S.A. with beam & column. The connection angle used in this investigation gives satisfactory results in comparison to M.C.1

Of all the three precast joints the energy dessipation properties of joint P.C.1 is most satisfactory under gravitational loads, owing to its better joint configuration & anchoraging with column. The behaviour of joint P.C.2 is least satisfactory as it is connected with column only by reinforcement bars & is supported by corbel prtuding from column face . Once the corbel fail it may cause imegiate failure of joint.

5.2.4 Strength & ductility of beam column joints under cyclic loads :-

1) From the data of hysteresis loops & energy dessipation at each cycle of P.C.1 in comparison to M.C.1 it can be seen that deterioration of strength of P.C.1 is at same rate as those of monolithic connection with increasing cyclic displacements & thus this type of joint may behave satisfactarely during cyclic deformations in strucutre.
2) From the data of energy dessipation at each cycle of P.C.2 in comparison to M.C.1 it can be seen that deterioration of strength of P.C.2 is much larger with increasing cyclic displacements & thus this type of joint may not behave satisfactarely during cyclic deformations in strucure. The reason behind this is that once the steel from beam fitting into the column losses its anchorage this joint is not abel to give much resistance to cyclic displacements.
3) The behaviour of P.C.3 is governed by the strength, yield capacity , size & connection strength of I.S.A. with beam & column. The connection angle used in this investigation gives satisfactory results in comparison to M.C.1 under cyclic displacements upto 20mm

The results of cyclic displacements of precast beam – column joints shows that properly anchoraged & detailed precast joint such as P.C.1 behaves sufficiently under cyclic loadings that are induced by seismic forces.

5.2.5 Behaviour of precast frame during its erection stage .

1) The analysis of precast frame during its erection stage under cyclic loads revels that these frame requires special supporting mechanism during erection

2) Even at the small displacement cycles of +5,-5mm the precast frame behaved adversely and can even collapse if not properly supported.
3) The reason for less lateral resistance of these frame during erection stage can be attributed to less stiffness of these frames during incomplete stage. The connection consist of beam – column held together by anchoraging steel & not by the bond between concrete of members which can help to dissipate higher energ & to transfer forces between frame members as in monolithic frames.
4) Thus during erection stage these frames should be properly supported so that any lateral force occurring on the frame can be properly distributed among various elements of frame to prevent collapse of frame.

5.3 Recommendations :-

The literature review and analysis procedure utilized in this thesis has provided useful insight about the behaviour of precast joints & frame . FEM model helps in accessing & comparing the results between precast & monolithic joints. The deformed shape , crack development stages & stress contours obtained by ATENA are helpful in understanding the load distribution pattern & critical areas of a structure. This can be usefull in in future researches on R.C.C. members & frames.

5.4 Future Scope

In the present study the behavior of three types of joints used in precast structures are investigated. Further work can be done on improving the detailing of these connections in term of bearings, anchoraging of reinforcement , ease of construction & support mechanisms of precast joints to develop a better details for precast joints. Also in this work only the seismic behavior of a single storied precast frame during its erection stage is accessed. Further work can be done on investigating the behavior of a completed precast frame under seismic forces.

REFRENCES

1) **Kim S. Elliot (2002),** Precast Concrete Structures, Great Britain, Antony Rowe Ltd.

2) **Englekirk, R. E.,** "Seismic Design Considerations for Precast Concrete Multistory Buildings," PCI JOURNAL, V. 35, No. 3,May-June 1990, pp. 40-51.

3) **Park, R.,** "A Perspective on the Seismic Design of PrecastConcrete Structures in New Zealand," PCI JOURNAL, V. 40,No. 3, May-June 1995, pp. 40-60.

4) **IS 10297 : 1987, Bureau of Indian Standards, New Delhi.** Code of practice for design and construction of floors and roofs using precast reinforced / prestressed concrete ribbed or cored slab unit,
5) **IS 10505 : 1983, Bureau of Indian Standards, New Delhi**. Code of practice for construction for floors and roofs using precast concrete waffle units,

6) **IS 11447 : 1985, Bureau of Indian Standards, New Delhi.** Code of practice for construction with large panel prefabricates, **IS 11447 : 1985, Bureau of Indian Standards, New Delhi.**
7) **IS 4326 : 1993, Bureau of Indian Standards, New Delhi.** Indian standard code for earthquake resistant design and construction of buildings,

8) Structural Engineering Design Provisions, Uniform Building Code 1997: Part 2, International Conference of Building Officials, Whittier, CA, USA.

9) Building code requirement for structural concrete, ACI 318-1995, American Concrete Institute, MI, USA.

10) Code of practice for the design of concrete structures and commentary NZS 3101, Part 1, (1995), Standards Association of New Zealand, Wellington.

11) **Mitchell D, DeVall, RH, Saatcioglu, M, Simpson R, Tinawi R, and Tremblay R**.,Damage to concrete structures due to the 1994 Northridge earthquake, *Canadian Journal of Civil Engineering*, 22(1995) 361-77.

12) METU, The Ceyhan–Misis Earthquake of 27 June 1998: A Preliminary Engineering Reconnaissance Report. Technical Report, Middle East Technical University Disaster Management, Implementation and Research Center, Ankara, Turkey, 1998.

13) Vidjeapriya and K.P. Jaya (2011), Behaviour of precast beam-column mechanical connections under cyclic loading. Asian journal of civil engineering (building and housing) VOL. 13, NO. 2 (2012) Pages 233-245

14) IS 1893:2002, Code of practice for Criteria for earthquake resistant design of structures Part 1 General provisions and buildings, Bureau of Indian Standards, New Delhi, 2002.

15) IS:456-2000, Code of practice for plain and reinforced concrete (fourth revision), Bureau of Indian Standards, New Delhi, 2000.

16) .IS:13920-1993, Code of practice for Ductile Detailing of reinforced concrete structures subjected to seismic forces, Bureau of Indian Standards, New Delhi, 1993.

17) Manoj K. Joshi, C.V.R. Murty and M. P. Jaisingh, Cyclic behavior of precast RC connections, The Indian Concrete Journal , November 2005, Pages 43-50

18) Ehsan Noroozinejad Farsangi (2010), Connections Behaviour in Precast Concrete Structures Due to Seismic Loading, GUJ Sci23(3):315-325 (2010)

19) Korkmaz, Husnu, Hasan., et al (2005) Performance of a precast concrete beam to-beam connection subject to reversed cyclic loading, T. Tankut/ Engineering Structures 27 (2005) 1392–1407

20) Rahman, Ataur, M., et al Performance-Based Seismic Evaluation of Two Five-Story Precast Concrete Hybrid Frame Buildings, Journal of structural engineering © asce / November 2017, Pages 1489 -1500

21) Libor Jendele and Jan Cervenka , ATENA theory manual, part 1 from Vladimir Cervenka.

22) B.G. Shirkey ,(2008) A detailed report on 3-S system of precast construction.